INL/RPT-22-69038-Revision-0

Enhancing Local Grid Resilience with Small Hydropower Hybrids Proving the concept through demonstration, simulation, and analysis with Idaho Falls Power

S M Shafiul Alam, Rojan Bhattarai, Tanveer Hussain, Vahan Gevorgian, Shahil Shah, Yaswanth Nag Velaga, Matthew Roberts, Thomas M Mosier, Jhair A. Alzamora, Ben Jenkins, Przemyslaw Koralewicz

Changing the World's Energy Future

Idaho National Laboratory

INL is a U.S. Department of Energy National Laboratory operated by Battelle Energy Alliance, LLC

INL/RPT-22-69038-Revision-0

Enhancing Local Grid Resilience with Small Hydropower Hybrids Proving the concept through demonstration, simulation, and analysis with Idaho Falls Power

S M Shafiul Alam, Rojan Bhattarai, Tanveer Hussain, Vahan Gevorgian, Shahil Shah, Yaswanth Nag Velaga, Matthew Roberts, Thomas M Mosier, Jhair A. Alzamora, Ben Jenkins, Przemyslaw Koralewicz

September 2022

Idaho National Laboratory
Idaho Falls, Idaho 83415

http://www.inl.gov

Prepared for the
U.S. Department of Energy
Under DOE Idaho Operations Office
Contract DE-AC07-05ID14517

HydroWIRES
U.S. DEPARTMENT OF ENERGY

Enhancing Local Grid Resilience with Small Hydropower Hybrids

Proving the concept through demonstration, simulation, and analysis with Idaho Falls Power

September 2022

S M Shafiul Alam
Rojan Bhattarai
Tanveer Hussain
Vahan Gevorgian
Shahil Shah
Yaswanth N. Velaga
Matthew Roberts
Thomas M. Mosier
Jhair A. Alzamora
Ben Jenkins
P. Koralewicz

INL/RPT-22-69038

Acknowledgments

This work was authored by the Idaho National Laboratory (INL), operated by Battelle Energy Alliance, under Contract No. DE-AC07-05ID14517; and National Renewable Energy Laboratory, operated by Alliance for Sustainable Energy, LLC, for the U.S. Department of Energy (DOE) under Contract No. DE-AC36-08GO28308 and supported by the HydroWIRES Initiative of the Energy Department's Water Power Technologies Office (WPTO).

Thank you to Idaho Falls Power for their leadership on the field demonstration, making their facilities and staff available to support it, and other technical facilitation.

We would like to thank Abhishek Banerjee who developed the Simulink hydropower model used in storage sizing simulation; Cliff Loughmiller, Brion Bennett, and Nicholas Smith who provided essential contributions for hardware installation, operation, and technical support. Thanks to Shiloh Elliott who provided information on irrigation modernization project and developed the map of the United States showing small hydro fleet and critical infrastructure density. Thanks to Muhammad Usama Usman for providing information about the non-powered dams.

We would also like to thank Mark Christian, Shijia Zhao, Matthew Mahalik, and Vladimir Koritarov from Argonne National Laboratory who summarized costs associated with power system outage.

The team would also like to thank WPTO including Marisol Bonnet, Hill Balliet, Sam Bockenhauer, and Tim Welch for their support, discussions, and contributions to the project design and review.

HydroWIRES

In April 2019, DOE's WPTO launched the HydroWIRES Initiative[1] to understand, enable, and improve hydropower and pumped storage hydropower's (PSH) contributions to reliability, resilience, and integration in the rapidly evolving U.S. electricity system. The unique characteristics of hydropower, including PSH, make it well-suited to provide a range of storage, generation flexibility, and other grid services to support the cost-effective integration of variable renewable resources.

The U.S. electricity system is rapidly evolving, bringing both opportunities and challenges for the hydropower sector. While increasing deployment of variable renewables such as wind and solar have enabled low-cost, clean energy in many U.S. regions, it also creates a need for resources that can store energy or quickly change their operations to ensure a reliable and resilient grid. Hydropower (including PSH) is not only a supplier of bulk, low-cost, and renewable energy, but a source of large-scale flexibility and a force multiplier for other

[1] Hydropower and Water Innovation for a Resilient Electricity System ("HydroWIRES")

renewable power generation sources. Realizing this potential requires innovation in several areas: incorporating new operations into planning and licensing decisions, predicting new operations and management (O&M) patterns and costs to prevent unplanned outages, and designing new turbines and control systems for fast response and frequent ramping while maintaining high efficiency.

HydroWIRES is distinguished in its close engagement with the DOE national laboratories. Five national laboratories—Argonne National Laboratory, INL, National Renewable Energy Laboratory, Oak Ridge National Laboratory, and Pacific Northwest National Laboratory—work as a team to provide strategic insight and develop connections across the HydroWIRES portfolio as well as broader DOE and national laboratory efforts such as the Grid Modernization Initiative.

Research efforts under the HydroWIRES Initiative are designed to benefit hydropower owners and operators, ISO/RTOs, regulators, original equipment manufacturers, and environmental organizations by developing data, analysis, models, and technology R&D that can improve their capabilities and inform their decisions.

More information about HydroWIRES is available at https://energy.gov/hydrowires.

Enhancing Local Grid Resilience with Small Hydropower Hybrids

Proving the concept through demonstration, simulation, and analysis with Idaho Falls Power

S M Shafiul Alam[1]
Rojan Bhattarai[1]
Tanveer Hussain[1]
Vahan Gevorgian[4]
Shahil Shah[4]
Yaswanth Nag Velaga[4]
Matthew Roberts[2]
Thomas M. Mosier[1]
Jhair A. Alzamora[3]
Ben Jenkins[5]
Przemyslaw Koralewicz[4]

September 2022

[1] Idaho National Laboratory
[2] Emerson
[3] Stony Brook University
[4] National Renewable Energy Laboratory
[5] Idaho Falls Power

Abstract

Large hydropower, connected to the transmission system and typically possessing significant ability to balance grid frequency, has long been central to black start plans in regions where it is present. Small hydropower possesses most of the attributes required for black start but is often connected to distribution or sub-transmission systems and has less ability to balance grid frequency. Integrating energy storage such as batteries or ultracapacitors increases the combined asset's ability to balance frequency. This asset integration enables a bottom-up grid restoration paradigm in which critical electric loads on the local distribution system can be powered even when the regional transmission system is down. This report presents a field demonstration conducted with Idaho Falls Power that proved this concept. The contribution of energy storage in restoring the small hydro-dominated distribution grid and its operational sensitivity across different control settings are further analyzed using high-fidelity simulations. Readers will learn about technical details on the field demonstration setup, energy storage contribution to black start, detailed simulation steps of islanded distribution grid restoration, and usage of field demonstration measurements for transient model refinements. Collectively this report points to a great opportunity for small hydropower to enhance resilience of local electric grids.

Acronyms and Abbreviations

BPA	Bonneville Power Administration
CB	City Bulb – Idaho Falls Power's 8.9 MVA City Bulb Plant (one horizontal Kaplan "bulb" unit)
CT	Current transformer
DER	Distributed energy resources
DGBS	Distribution grid black start
DOE	Department of Energy
f-Watt	Frequency-Watt
GFM	Grid forming
IBR	Inverter-based resource
IEEE	Institute of Electrical and Electronics Engineers
IFP	Idaho Falls Power
INL	Idaho National Laboratory
LB	Lower Bulb - IFP's 8.9 MVA Lower Bulb plant (one horizontal Kaplan "bulb" unit)
NBSU	Non-black start unit
NERC	North American Electric Reliability Corporation
NWPPA	Northwest Public Power Association
O&M	Operations and management
OL	Old Lower – IFP's Old Lower plant (consists of two 1.8 MVA Francis units. Only one was operated during the demonstration)
PID	Proportional-Integral-Derivative – one form of hydrogovernor control with gains {P, I, D}
PLC	Programmable logic controller
PLL	Phase-locked loop
PMU	Phasor measurement unit
PSH	Pumped storage hydropower
PSPS	Public safety power shutoff
PT	Potential transformer
ROCOF	Rate-of-change-of-frequency
ROR	Run-of-river
SoC	State of charge
USGS	United States Geological Survey
VAR	Volt-Ampere reactive
WPTO	Water Power Technologies Office

Contents

Figures

Tables

1. INTRODUCTION

Key Takeaways:

- Large hydropower's contribution to bulk grid resilience is recognized. However, small hydro's value in post blackout local grid resilience is yet to be explored.
- The complexity and speed of black start and grid restoration are primarily driven by cranking power requirement of non-black start units and ramping speed of individual generation units.
- Black start restoration strategies can be divided into four categories: (1) top-down from high-voltage transmission system, (2) bottom-up restoration from sub-transmission system, (3) bottom-up restoration from distribution system, (4) combined restoration.
- The "bottom-up" distribution grid black start can reduce outage area and time, enhance socioeconomic value through reduced downtime and component costs. Yet, its success depends upon factors, such as the presence and black start ability of small synchronous generator(s), system reconfiguration capability, protection settings flexibility, deciding the priority/order in which loads will be restored.
- Large hydropower plants have long been serving as black start units. Small hydropower plants possess similar requirements of such operation but suffers from islanded grid frequency

The reliability and resilience of the current electric grid are increasingly challenged by various threats ranging from weather events to cyber vulnerabilities. The resulting disturbance defined by "off normal" operating conditions occurs in electric grids all the time. The overwhelming majority of them are within planning margins and therefore are not noticed by anyone other than operators. Yet, some events are too large for the system to continue operating normally, leading to blackouts. Typical causes of blackouts as derived from natural and manmade threats include significant unplanned reductions in generation, limitations in transmission to balance regional generation and load, loss of a critical piece of equipment such as a large transformer, and inadequate reactive power reserves.

Transmission operators, in the face of extreme weather or cyberthreats, can sometime disconnect the distribution grid to maintain reliability of the transmission system. One such example is the public safety power shutoff (PSPS). This planned and regional outage is intended to limit the likelihood that the bulk power system would ignite a wildfire when conditions are particularly dangerous (typically hot, dry conditions with high winds). The execution of PSPS has become more frequent after a utility's bankruptcy due to legal liability in starting wildfires [1]. Now, PSPS events are common in California and are spreading to other Western states. On the other side of extreme weather, ice storms can knock off power lines in the winter, cutting off electricity supplies to rural customers whose connections to the transmission are "radial" (i.e., not redundant). Consequently, the independence of a distribution grid for post-blackout restoration is becoming increasingly important for local grid resilience.

In the context of generation assets for blackout mitigation and grid restoration, large hydropower plants' contribution to bulk power system reliability and resilience is widely recognized [2]. However, small hydropower plants (capacity: 100 kW ~ 10 MW), which are typically connected to sub-transmission or distribution systems, are yet to be explored for local grid resilience.

This report focuses on the role that small hydropower, when integrated with additional energy storage, can play in enabling the distribution grid black start. This bottom-up restoration strategy does not replace the need for transmission or sub-transmission-level black start resources. Rather, the goal is to enable greater overall system resilience by enabling multiple black start approaches. While the entire grid condition will determine the feasible mix of these restoration approaches, it will enable quicker restoration and operability of distribution system critical loads.

1.1 Black Start – Definitions, Requirements, and Processes

The process of restoring the grid after a blackout is called "black start." The formal definition of a black start resource established by the North American Electric Reliability Corporation (NERC) is:

> A generating unit(s) and its associated set of equipment which has the ability to be started without support from the System [i.e., electric grid] or is designed to remain energized without connection to the remainder of the System, with the ability to energize a bus, meeting the Transmission Operator's restoration plan needs for Real and Reactive Power capability, frequency and voltage control, and that has been included in the Transmission Operator's restoration plan [2].

Generation units that can satisfy the above definitions are referred to as black start units. The term non-black start unit (NBSU) refers to generation units that cannot start from complete shutdown without external auxiliary power support.

A post-blackout restoration plan typically includes the following stages [3]:

- System status identification to determine blackout boundaries and locations in respect to critical loads, status of circuit breakers and other protective devices, locations, and capacities of available black start units, etc.
- Starting at least one black start unit to establish cranking power path to NBSUs such as nuclear or large thermal power plants.
- Progressive restoration based on prioritized and step-by-step supply to loads avoiding over and under-voltage conditions.

The overall time of restoration depends upon (a) individual component's starting time (aggregation of cranking and ramping time), (b) cranking power requirement across the generation fleet and power grid, (c) energization sequence, and (d) the amount of load to be restored. Starting time, for example, varies across different components (see Table 1-1) [4], [5], [6], [3]. Cranking time, which is one of the contributors to starting time, shows smaller variation across generation capacity (see Figure 1). Ramping time (the other contributor to starting time), however, increases with generation capacity (see Figure 2) [4], [7], [8]. For an NBSU unit, both the cranking and ramping times are counted from the moment the external auxiliary power is available.

Table 1-1. Typical ranges of grid component start-up times.

Grid Role	Component	Cranking Time (min)		Ramping Time (min)	Average Starting Time (min)
		Minimum	*Maximum*		
Black Start Generation	**Hydro Reservoir**	0.02	60	6.7	**37**
	Diesel Generator	1	2	5	**7**
	Combustion Turbines	15	30	5	**28**
	Gas Turbine Combined Cycle	45	120	12.5	**95**
Non-Black Start Generation	**Geothermal**	60	300	20	**200**
	Steam Plants (gas, oil)	100	180	14.3	**154**
	Concentrated Solar Power	120	300	16.7	**227**
	Coal Power	160	180	16.7	**187**
	Bioenergy	160	180	12.5	**183**
	Lignite	340	360	25	**375**
	Nuclear	1400	1440	50	**1470**
	Utility-scale Renewable Energy Power Source	1	3	10	**12**
	Distribution-level Battery Energy Storage Systems	0.5	2	10	**11**
Transmission System	**Energize Bus Bar**	5	10	0	**8**
	Energize Transmission Line	5	10	0	**8**
	Energize Transformer	0.02	0.03	0	**0**
Distribution System	**Energize Substation**	1	5	0	**3**
	Energize Distribution Line	1	5	0	**3**
	Pickup Load	5	10	0	**8**

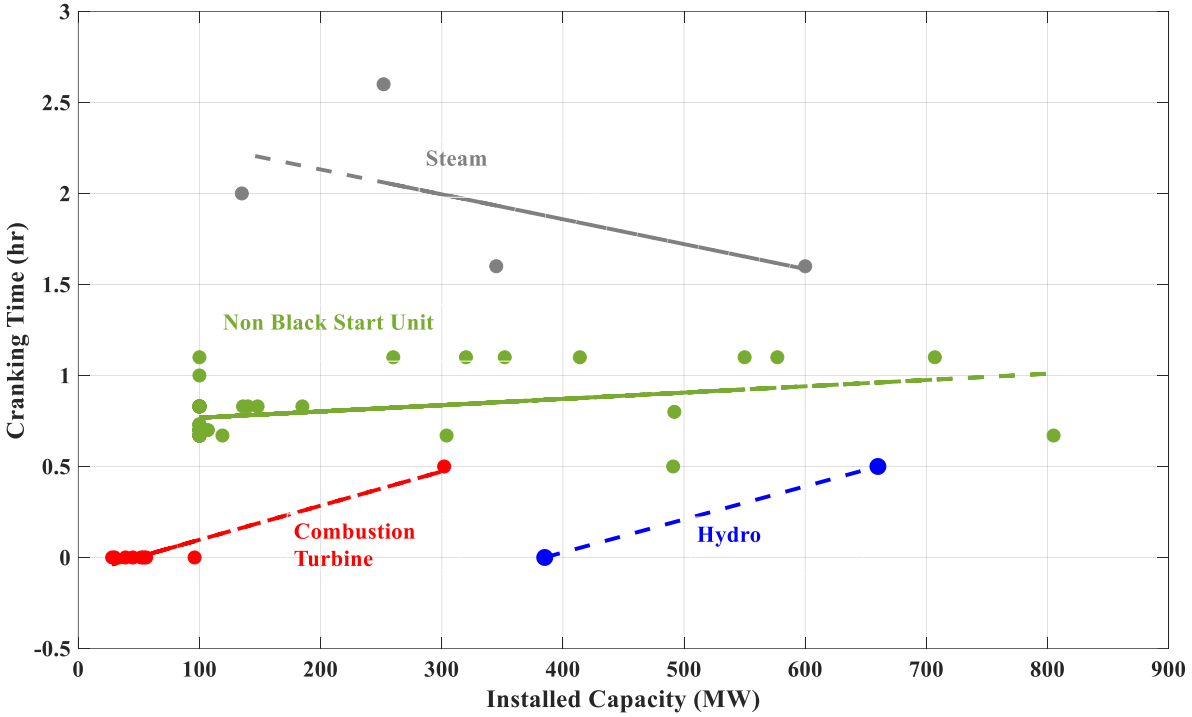

Figure Notes: Cranking time, which is one of the contributors to starting time, shows smaller variation across generation capacity.

Figure 1. Cranking time sensitivity based on generation type and installed capacity. Data Source: [7], [8].

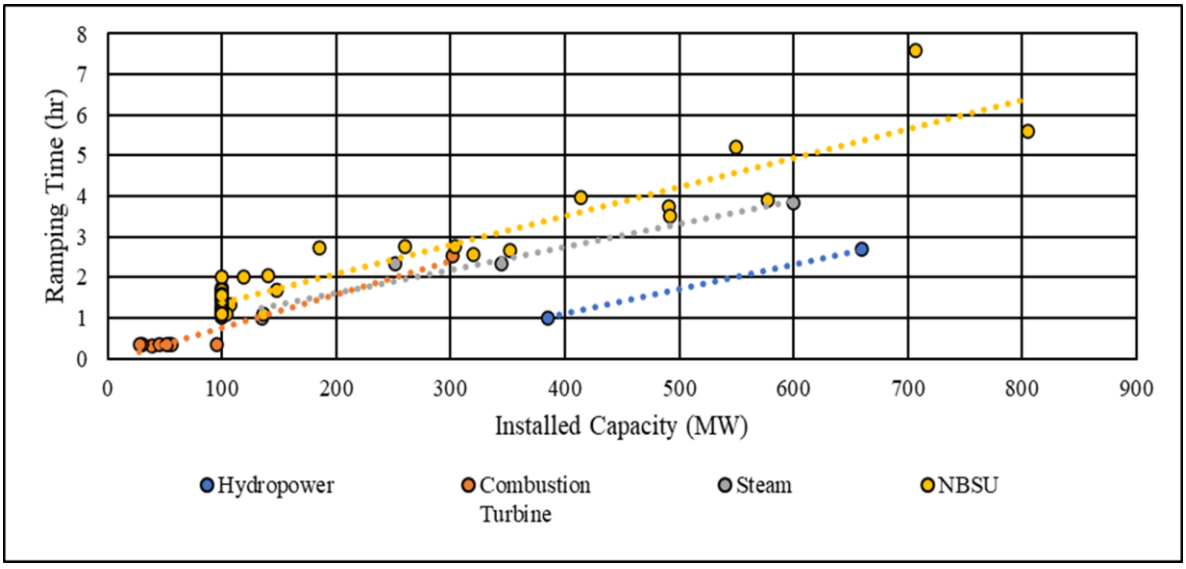

Figure Notes: Ramping time (the other contributor to starting time), however, increases with generation capacity.

Figure 2. Ramping time sensitivity based on generation type and installed capacity. “NBSU” stands for Non-Black Start Unit. Data Source: [7], [8].

The cranking power—the power that must be available at the site to energize the component—is largely a function of the capacity of the NBSU (Figure 3). The cranking power requirements of individual NBSU and their interconnections primarily determine the portion of the grid that must be energized to reliably transfer such power. Thus, the energized portion of the grid for cranking power transfer is referred to as *cranking path*. Overall, it is the ramping time of the individual generation unit and NBSU's cranking power requirement that drives the black start and restoration complexity and determines the restoration speed.

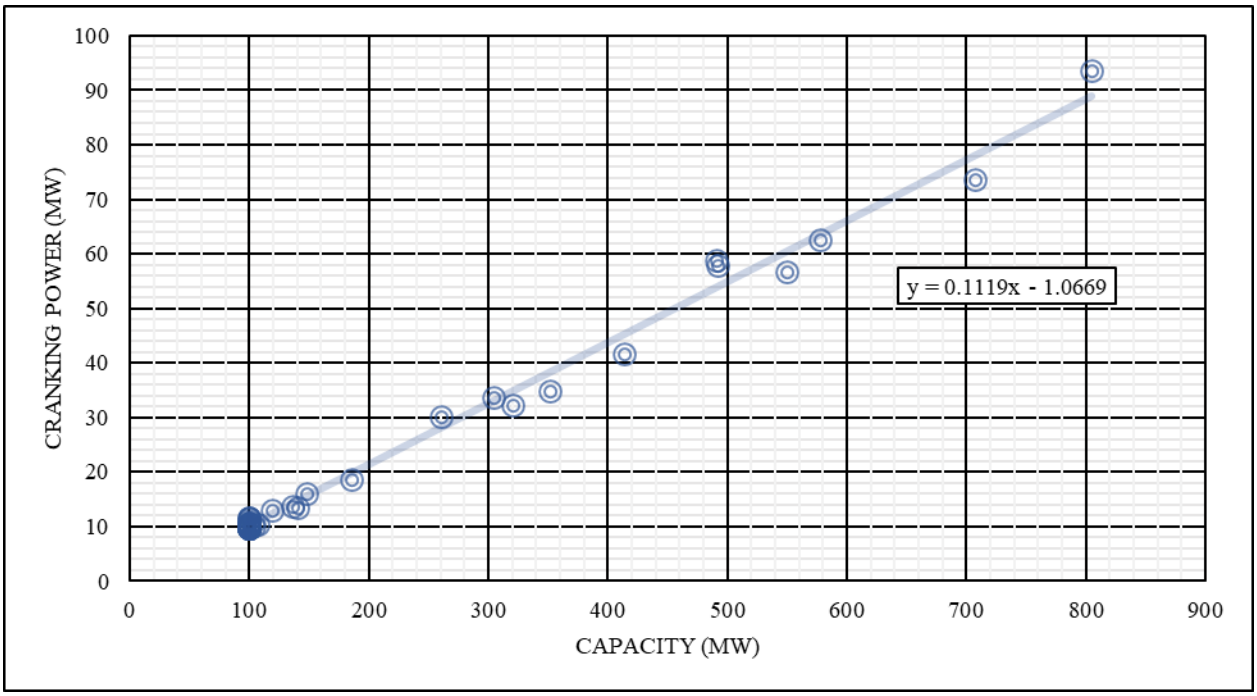

Figure 3. Necessary cranking power for non-black start units based on component capacity. Data Source: [8].

A reserve margin should also be provided between the local available power and the load pick up during the black start process. This differential is designed to compensate for load variability and compensate for electrical system dynamics while the islanded grid is still in a fragile state. This reserve margin should be set at 15% for primarily thermal generation systems and 10% for primarily hydropower-based generation systems [9], [10].

There are four main categories of black start restoration strategies [11], [12] (Figure 4):

- *Top-down restoration with high-voltage transmission system*: In this traditional approach, a few central black start units are restored first. These units then energize the high-voltage transmission system. Next the sub-transmission network to non-black start units is energized to establish the cranking path and eventually restore distribution grid and load services. Hydropower has long been a key transmission-level black start resource in many locations within the United States.
- *Bottom-up restoration with a sub-transmission system*: In this strategy, the black start units first energize the sub-transmission network and establish cranking path to larger but non-black start generation plants. A parallel multi-island restoration is executed, and then, the high-voltage transmission system is energized on the way to entire grid restoration.
- *Bottom-up restoration with a distribution system*: Referred to as distribution grid black start, this approach has the potential to leverage DERs, adaptive protection settings, and smart switching

capability to restore part or all the distribution grid. This approach is independent of transmission system restoration status. Furthermore, this is consistent with the concept of a microgrid that has all required grid capabilities and can connect or disconnect from the broader grid [13]. As we will see in Section 1.4, many small hydropower plants exist in proximity of the nation's critical infrastructure, but most are not used as black start resources.

- *Combined restoration*: Both the top-down transmission side and bottom-up distribution side restoration are executed in parallel; stability of respective frequency and voltage profiles are ensured and finally synchronized at the point of interconnection.

The current predominant black start scheme is referred to as "top-down." Traditional grid planning and operation are conducted using balancing authorities, an entity that is responsible for keeping generation and electric load in balance for a given geographic region. Part of the balancing authority's obligation is to maintain adequate black start resources and a corresponding plan for restoring their portion of the electric grid after a disturbance. Historically, most of the generation and storage assets have been large (hundreds of megawatts) and connected to the transmission system.

The transmission system connects each distribution system within the balancing authority, and therefore, the fastest and more reliable approach to ensuring adequate black start resources has historically been to utilize transmission-level generation and storage assets. The increasing prevalence of distribution-level generation and storage (i.e., distributed energy resources [DERs]) is enabling a new set of possibilities. With the cost of energy storage declining and advanced controls capability of DERs, a "bottom-up" approach for system restoration starting at distribution system can now be achieved.

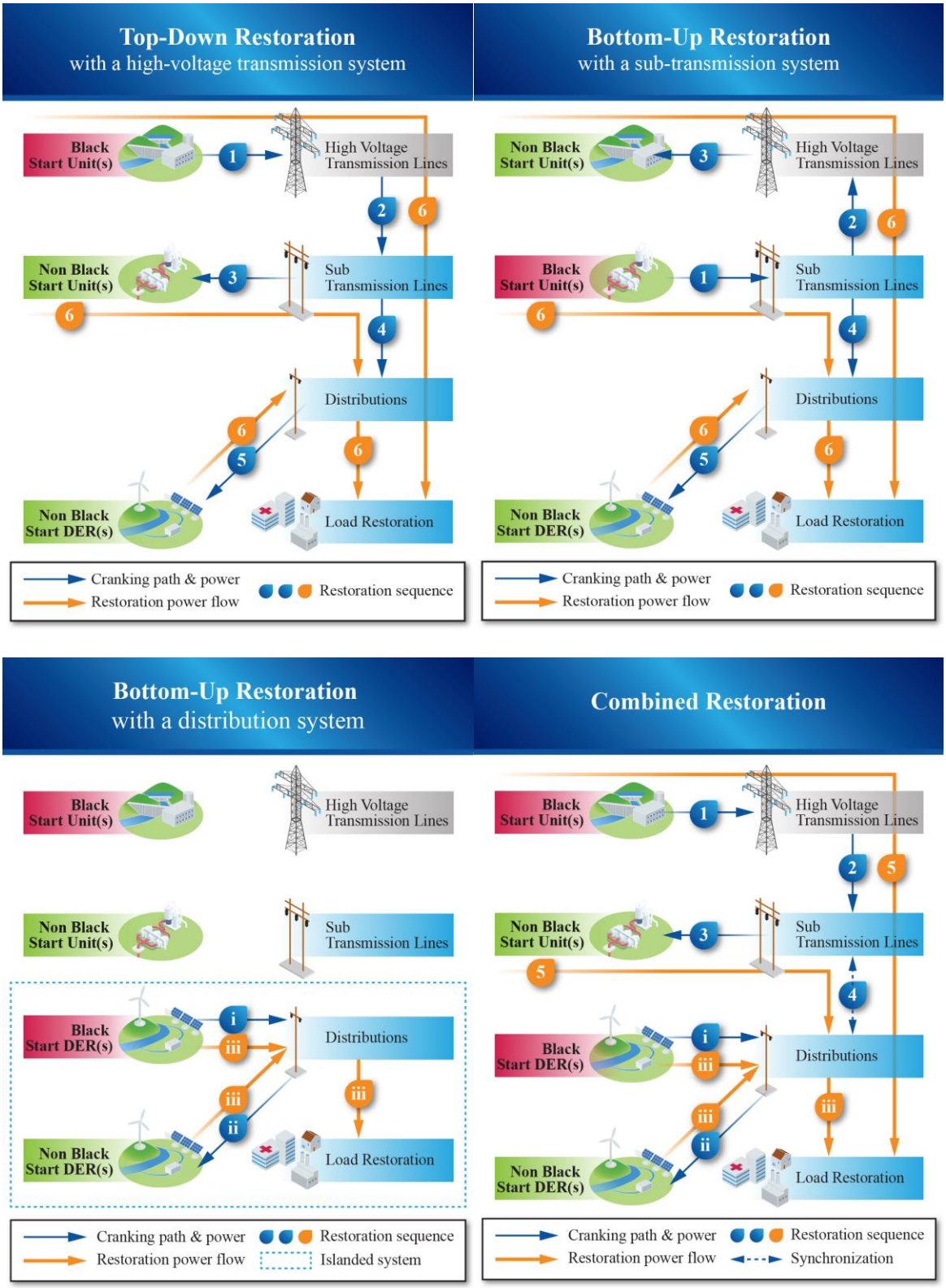

Figure 4. Hydropower can enable an alternative restoration strategy centered on the distribution grid.

1.2 The Benefits of Distribution Grid Black Start

The "bottom-up" distribution grid black start (DGBS) has the potential to increase reliability and resilience of the power system against natural and manmade threats by leveraging DERs and executing an independent yet parallel grid restoration scheme. Furthermore, the DGBS can reduce power outage duration and pick up all or a portion of the distribution loads. Consequently, this would reduce load downtime costs. The resulting impacts on local communities and business can be realized by looking into two aspects.

First, DGBS can relieve local businesses of financial crisis by helping reduce the system component level costs [14], [15], [16] and load downtime costs (see Table 1-2).

Table 1-2. Example downtime costs and sensitivities (summarized from [17]). Large (small) loads correspond to annual consumption greater (smaller) than 1 GWh.

	Large Loads ($/kw-hr)			**Small Loads ($/kw-hr)**		
	By percentile			*By percentile*		
Load Type	*5th*	*50th*	*95th*	*5th*	*50th*	*95th*
Agriculture	13	33	97	42	65	136
Mining	36	102	324	42	65	136
Construction	13	33	97	33	52	110
Manufacturing	21	55	168	29	47	99
Transportation/Communications	13	33	97	23	38	82
Wholesale/Retail	13	33	97	42	65	136
Finance/Real-estate	13	33	97	29	47	98

Second, DGBS can help reduce the socioeconomic costs associated with the power outage to vital resources (municipal water, communications, and health care) or major economic drivers (industrial loads, data centers, and commercial centers). It should be noted that these costs are significant and can vary based on duration and use cases. For example, the estimates for 1 hour outage cost can vary between $500/hr and $1,500,000/hr with the broader U.S. economy losing over $100 billion/year from outages and over $15 billion/year due to power quality issues [18], [19].

The DGBS can also mitigate cold load pickup issues (e.g., flow of inrush currents of 8 ~10 times of rated current magnitude due to simultaneous energization of reactive and thermostatically controlled loads [11]) and expedite transmission system black start even with generators of limited ramping capability. This would help reduce component level costs. Overall, the reduction in outage area and time due to DGBS would enhance socioeconomic value through increased customer satisfaction and reduced downtime and component costs.

1.3 Elements and Considerations for Distribution Grid Black Start

Distribution system service restoration is a practice that has been in place for years, in which the distribution utilities take a coordinated approach to restore power supply to out-of-service consumers while ensuring continuity of power supply to other consumers after events like faults in the system. For the service restoration, the goal is to reenergize a portion of the distribution system, isolated by protective devices which open part of the system after detecting a sustained fault. DGBS can be considered as a special case of service restoration in which all the distribution systems were fully de-energized before performing DGBS. However, the viability of a stable and reliable DGBS depends upon various considerations. The power distribution system differs from its transmission counterpart on various characteristics, including topologies, level of balancing, and reactance to resistance ratio [20]. For example, the distribution grid of radial topology, spanning from the distribution substation all the way to customers at the feeder ends, consists of phase and power imbalanced mixture of loads, synchronous

generators of smaller capacity, inverter-based resources (IBRs) with lower short circuit ratio [21], limited remote control, and restrictive frequency trip settings [22].

Consequently, the success of a DGBS depends upon factors such as the presence and black start ability of small synchronous generator(s), system reconfiguration capability, protection settings flexibility, deciding the priority/order in which loads will be restored, best possible ways to minimize the downtime for customers, etc.

Not all generation units are well-suited to act as a "black start" unit. Preferred black start unit characteristics are as follows [3]:

- Needs minimal time, fuel, and equipment to restart.
- Can be relied upon at any time to be available for black start with fuel on hand.
- Can operate in isochronous (i.e., 0% droop) mode of prime mover governor control [23]. During black start, isochronous mode enables full range dispatch of the black start unit to continuously maintain grid frequency at nominal value.
- Is equipped with adequate start-up power support at the station (e.g., DC batteries and small diesel generator) to start in islanded mode (i.e., absence of external grid support).
- Has sufficient nameplate capacity to provide real and reactive power to energize cranking paths and restart other DERs.
- Can operate quickly after a blackout during early grid restoration operations, can continue to operate when frequency swings are expected and occur, and can help stabilize system frequency.
- Can provide station and start-up power to non-black start units with a minimum of transformations (transformers in the path) and electric line switching operations.

The start-up power is needed, for example, to keep the oil and lubrication system running and maintain the station switching, control, and communication system, until the black start unit comes online and is ready to deliver power to the station and energize the cranking path.

It should be noted that energy storage with a GFM inverter can also act as a black start unit, by co-locating with a distribution substation, for instance, and leveraging high-DER penetration [24]. Yet, widespread deployment of GFM solutions has a long way to go from a handful of pilot projects [25].

The cranking path for DGBS depends upon the distribution grid topology—sequencing the start of black start and non-black start resources around a ring bus versus establishing reliable and stable cranking paths toward non-black start resources across radial topology [26]. The cranking path should have a point of interconnection to available non-black start units, and the number of transformers and switchgears through the cranking path should be as low as possible to ensure seamless energization of non-black start units and formation of a stiff distribution backbone [3], [11].

In the presence of DERs (both synchronous generators and IBRs), coordination of controlling individual generation assets and load entities is of the utmost importance to ensure reliable and stable post-blackout restoration. This applies to both DGBS and combined top-down and bottom-up restoration methods. According to the NERC, coordination is needed between governor and inverter control according to the time, magnitude, and repeatability of the respective frequency responses [27]. The ideal case would be to make the IBR control adaptive (e.g., transition between inertial and fast frequency response) to the dynamics of the frequency excursion, within the boundaries set by the IBR's recommended state of charge.

Depending on the availability of black start capable units, the control coordination complexity, and the accepted outage time [28], load restoration can take place either in parallel at multiple islanded grids or after spanning the cranking path to bring all generation resources and the grid online [29].

In some cases, distribution network reinforcement may be needed depending on DER locations since more sectionalizing switches would be necessary for feeder reconfiguration during black start. Availability of a distribution management system, monitoring infrastructure, and communication networks for distributed generation is also important for successful restoration services.

1.4 Opportunities and Challenges for Hydropower to Provide Distribution Grid Black Start

Hydropower has long been a traditional black start unit because it meets all the black start requirements, and large hydropower plants are tied to the transmission system. A benefit is that their "fuel" (water) is naturally stored across the landscape (e.g., as snow) and in the upstream river system, although the amount of water depends on the season. Internal power consumption of hydropower plants is low compared to thermal ones, and start-up times are faster thanks to their fast primary frequency response and steep ramping capabilities [11]. In the United States, about 40% of all units that are maintained and tested for providing black start are hydropower turbine generators, even though hydropower makes up only about 10% of overall U.S. generating capacity [3]. According to U.S. Energy Information Administration, most of these large (at least of 10 GW capacity) hydropower-based black start units have a starting time less than 10 minutes [30]. There are also significant opportunities for small hydropower to enhance distribution system resilience by enabling DGBS capabilities for a larger number of locations through the nature-driven geographic diversity and proximity to critical infrastructures (see Figure 5).

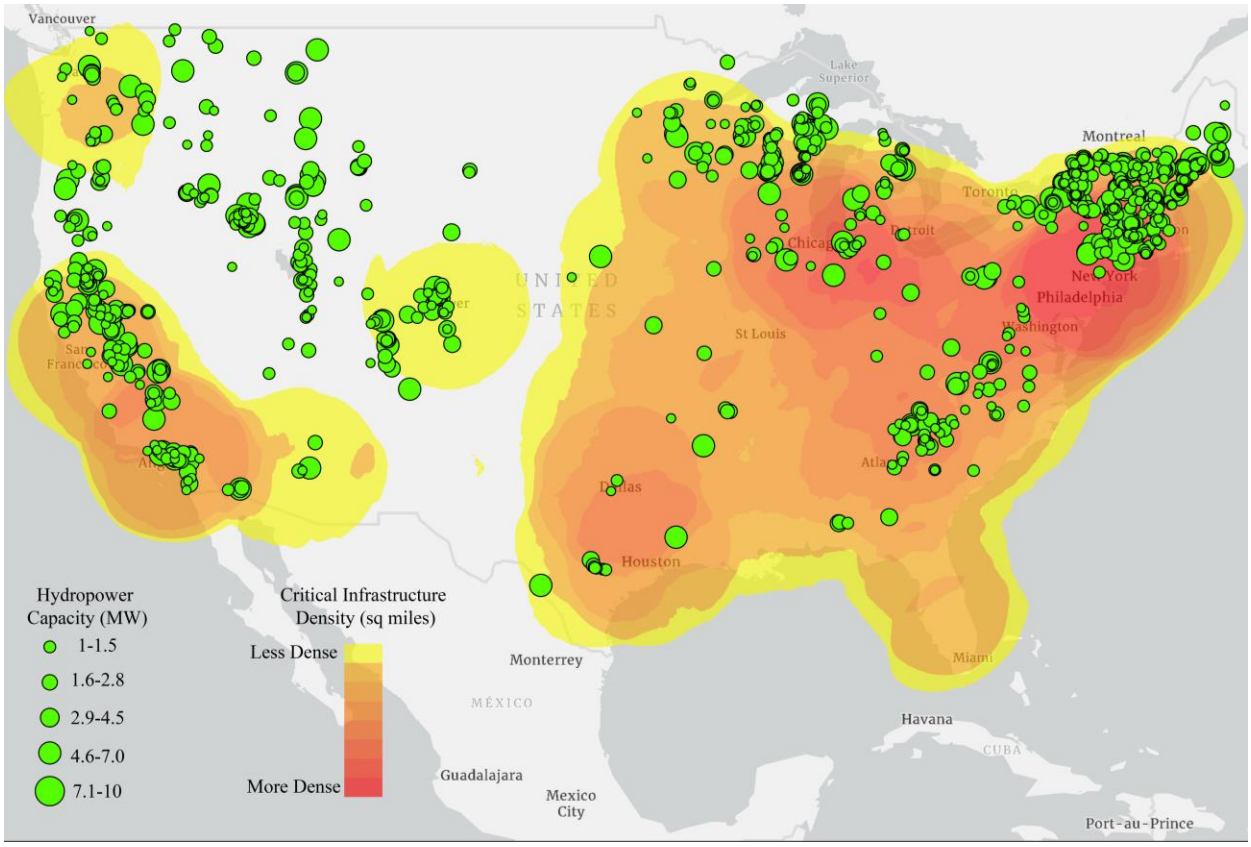

Figure 5. U.S. critical infrastructure and small hydropower co-location [31].

Many public, cooperative, and municipal utilities have more than one hydropower unit in their systems. These municipal small hydropower units are usually small projects capturing energy from low-head and diverted stream flows or using existing dams in irrigation infrastructure [32], [33]. Such run-of-

river (ROR) hydropower units are normally set to run at the maximum efficiency with wicket gates and turbines that adapt and move as the stream does. Considering the fuel, fast start-up, and station power requirements, these units are, in principle, black start capable. But they suffer from maintaining stable frequency without the external grid support—posing the challenge of seamless load restoration during the DGBS. This is because small hydropower units, such as ROR, have lower inertia and have lower momentum in the moving water and the machinery, as compared to reservoir-based large hydropower units. Consequently, small hydropower units have less ability to bear the transients of load restoration during DGBS. This showcases the irony of remote and hydro-reach island communities, such as those in Alaska, who mostly rely on their diesel generation for DGBS.

Accordingly, turbine and governor specific control modification and improvements (e.g., designing control set points exclusively for islanded operation) may be needed to provide stable operation during islanded conditions. Such control adjustment may enhance stability at the expense of compromised efficiency. In some cases, enhancing technologies such as integrating energy storage is needed to address stability problems during DGBS with small hydropower.

The rest of this report presents the option of energy storage integration with ROR hydropower through (1) a black start field demonstration with a municipal utility and report frequency stability performance (Section 2) and (2) a DGBS simulation with energy storage and multiple ROR hydropower plants (Section 3). The sensitivity of energy storage configuration to black start frequency stability is also reported (Section 4), and the importance of onsite demonstration is illustrated through simulation and actual response comparison (Section 5). Finally, the findings and lessons learned are summarized with the mention of next steps for accelerating energy storage integration with small hydropower for enhanced grid resilience.

2. ENERGY STORAGE CAN IMPROVE SMALL HYDROPOWER'S BLACK START CAPABILITY

Key Takeaways:

- Idaho Falls Power and Idaho National Laboratory conducted a field demonstration that included isolated operation of three small hydropower plants and an ultracapacitor system.
- Use of the ultracapacitor system increased operational stability, as characterized by reducing the magnitude and duration of frequency excursions during tests to emulate a distribution-level black start process.
- Isolated mode tuning of hydrogovernor control further contributed to operational stability enhancement.
- Multi-plant black start increased individual plant's contribution to load restoration.

As mentioned in the previous section, small hydropower, such as ROR satisfies almost all major criteria to act as a black start unit but suffers from inherent stability issues when loads are being restored without external grid support. This is first observed during a black start test conducted by Idaho National Laboratory (INL) and Idaho Falls Power (IFP) in December 2017 [34]. IFP is a publicly owned municipal-run electric utility in the city of Idaho Falls, Idaho, USA. This hydro-dominated utility owns and operates five hydropower plants with a total generation capacity of 52.9 MW (see Table 2-1).

Table 2-1. IFP's hydropower fleet.

Generation	Capacity (MW)	Number of Units	Turbine Type
Upper Bulb (UB)	8.9	1	Horizontal Bulb-Kaplan
City Bulb (CB)	8.9	1	Horizontal Bulb-Kaplan
Lower Bulb (LB)	8.9	1	Horizontal Bulb-Kaplan
Old Lower (OL)	3.6	2	Vertical Francis
Gem State	22.6	1	Vertical Kaplan
Total	**52.9**		

Among these, the Upper, City, and Lower Bulb plants operate horizontal axis Kaplan turbines at approximately 19 ft head and require at least 6,000 cubic ft/sec (CFS) of river flow rate for optimal operation. The Old Lower (OL) plant, co-located with the Lower Bulb (LB) plant, consists of two vertical axis Francis turbines and operates when the flow rate exceeds the optimal limit or when the LB plant is shut down. The 22.6 MW Gem State project is operating at 43 ft head and located about 5 miles south of the city. All these plants are sited along the Snake River spanning from the Northern (Upper Bulb) to the Southern (Gem State) side of Idaho Falls (see Figure 6). Based on IFP's 2017 annual report, this hydropower fleet served approximately 23% of the city's total energy demand. IFP serves the rest of the energy demands through receiving purchased power from the PacifiCorp (Rocky Mountain Power) via the Goshen substation [32], [35], [36], [37]. This substation is IFP's single point of interconnection with PacifiCorp and caused two major blackouts to IFP and its customers. The first one occurred on December 4, 2013 leaving about 53,000 southeast Idaho residents without power in subzero cold for 3 hours [38]. After this event, IFP started a collaborative research effort with INL to assess the black start capability of IFP's hydropower fleet. In the meantime, IFP experienced the second blackout in summer of 2016 leaving 27,000 customers out of power for at least 2 hours [39]. Consequently, the December 2017 black start test with IFP's LB plant played an important role to assess black start and IFP's grid islandability should there be a next major blackout. This black start test identified ROR hydropower's frequency stability issues, specifically excessive lowering of frequency nadir that resulted in multiple trip offs of the LB hydropower plant. This restricted the load restoration up to only 3 MW, and further

investigation was recommended for islanded mode hydrogovernor control, generator protection settings adjustment, and viability of energy storage integration.

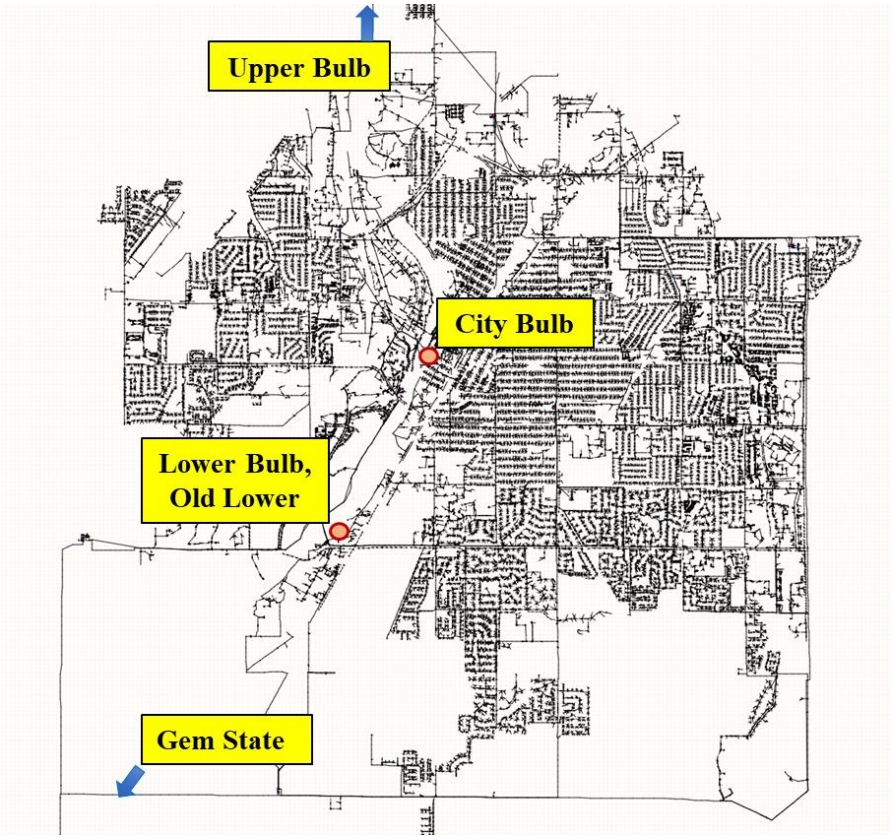

Figure 6. Electrical map view of IFP grid, including location of hydropower plants.

Based on these recommendations, IFP revised the generator protection settings to relax underfrequency trip settings from islanded mode. Specifically, the islanded LB plant is allowed to operate at 55 Hz for 5 seconds—a relaxation from the typical IEEE C37.102-2007 (AC Generator Protection) setpoints [40]. INL, in collaboration with IFP, and Emerson developed a high-fidelity model of the LB plant [41]. This model is utilized in digital real-time simulation with an ultracapacitor energy storage system hardware-in-the-loop test [42]. This test enabled tuning the ultracapacitor's frequency (f)-Watt control with a goal to improve frequency nadir and other stability aspects while restoring load from the LB plant.

During the week of April 19, 2021, the ultracapacitor system with lab-tested f-Watt control setpoints was transported to IFP's Rack substation to conduct a 4-day-long field demonstration of black start. Two 4 MW load banks have been rented to provide step loading to the hydropower units during this demonstration (Figure 7).

Figure 7. Satellite image and photos showing the Rack substation, ultracapacitor system, Old Lower, and Lower Bulb plants. Satellite image courtesy: Google Maps.

Beside LB, IFP's OL and City Bulb (CB) plants were involved in the field demonstration. During multi-plant operation, OL plant was manually synchronized to LB first, and then CB plant was manually synchronized to OL and LB plants. Figure 8 illustrates the hydrogovernor droop and speed reference settings for these plants during the field demonstration. It should be noted that, during this period of demonstration, the river flow rate was reported below 6,000 CFS by the nearby U.S. Geological Survey (USGS) stream gauge # 13060000 [43]—suggesting less stable behavior from these hydropower plants.

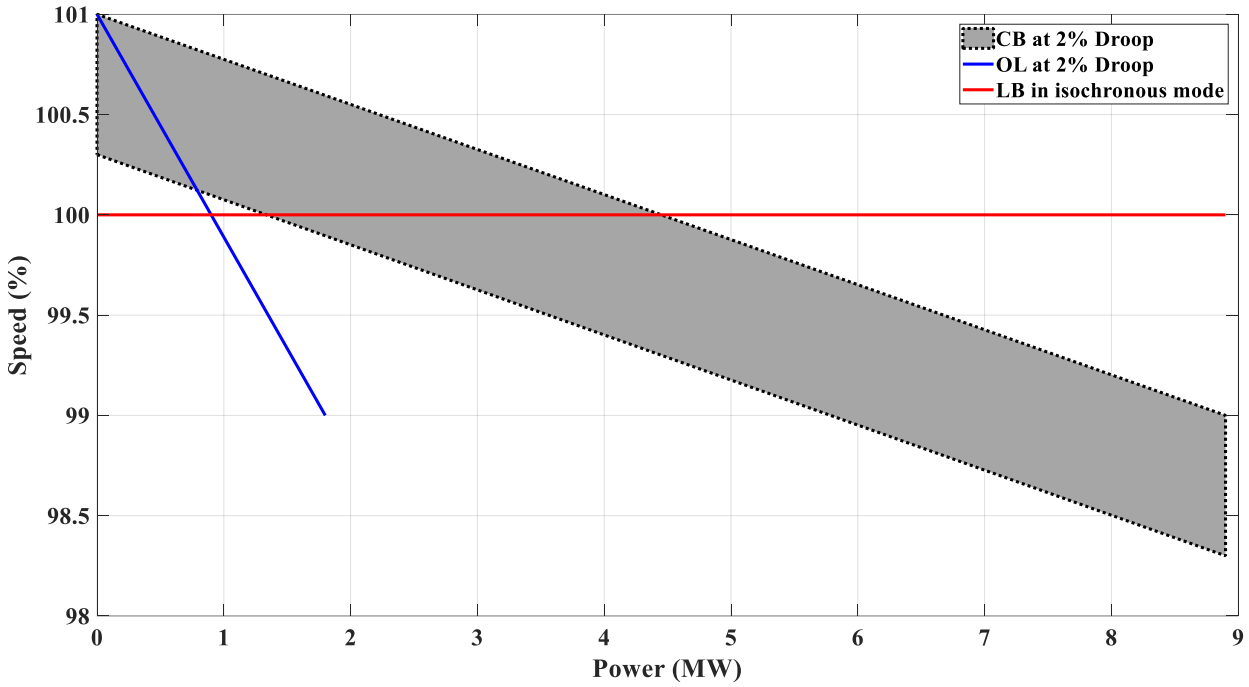

Figure Notes: Isochronous mode corresponds to 0% droop. The shaded region represents the range of speed references used for the CB plant during the field demonstration. This enabled adjustment of CB's generation dispatch across different loading conditions. CB's speed reference was raised with higher loading to match LB generation.

Figure 8. Speed reference and droop settings used during the black start field demonstration.

Three micro-phasor measurement units (micro-PMU) have been installed to capture high-resolution data during the demonstration (Figure 9). The micro-PMU data thus collected has been postprocessed and analyzed (see Appendix A) to capture (a) frequency at the LB interconnection (PMU 3) and (b) active power response from ultracapacitor (PMU 2) for each electric loading (PMU 1). Each day of the demonstration focused on a specific scenario [40].

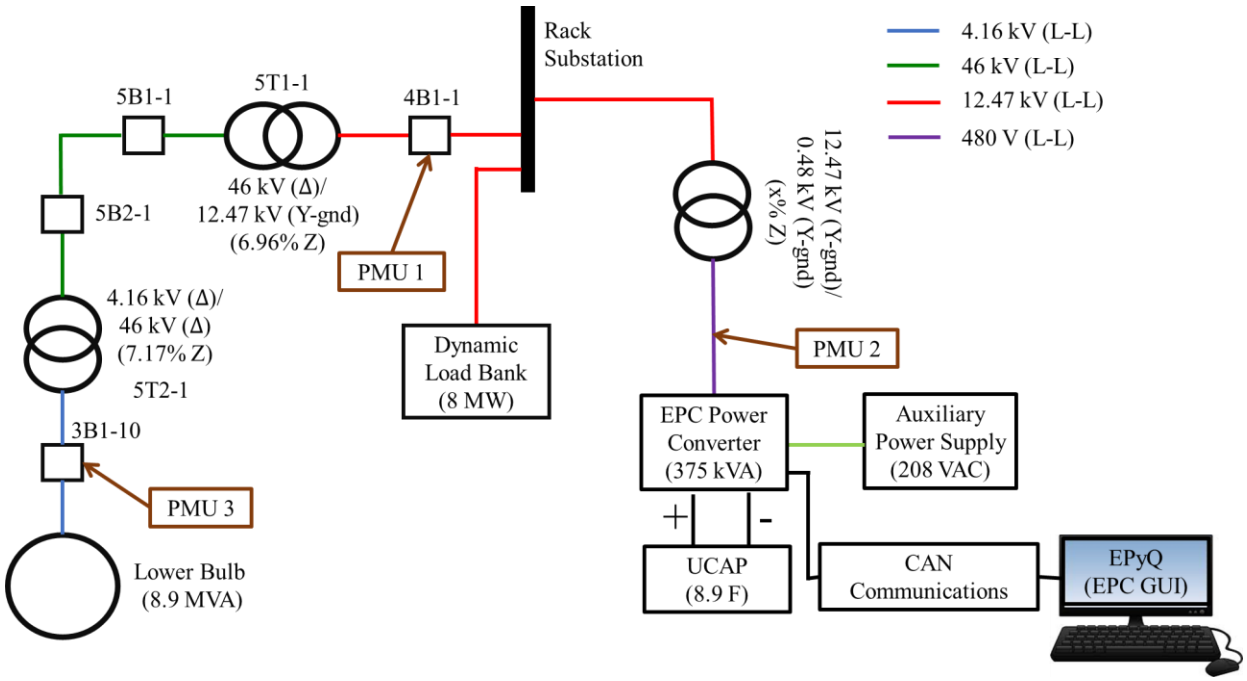

Figure 9. Micro-PMU, load bank, and ultracapacitor (UCAP) interconnection with LB for black start field demonstration. Not shown are the OL (2.4 kV, 1.8 MVA) and CB (4.16 kV, 8.9 MVA) that can interconnect with the 46 kV sub-transmission line.

The scenarios included electrical loading (through 500 kW step load up) of single or multiple hydropower units in the absence or presence of ultracapacitor (see Table 2-2).

Table 2-2. Loading test scenarios used during the black start field demonstration.

Scenario	Units Involved	Execution Date
1A	LB (Old settings of hydrogovernor, 0% droop)	Monday, April 19, 2021
1B	LB (Old settings of hydrogovernor, 0% droop) + UCAP (f-Watt Setting # 1)	Monday, April 19, 2021
2A	OL (2% droop) + LB (Old settings of hydrogovernor, 0% droop)	Tuesday, April 20, 2021
2B	OL (2% droop) + LB (Old settings of hydrogovernor, 0% droop) + UCAP (f-Watt Setting # 2)	Tuesday, April 20, 2021
3A	OL (2% droop) + LB (Old settings of hydrogovernor, 0% droop) + CB (Sharing no/equal load with LB)	Wednesday, April 21, 2021
3B	OL (2% droop) + LB (Old settings of hydrogovernor, 0% droop) + CB (Sharing equal load with LB) + UCAP (f-Watt Setting # 2N)	Wednesday, April 21, 2021
4	LB (New settings of hydrogovernor, 0% droop);	Thursday, April 22, 2021

Scenario	Units Involved	Execution Date
	Blade biasing; UCAP (with different f-Watt Settings)	

For ultracapacitor integration in grid-following mode, four frequency-Watt (f-Watt) settings have been considered (see Figure 10) for fast frequency response.

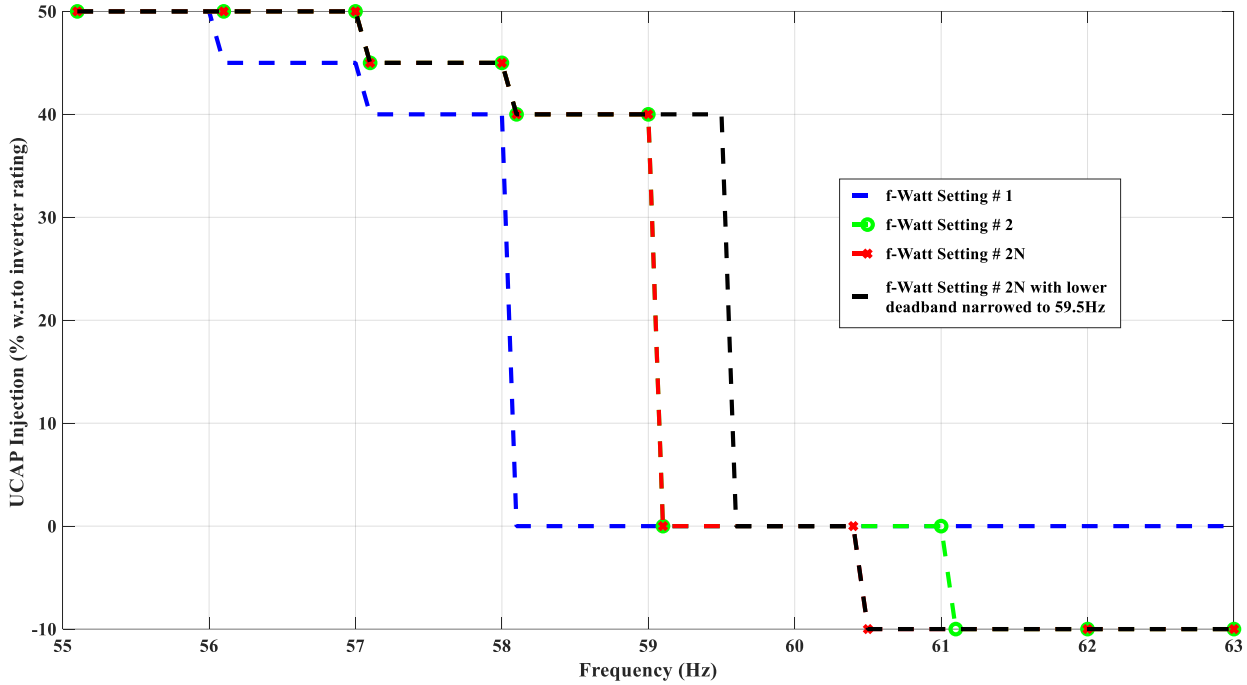

Figure Notes: Setting "# 2N" is obtained by narrowing the upper deadband to 60.4 Hz.

Figure 10. Frequency-watt (f-Watt) settings used during the field demonstration.

Before looking into the detailed black start performance across these scenarios and f-Watt settings, we want to illustrate the islanded LB plant's response to electric loading with and without ultracapacitor. Given a 500 kW step load change, the goal is to observe whether the generation units can withstand the resulting frequency instability and if ultracapacitor integration can contribute to improve such instability. In scenario 1A, for instance, the 8.9 MVA LB plant experienced frequency excursion with a nadir as low as 54.15 Hz during a load increase from 2.5 MW to 3.0 MW (see Figure 11).

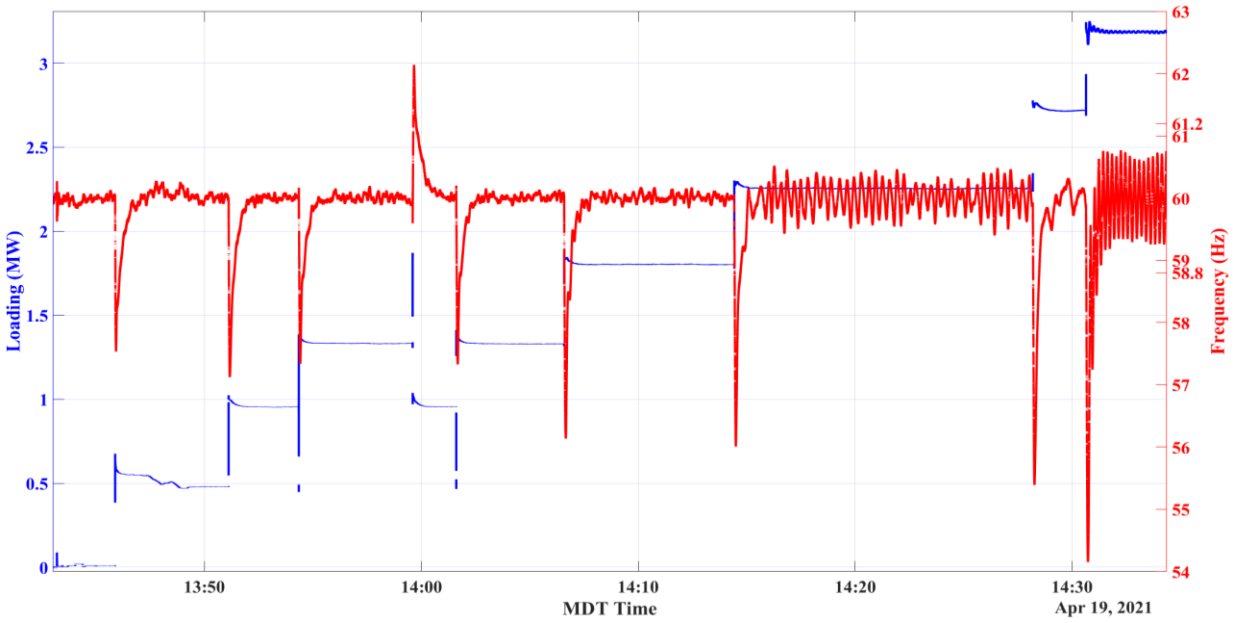

Figure 11. LB's frequency excursion in Scenario 1A (no ultracapacitor used).

With the integration of ultracapacitor, and for the same load step, the frequency nadir recorded is 56 Hz (see Figure 12). This 2 Hz improvement reduces the risk of an under-frequency trip of the LB plant and hence paves the path to successful black start and enhanced load carrying capability. The improved nadir also offers greater adherence to IEEE C37.102-2007. The corresponding response from the ultracapacitor, such as its precharging (i.e., before load steps), active power injection (caused by frequency nadir), and active power absorption (caused by frequency overshoot), are also illustrated (see Figure 12).

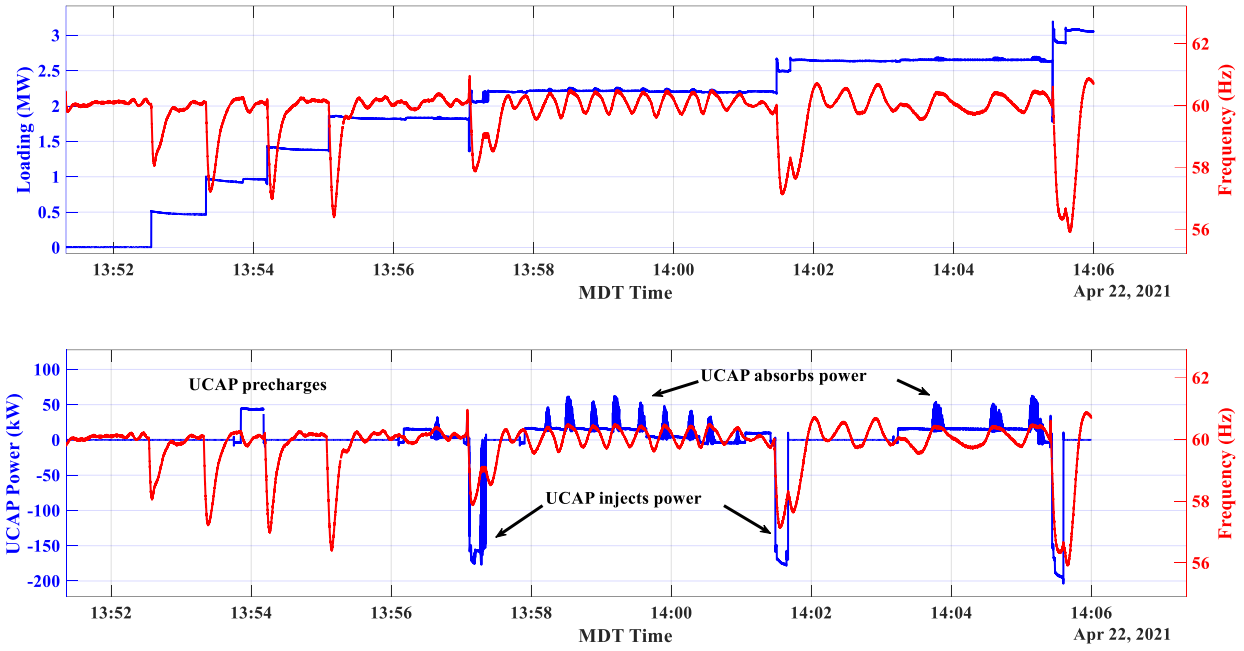

Figure Notes: The second frequency dip is attribuable to DC under-voltage ultracapacitor trip.

Figure 12. Electric loading of LB in presence of ultracapacitor ("UCAP"). This experiment corresponds to Scenario 4 using f-Watt setting # 2N.

With such illustrated improvement in frequency nadir for the single plant black start, we conduct a comprehensive analysis of stability performance across the stated four scenarios (Table 2-2) and ultracapacitor's f-Watt settings (Figure 10).

Four metrics (see Figure 13), namely frequency nadir, duration of frequency below 59 Hz, duration of frequency below 58 Hz, and 2% criteria of frequency settling, have been captured for each scenario and loading test. The most important metric, the frequency nadir, reflects the recommended protection settings. Duration of frequency below a certain value is the second most important metric that reflects the plant's under-frequency ride through capability. The third most important metric is the 2% settling criteria that showcases whether the islanded hydropower plant, gradually being loaded, can steadily maintain the islanded frequency at the nominal value. Given the plant is not tripped and able to ride through under-frequency excursions, the load carrying capability is determined by the maximum electric loading beyond which the islanded grid frequency does not settle within 2% of 60 Hz. In the upcoming subsections, we utilize these metrics to assess frequency stability and load restoration performance of the single and multi-plant configuration. We further utilize these metrics to investigate the effect of different hydrogovernor settings (including blade bias) on single plant black start.

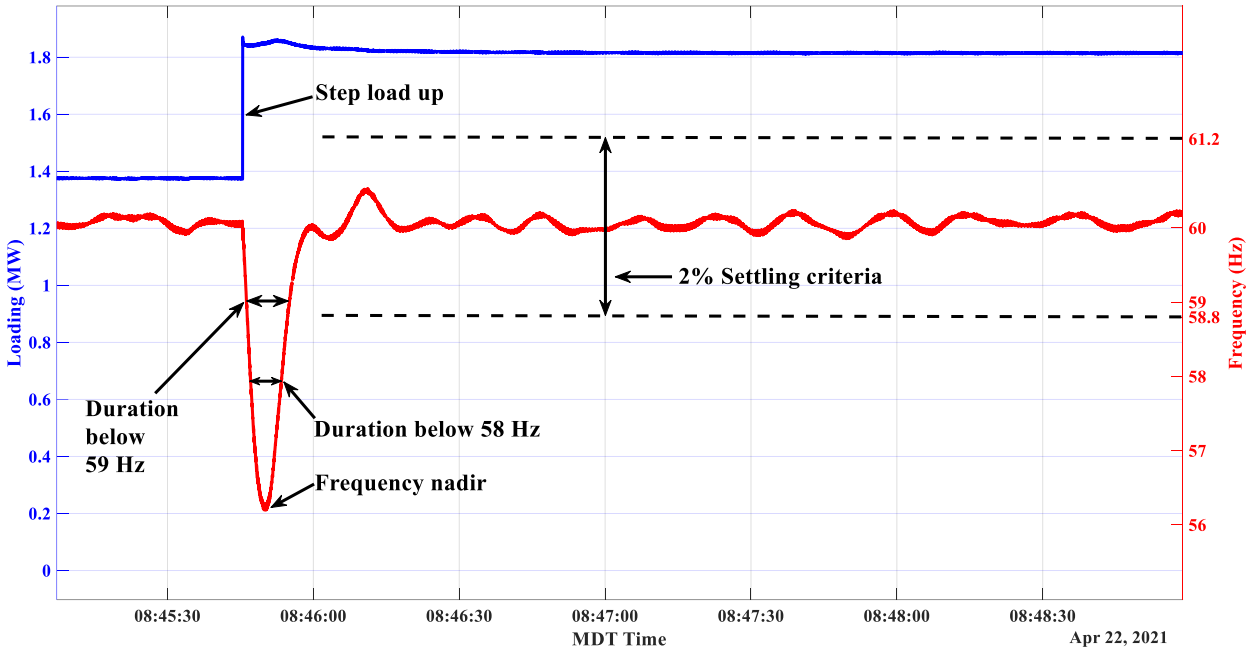

Figure 13. Illustrative definition of frequency stability metrics used in this section.

2.1 Single Plant Black Start: Frequency Nadir

It has been observed that active power injection from ultracapacitor improves frequency nadir while a single ROR unit (LB) is being loaded in step during the black start. Primary frequency response from a smaller hydropower unit (OL) also contributes to frequency nadir improvement. The best improvement in frequency nadir was observed when both the active power injection (from ultracapacitor with *narrower* f-Watt setting #2) and primary frequency response (from OL) supported the ROR unit (LB) during the black start (see Figure 14). With the increase in electric loading, however, a gradual drop in frequency nadir has been observed irrespective of generation and storage mix.

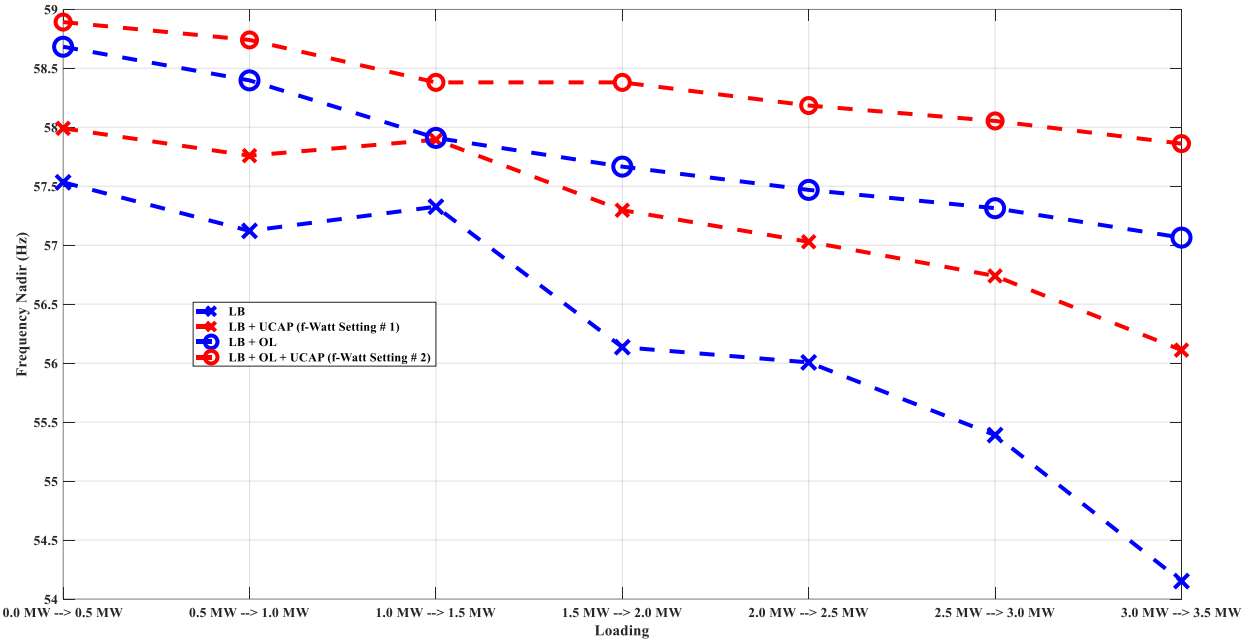

Figure Notes: LB is operating with original proportional-integral-differential ("PID") settings. OL is dispatching 810 kW (45% of one unit's capacity).

Figure 14. Integration of Old Lower Plant ("OL") and ultracapacitor ("UCAP") each improve LB frequency nadir.

2.2 Single Plant Black Start: Duration of Frequency Below 58 Hz and 59 Hz

The integration of ultracapacitor and OL has reduced the duration of frequency below 58 Hz in similar fashion. However, the duration below 59 Hz increased at high loading of LB + ultracapacitor system (see Figure 15). Following f-Watt setting # 1, the ultracapacitor's power injection cuts off near 58 Hz, apparently before the primary frequency response from the hydrogovernor settles the power imbalance. This results in the second dip in system frequency and causes longer duration below 59 Hz. With f-Watt setting # 2 (lower deadband at 59 Hz), however, the ultracapacitor power injection further reduced the duration below 59 Hz compared to the LB + OL system.

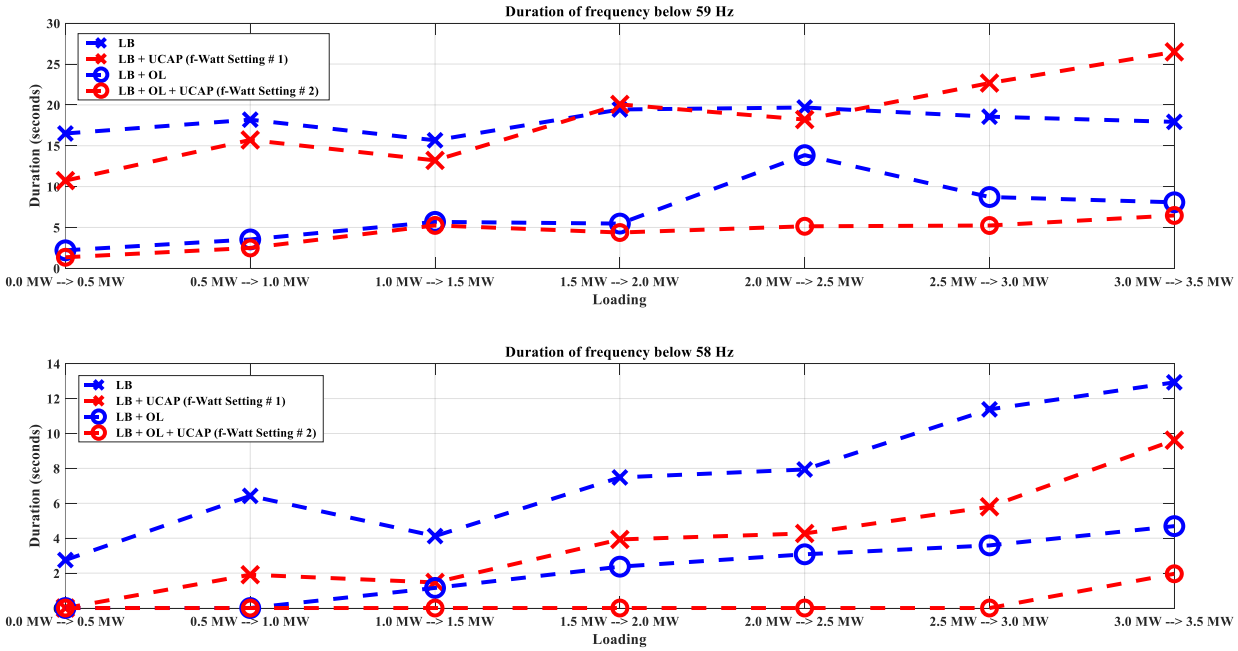

Figure Notes: LB is operating with original proportional-integral-differential ("PID") settings.

Figure 15. Integration of Old Lower Plant ("OL") and ultracapacitor ("UCAP") each reduce duration of frequency excursion for most experiments. LB is operating with original PID settings.

2.3 Single Plant Black Start: 2% Frequency Settling Criteria

For step load increase up to 3.5 MW, the frequency at the LB unit interconnection settled within 2% of 60 Hz after the primary frequency (i.e., hydrogovernor) response to each step load change. Beyond that, the 2% settling criteria was violated, setting the LB unit's load carrying capability to 3.5 MW (i.e., up to 39% of generation capacity). Increasing LB unit's load carrying capability up to 4 MW was achieved through either primary frequency support from the OL unit or LB unit's hydrogovernor settings adjustment and blade biasing. However, no additional improvements in load carrying capability were observed through ultracapacitor's (grid-following mode) active power injection.

2.4 Multi-Plant Black Start Demonstration

On the third day of the field demonstration, a multi-plant black start scenario was tested by running the OL, LB, and CB unit altogether. OL unit provided the primary frequency response as on the second day, and the CB unit shared the load with the LB unit. With gradual increase in CB unit's load share, the multi-plant configuration was initially able to support up to 7.5 MW (the 2% frequency settling criteria was violated at 8 MW). Further adjustment in the speed reference of CB unit's hydrogovernor helped to reach 8 MW—the maximum aggregate capacity of the rented load banks. For IFP, it was discovered that while a single ROR hydropower plant can support load restoration up to 34% of its capacity, two ROR hydropower plants, when combined, can raise that support at least to 50% of their total capacity. Although this speed reference adjustment approach increased the load restoration capacity, it lowered the frequency nadir. Integration of ultracapacitor ultimately improved the frequency nadir in this multi-plant black start scenario (see Figure 16).

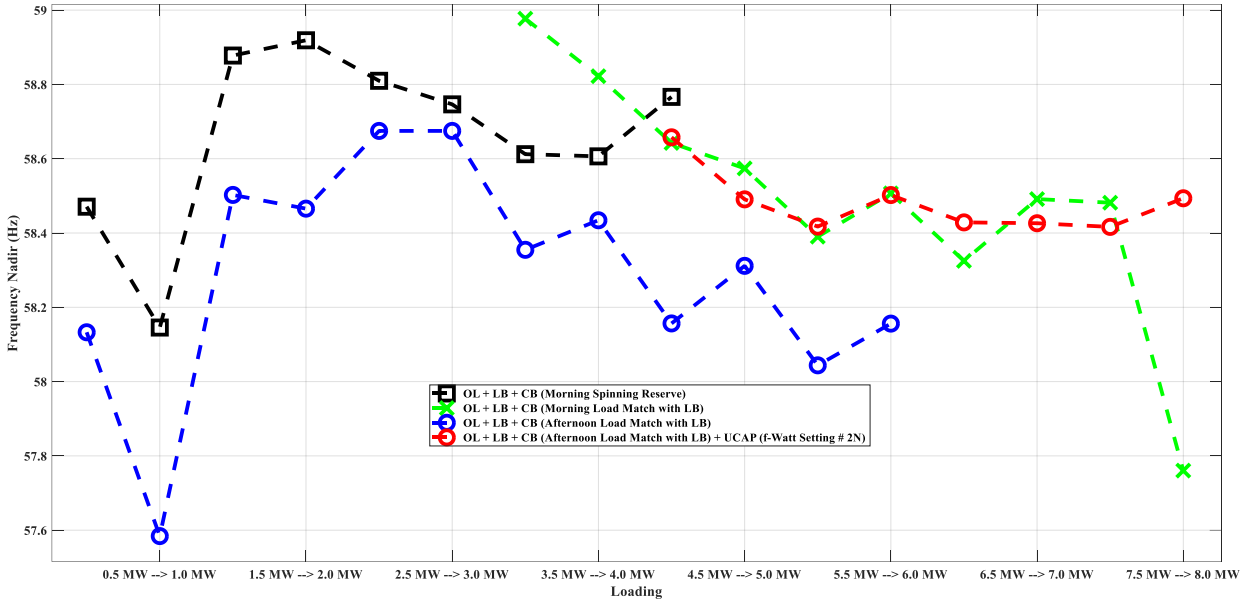

Figure Notes: LB is operating with original PID settings. The CB is set to spinning reserve by operating at speed reference of 100% in the morning. For the rest of the multi-plant black start test, CB's speed reference is adjusted to match its generation dispatch with that of LB.

Figure 16. Frequency nadir observed during the multi-plant black start scenario.

2.5 Impact Of Hydrogovernor Settings On Single Plant Black Start

The tests and observation mentioned above do not capture sensitivity to hydrogovernor settings and blade biasing of the LB unit. On the fourth day of the field demonstration, additional loading tests have been carried out on the LB unit with blade biasing (see Figure 17) and different hydrogovernor settings.

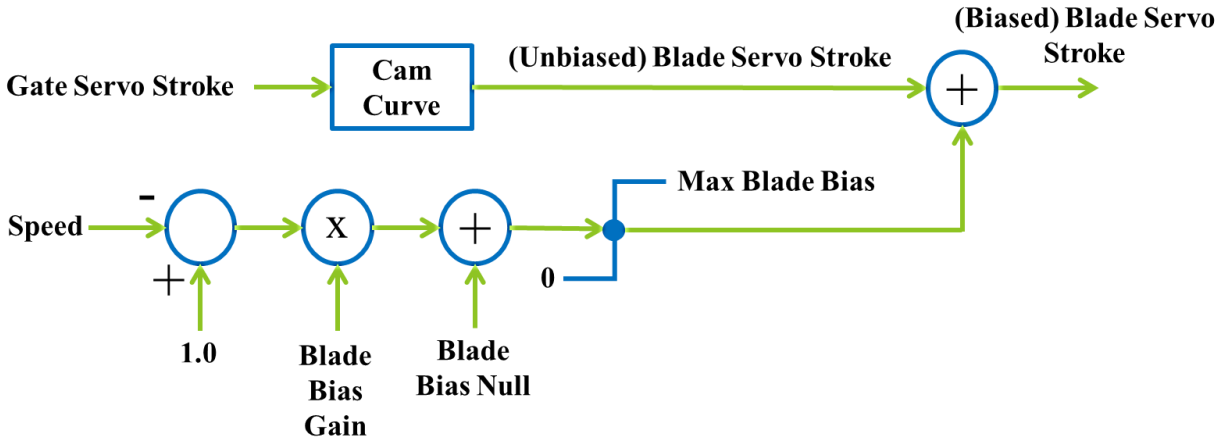

Figure Notes: The phrase "Cam Curve," which is commonly used in the hydropower industry, refers to the blade versus gate curve [44].

Figure 17. Control scheme with addition of blade servo stroke bias.

Given the step load change, it has been observed that blade bias can improve the frequency nadir but less significantly than with the ultracapacitor power injection. The best performance in frequency nadir,

however, comes through a combination of blade biasing, ultracapacitor power injection, an effective increase in integral (I) gain and reduction in proportional (P) and derivative (D) gain (see Figure 18).

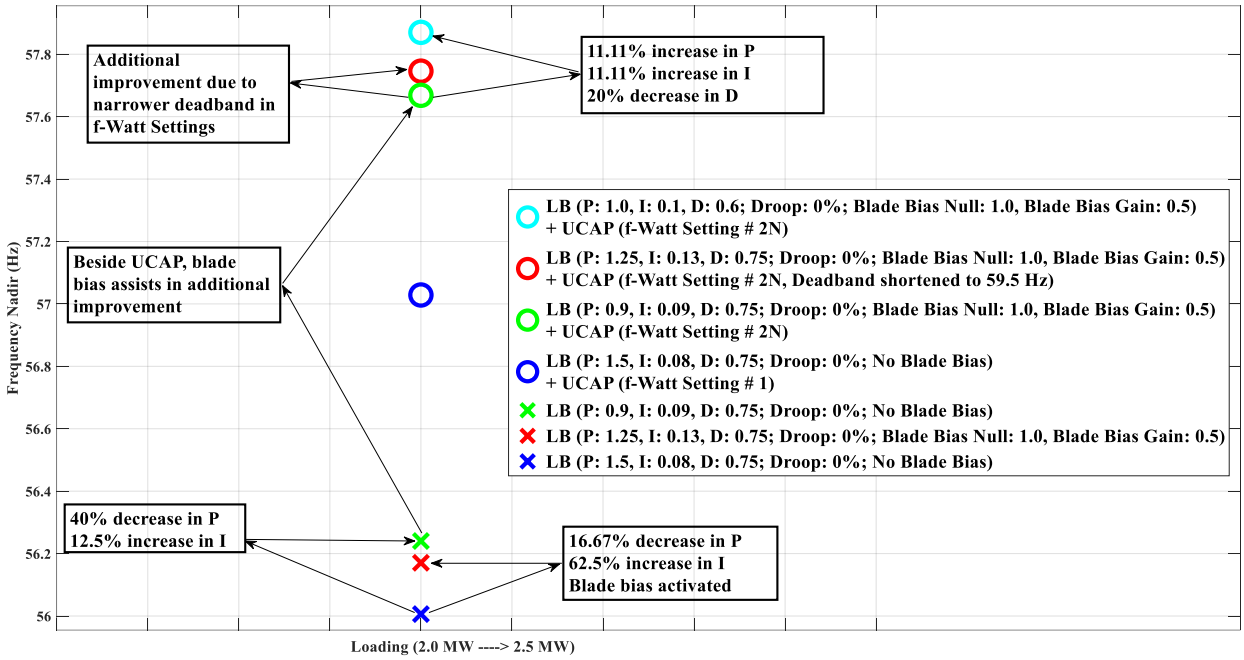

Figure 18. Frequency nadir sensitivity to hydrogovernor and storage settings. Integration of energy storage and activation of blade bias necessitates reduction in proportional and derivative gains and increase in integral gain.

Introducing the blade bias and hydrogovernor settings adjustment did not show a similar trend in reducing the duration of frequency either below 59 or 58 Hz, but ultracapacitor integration clearly reduced both these durations (see Figure 19). The LB unit and ultracapacitor settings for the best frequency nadir (see Figure 18), however, causes the longest duration of frequency below 59 Hz (see Figure 19). This reflects the “double dip” (see Figure 12 for example) caused by the DC under-voltage trip of the ultracapacitor and a direct consequence of a *narrower* f-Watt setting. Additional discussion on the effect of f-Watt settings on frequency stability can be found in Section 4.

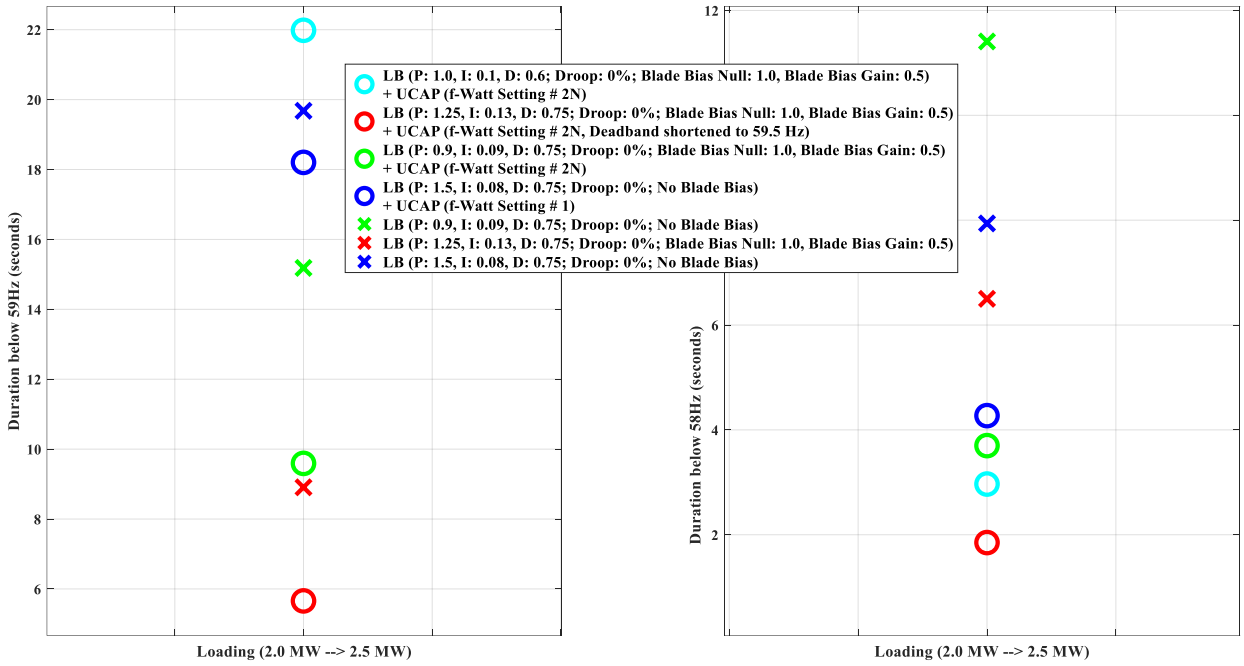

Figure 19. Duration below 59 Hz and 58 Hz sensitivity to hydrogovernor and storage settings.

The overall findings from this field demonstration are summarized in Table 2-3.

Table 2-3. Frequency stability metrics across different black start test scenarios.

Black start test scenario	Raise frequency nadir?	Reduce the frequency duration below 59 Hz?	Reduce the frequency duration below 58 Hz?	Enhance load carrying capability?
Isolated mode tuning of digital hydrogovernor control for single plant.	Yes—through blade biasing, effective increase in integral gain, and reduction in proportional and derivative gain.	Inconclusive.	Inconclusive.	No.
Single plant black start with ultracapacitor integration.	Yes—more significant contribution than that from isolation tuned hydrogovernor control.	Yes—through narrower deadband in ultracapacitor's f-Watt setting.	Yes.	No.
Multi-plant black start.	No.	Not investigated.	Not investigated.	Yes.
Multi-plant black start with ultracapacitor integration.	Yes.	Not investigated.	Not investigated.	Yes—improvement beyond just multi-plant contribution.

This field demonstration and associated frequency stability assessment do not involve IFP's entire distribution grid, the Upper Bulb, and Gem State hydropower plants. Furthermore, due to compact size, fast charging, and easy transportability, ultracapacitor has been used onsite with grid-following inverter configuration.

In the next section, we present multi-plant black start simulation for IFP's entire distribution grid utilizing all its hydropower fleet and a battery model with GFM inverter configuration.

3. MULTI-PLANT BLACK START SIMULATION FOR IDAHO FALLS POWER

Key Takeaways:

- Black start of Idaho Falls Power's distribution grid is simulated on a computer-based transient simulation platform. The simulation included dynamic models of the utility's entire hydropower fleet. Model of grid-forming inverter with battery storage is also included to simulate inrush current support.
- Battery storage located near the load center mitigates frequency oscillations during distribution grid black start.
- Battery capacity (MW) needed during distribution grid black start can be reduced through pre-synchronization of utility's hydropower fleet with the battery storage.
- Battery storage with grid-forming inverter enhances electric loading capability during multi-plant distribution grid black start.

The IFP grid consists of approximately 38 miles of high-voltage (161 and 46 kV) transmission facilities and over 400 miles of distribution facilities that operate at voltages ranging from 2.4 kV to 12.47 kV. The system currently includes 11 substations among which the Westside and Sugar Mill substation receives purchased power from the PacifiCorp (Rocky Mountain Power) via the Goshen substation and over the 161 kV lines [35], [37]. IFP's hydropower fleet is connected to the 46 kV transmission loop. The multi-plant black start capability for this distribution grid has been further investigated by considering its topology, load distribution, and integrating a battery with GFM inverter configuration. For this purpose, the model of IFP grid was converted to power systems computer-aided design (PSCAD) [44] from the original IFP system model developed in Milsoft [45].

The PSCAD model of IFP grid includes 161, 46, 12.5, 13.8, 4.16, and 2.4 kV circuits with loads connected to respective substations (see Figure 20). Existing IFP circuit breakers are included in the model, so it can be reconfigured to accommodate black start and load energizing for any desired scenario. The protection settings and protection coordination are not included in the model. The model of the IFP system was disconnected from 161 kV tie lines to island it from the Goshen substation and to simulate multi-plant black start. All of IFP's ROR hydropower plants are modeled in PSCAD based on the respective Simulink model [41]. These hydropower models are also equipped with synchronizing relays for the multi-plant black start simulation.

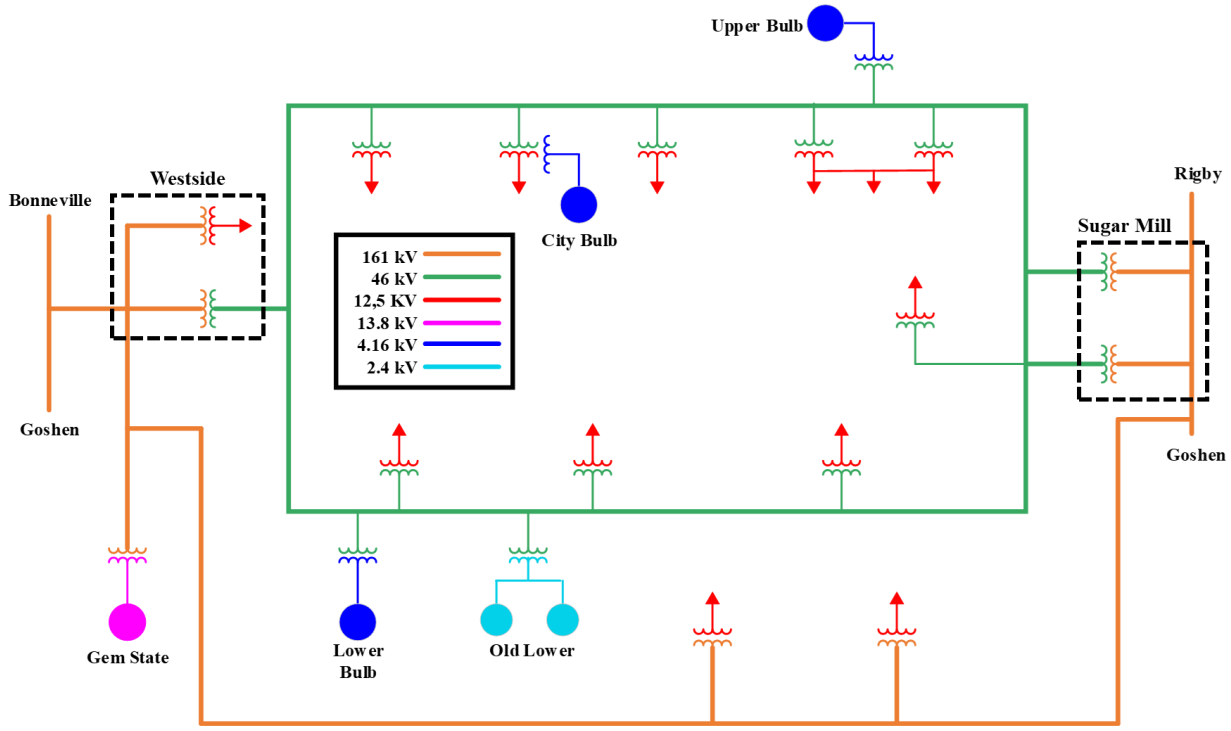

Figure 20. One line diagram of IFP grid.

There is about 94.5 MW of aggregate load connected to IFP's 46kV system distributed among nine substations (see Table 3-1).

Table 3-1. IFP 46 kV loads.

Substation	Real (MW)	Reactive (MVAR)
Rack	10.279	1.592
Milligan	9.799	1.717
Fifteenth	14.57	2.263
North Boulevard 2	6.77	1.901
North Boulevard	9.813	1.659
Sugar Mill	11.717	1.581
City	8.39	1.575
Temple View	9.101	1.327
Hatch	13.95	1.827
Total	**94.5**	**15.5**

Data shown in Table 3-1 is calculated from the IFP model with following assumptions:

- Reactive load is net load considering losses and charging VAR (volt-ampere reactive) (no capacitor banks are present in the IFP system)
- Capacity of ROR hydropower fleet is about one-third of total 46 kV load

- Combined capacity of ROR hydropower fleet and Gem State plant accounts for ~58% of total load.

Since IFP's local hydro-generation is smaller than load, only a portion of city loads can be using hydro resources during black start and islanded operation. Therefore, critical and high-priority loads need to be included into restoration plan.

One important aspect of black start when energizing all reactive components in the islanded grid, such as transformers and transmission lines, is the issue of inrush currents. Some of modern GFM battery inverters (such as SMA [System, Mess, and Anlagentechnik] inverters) can provide voltage ramping (or soft start). One example of tested voltage ramping is shown in Figure 21 using National Renewable Energy Laboratory's 1 MW battery. The lower plot in Figure 21 shows inverter-measured inrush currents when energizing 1/1 MVA transformer. The measured current in this case is only 2% of full inrush current that this transformer will consume during hard start. The same soft-start strategy is selected for GFM inverter in simulation using IFP model as well.

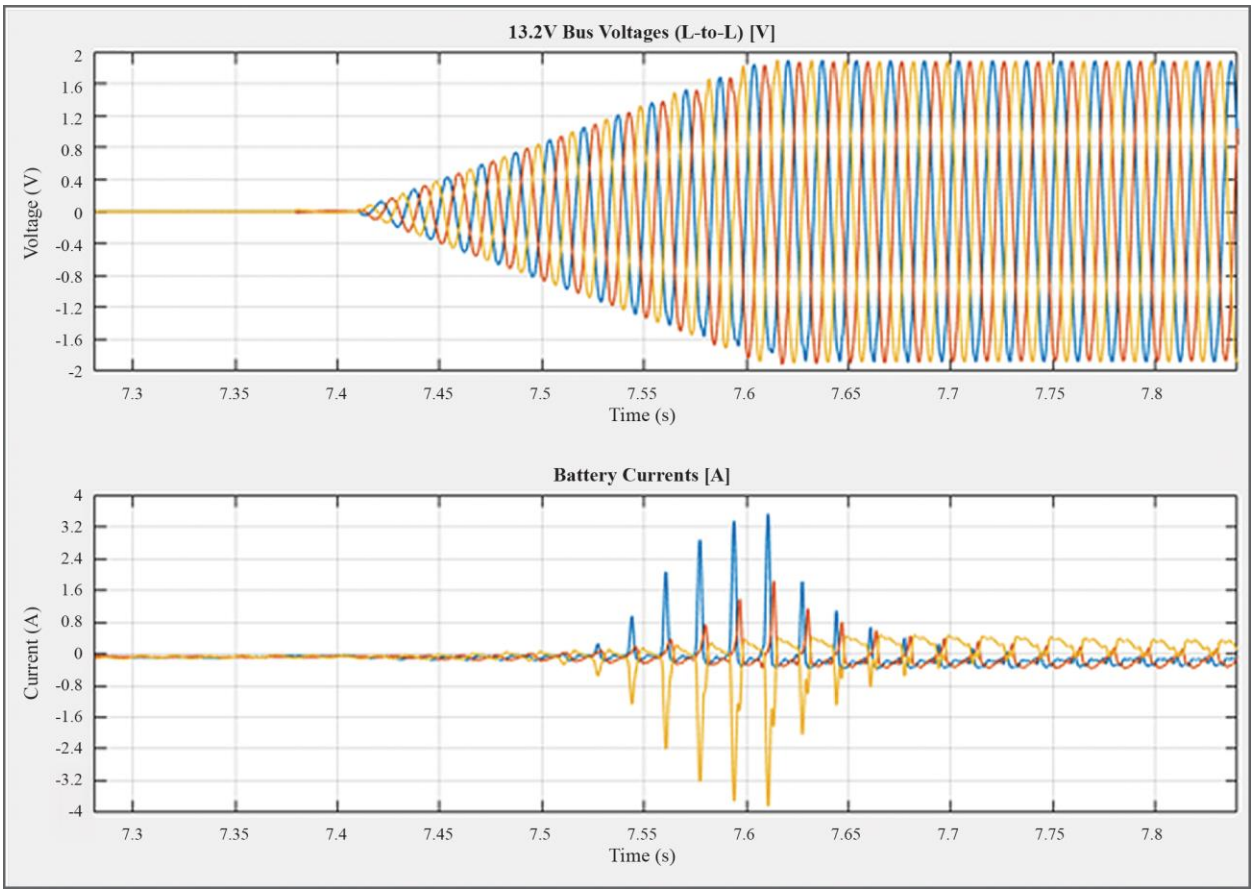

Figure 21. Battery soft start (measured at National Renewable Energy Laboratory's test site). Upper plot shows voltage ramp during GFM Battery Energy Storage System (BESS) inverter soft start. Bottom plot shows the transformer inrush current peaking at only 3% of transformer rating.

For multi-plant black start simulation, the following strategy is implemented:

1. GFM battery with current limiting control is set to soft-start mode (battery is operating with 5% f-Watt and 5% V-VAR droops).
2. All load circuit breakers are open.

3. Then some circuit breakers are configured to provide a path from GFM battery with soft start to energize the power lines and transformers of hydropower plants with minimum inrush currents, so the current limit of the battery inverter is not exceeded.
4. The battery is commanded to ramp up its 60 Hz voltage from zero to full voltage in 1 s energizing lines and transformers, so each IFP hydropower plant has energized transformer.
5. One IFP hydro plant at the time is started and synchronized with battery voltage.
6. After plant synchronization is complete, the hydropower plant is controlled to produce power by adjusting positions of the wicked gates and runner blades. The plant starts producing power that is fully absorbed by battery (charging mode).
7. Next, a high-priority load feeder is energized, and battery power goes back to zero.

Steps 6 and 7 are repeated until all hydropower plants are generating, and the full-size island is formed. GFM battery remains online providing generation-load balance during load changes and stable system operation. The IFP system has big load segments after each circuit breaker. Therefore, the battery capacity is chosen to be 10 MW for extreme load steps and sited at two locations to simulate multi-plant black start.

3.1 Battery Co-Located with Lower Bulb Plant

In the first case, the 10 MW battery is located near the LB plant and connected to 46 kV line via step-up transformer (see Figure 22). At the beginning of simulation, all loads are disconnected. Some circuit breakers in 46 kV system and 161 kV line are closed to provide single paths from the battery to the transformers of all hydropower plants. At t = 0 s, the GFM battery starts ramping its 60 Hz voltage energizing few segments of the 46 kV and 161 kV systems (upper plot in Figure 22). This is happening without any significant inrush current as can be seen in Figure 24 (battery current). Shortly after this, the generator at the LB plant is synchronized with the voltage formed by battery. At t = 7 s, the LB plant is controlled to produce 5 MW of power which is momentarily absorbed by the grid-forming battery. This operation brings the LB plant online with desired capacity of loading with no violation in transients. At t =10 s, a 5 MW segment of load is energized, so the grid-forming battery stops charging and dampens the resulting frequency transients. In a similar manner, all other plants (City Bulb, Upper Bulb, and Gem State) are operated until about 24 MW of city loads are energized.

Throughout this process, the state of charge of the battery needs to be below 50% to support the instance of individual plant interconnection. To demonstrate the stabilizing effect of GFM battery at t = 42 s, the battery that was discharging at about 1.4 MW is disconnected from the circuit. Immediately after, all generators start decelerating causing a large frequency dip to 58.7 Hz (lower plot in Figure 22). However, in the presence of GFM battery, the system frequency remains more stable with much smaller deviations from nominal (a zoomed in view of one load step change is shown in Figure 23). Battery current stays below rated during all stages of operation (upper plot in Figure 24). Notice the frequency overshoot and spikes in Gem State generation profile. These are caused by changes in frequency by GFM battery which in turn is caused by step changes in load since GFM battery controls its power by adjusting the phase angle causing system frequency to change, and generator speeds are following the frequency. It is important to note that BESS output frequency is measured using phase-locked loop (PLL). Speeds of generators are converted into frequency for easy comparison and are shown on the same plot. Voltages in all buses remain stable within acceptable limits (less than 2% deviation) during all stages of system black start.

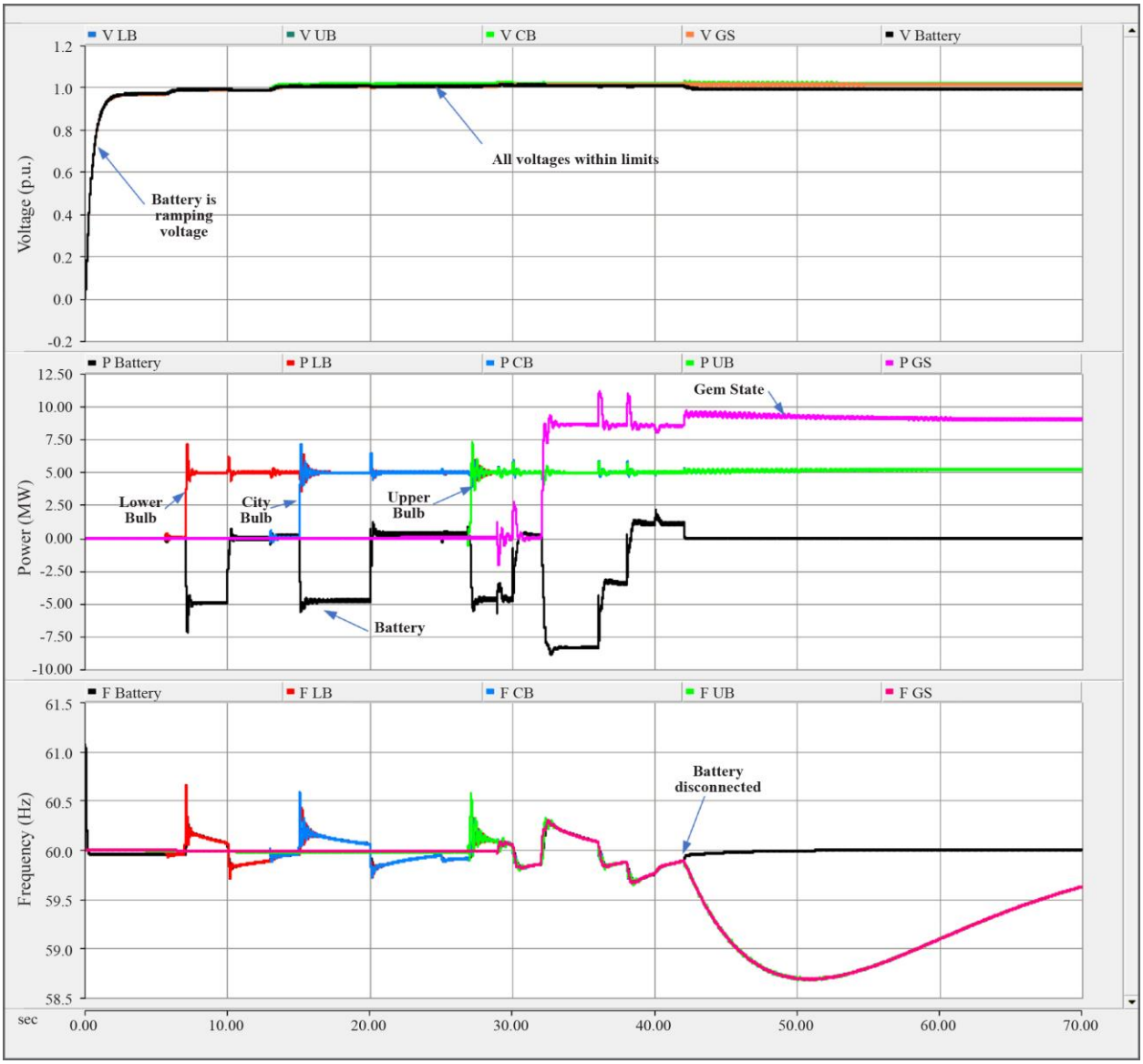

Figure 22. Multi-plant black start simulation for scenario in which battery is co-located with LB plant.

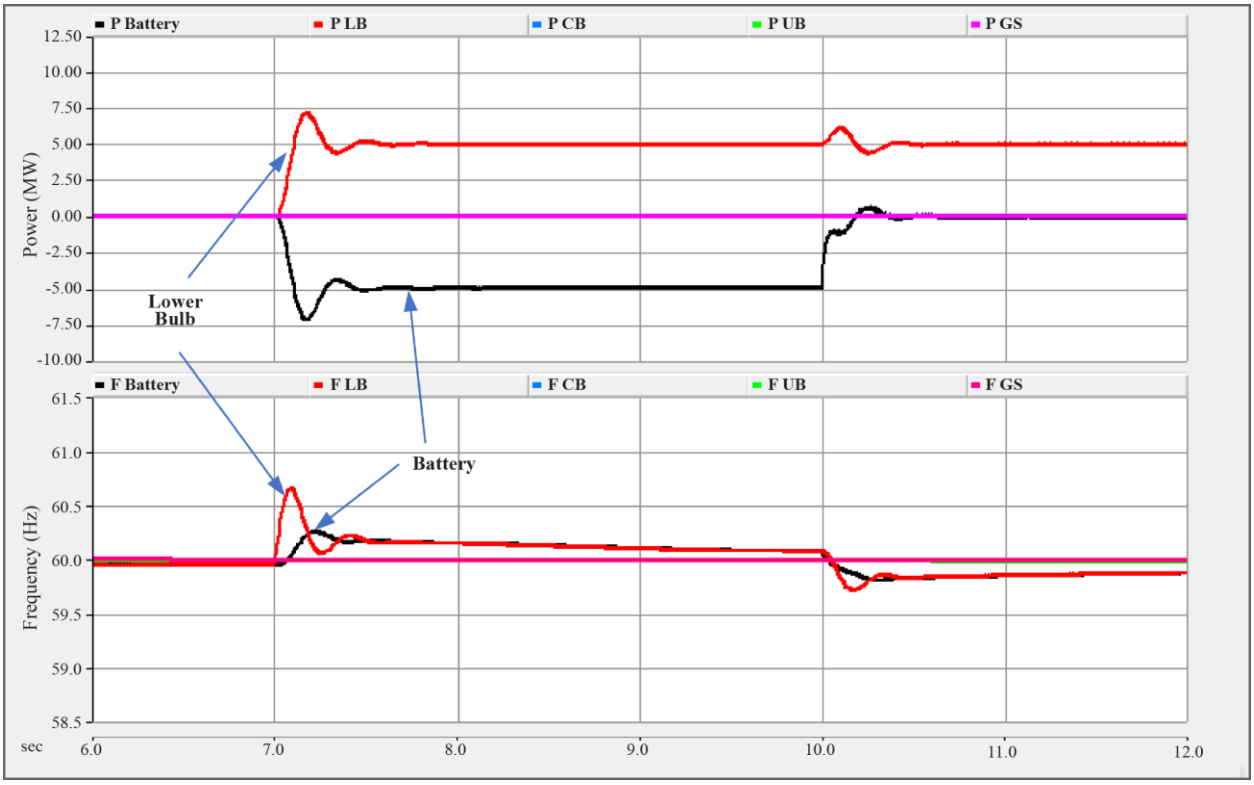

Figure 23. Enlarged view of electric loading for scenario in which battery is co-located with LB plant.

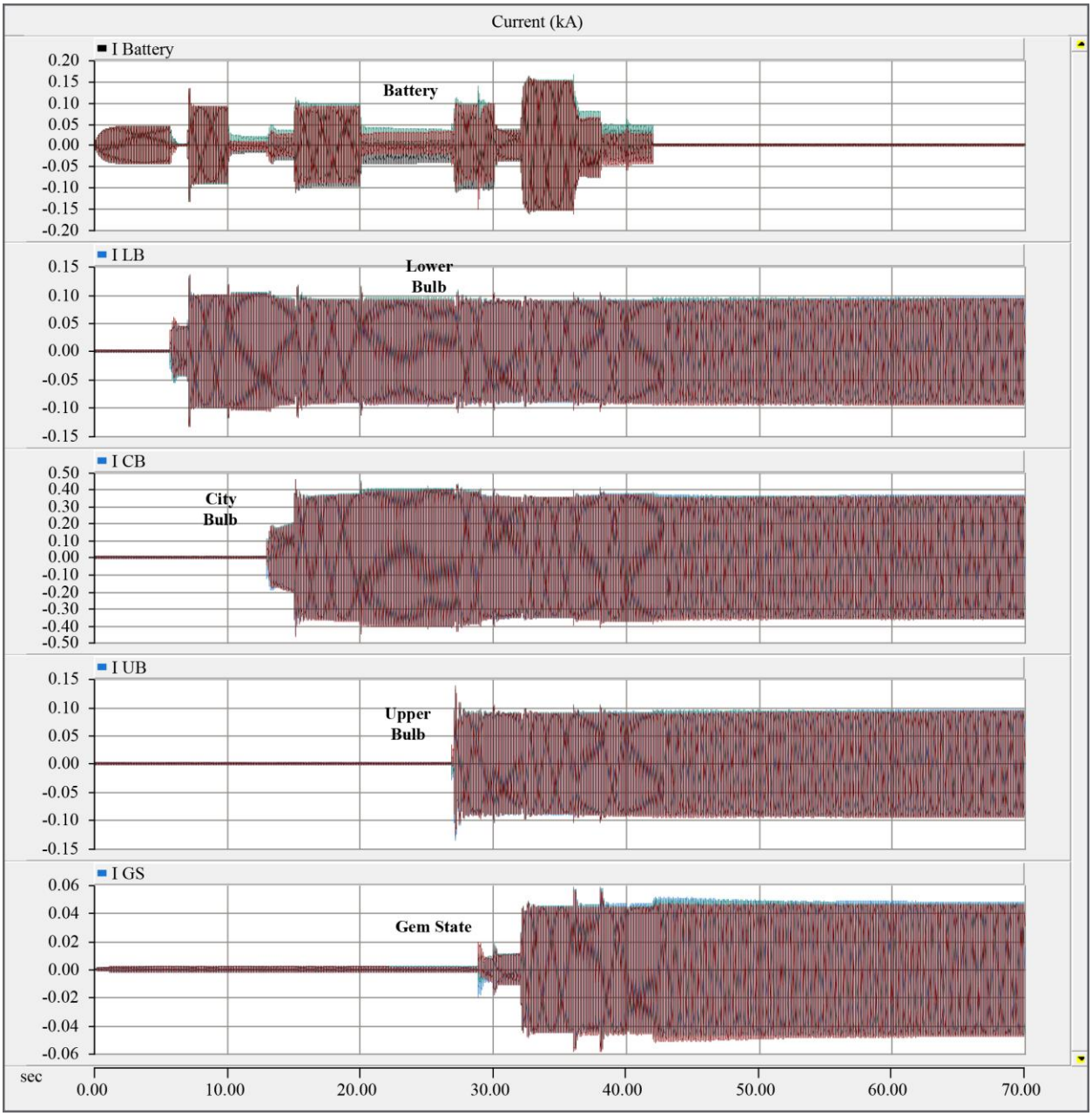

Figure 24. Instantaneous currents from individual hydropower plants and battery during multi-plant black start simulation for scenario in which battery is co-located with LB plant.

3.2 Battery Co-Located with Gem State Plant

In the second case, the 10 MW battery is located near the Gem State plant and connected to 161 kV line via step-up transformer. The sequence of system start operations is the same as in previous case. Except in this case, the Gem State plant starts first at t = 5 s (see Figure 25). At each step of black start, the battery acts as a load for hydro-generators, keeping the system frequency stable (lower plot in Figure 25). The battery current is below rated value during all steps (see Figure 26), and a load of 23.75 MW is being served. Some oscillations in generator speeds are observed after each load step but get dampened quickly (see Figure 27). These oscillations are caused by the larger impedance between Gem State plant and city loads. In the event of battery disconnection, however, a higher frequency nadir of 59.87 Hz (it

was 58.7 Hz for battery co-located with LB plant) is observed thanks to larger inertia of the Gem State plant. After black start is completed, the battery will continue supporting stable operation by balancing the system during load variations. Also, all hydro-generators have headroom to increase their production if more loads need to be energized.

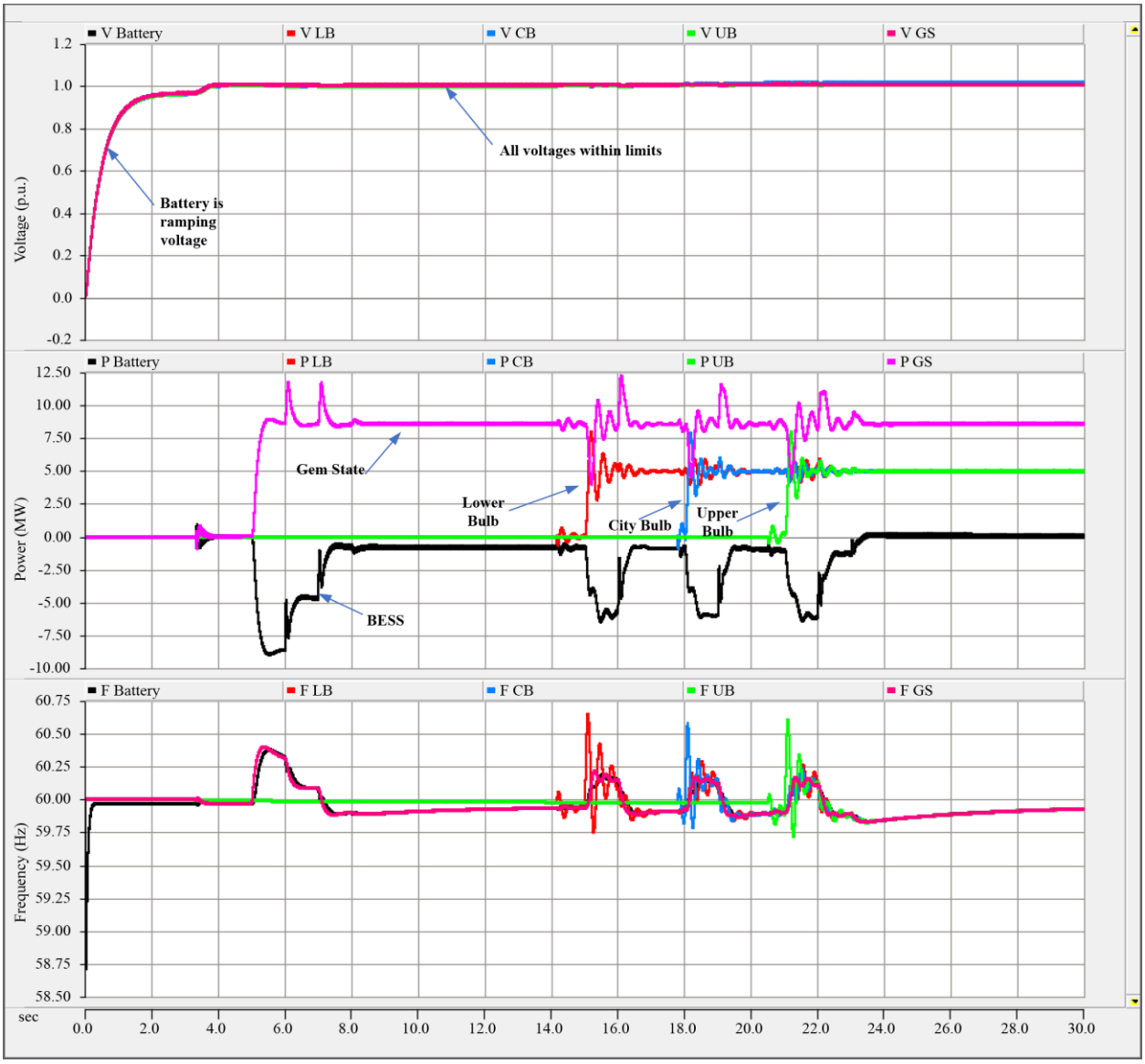

Figure 25. Multi-plant black start simulation for scenario in which battery is co-located with Gem State plant.

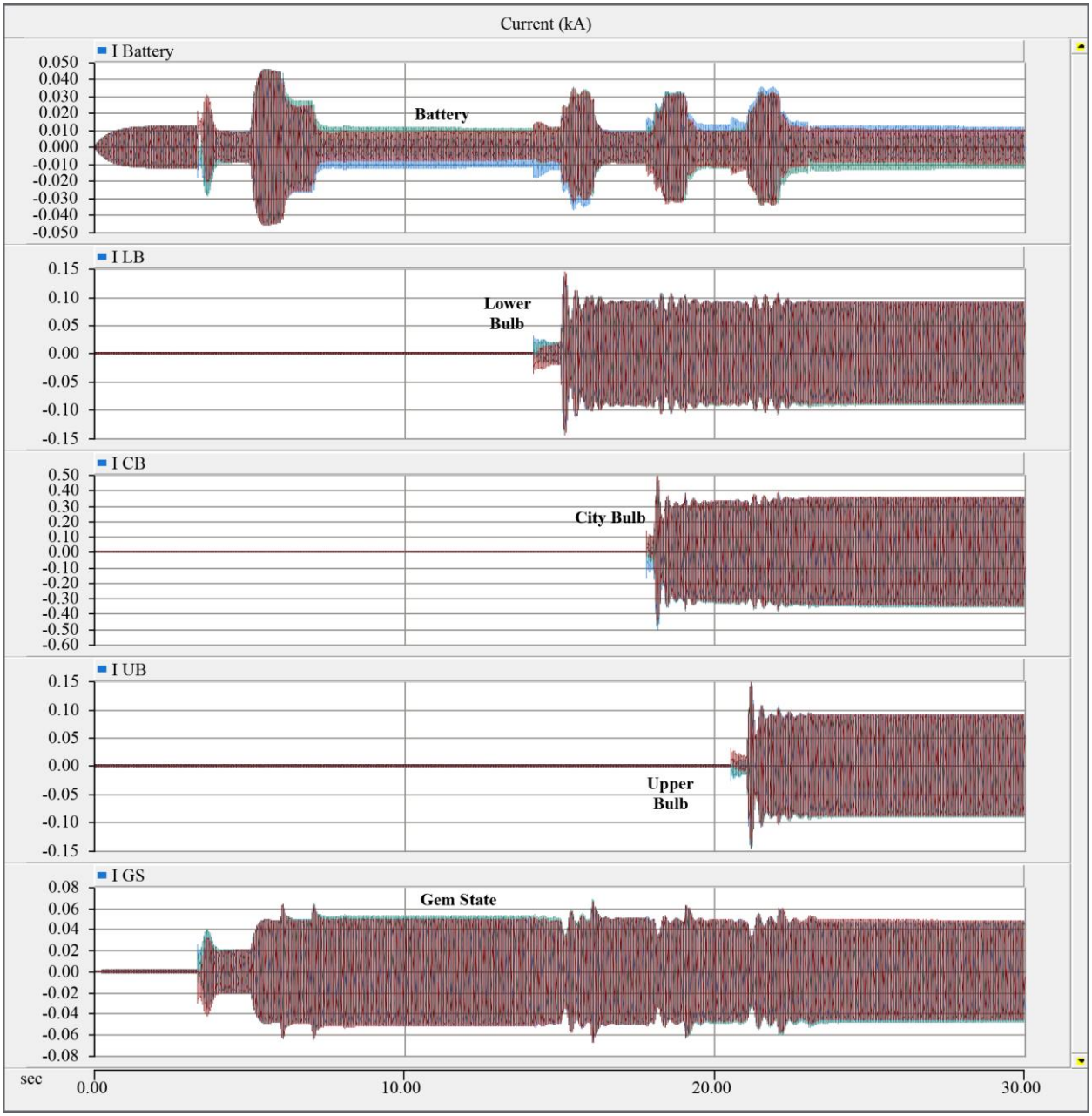

Figure 26. Instantaneous currents from individual hydropower plants and battery during multi-plant black start simulation for scenario in which battery is co-located with Gem State plant.

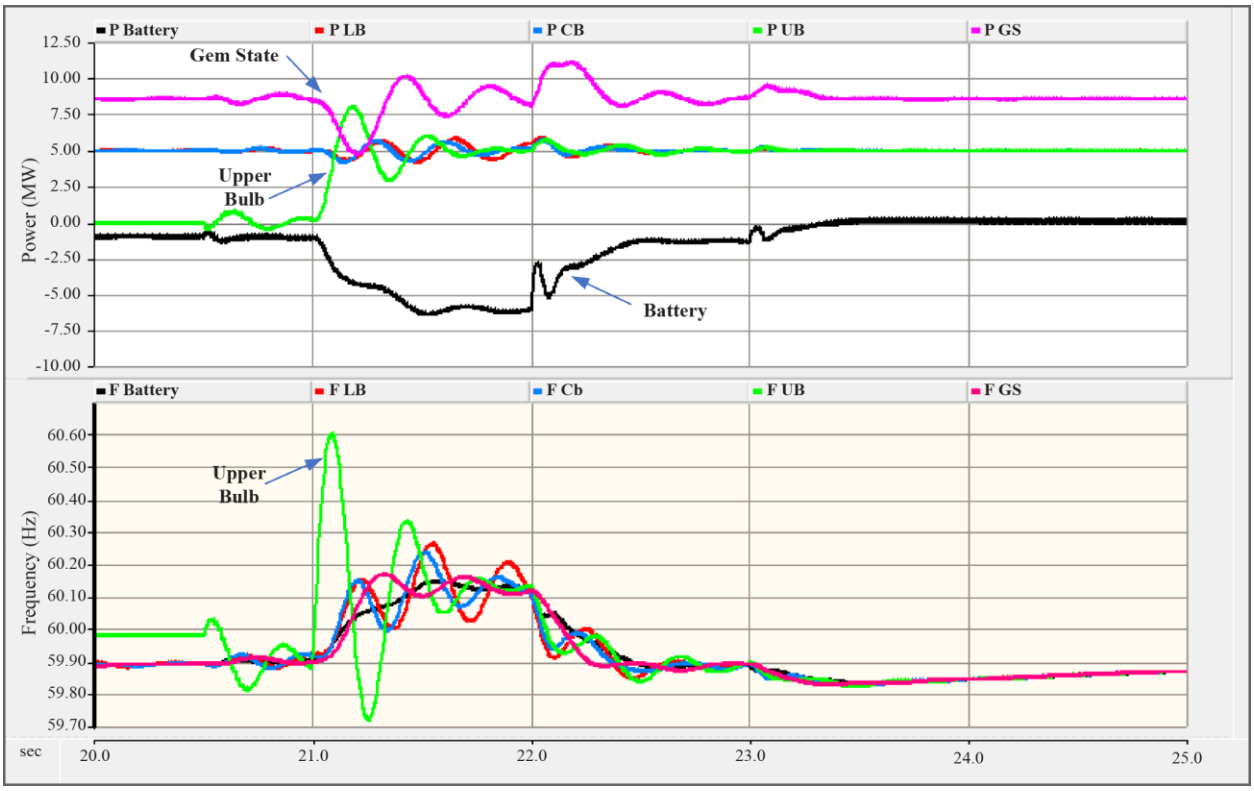

Figure 27. Oscillation of electric power and frequency during step load increase during multi-plant black start simulation for scenario in which battery is co-located with Gem State plant.

3.3 All Hydropower Plants Pre-Synchronize with Battery

The above described simulation results demonstrate that 10 MW GFM battery is more than sufficient to perform stable black start and islanded operation for a portion of IFP loads. More advanced start-up methods are possible if power control in each generator is coordinated with load increase. In such cases, the required battery power capacity can be significantly lower. One such hypothetical case is shown in Figure 28. All generators synchronize to GFM battery at t = 3.5 s. At t = 7 s, the Gem State generator is controlled to bring wicked gates and runner blades to the position corresponding to 7 MW load level. At the same time, one 8.75 MW feeder is switched on. The generator power ramps up to 8.75 MW. In the process, the battery injects power keeping the system in balance. The same is repeated for all remaining hydro plants serving a total load of 22 MW. If this approach is possible at all, it will end up with the battery discharge not exceeding 2 MW during the step load increase—a significant reduction in the required battery power rating.

In all the above cases, we assumed the most extreme scenarios with very large load steps to demonstrate the concept. The sizes of load steps were selected based on capacities of individual feeders in each substation. In some cases, it may be possible to implement even finer load steps causing less transient behavior and decreasing the size of required storage. In this study, we have demonstrated the black start process for a municipal grid with most extreme scenarios to demonstrate the benefits of GFM battery in the black start process.

Based on the findings from the black start field demonstration (Section 2) and DGBS simulation (Section 3), it is evident that energy storage can play a vital role in maintaining islanded grid frequency and voltage profile within acceptable range during black start of small hydropower plants and load restoration. These are primarily achieved through frequency-droop-based active power response from

grid-following inverter (black start field demonstration) and voltage-droop-based reactive power response from GFM inverter (black start simulation). However, it is important to understand how any variation across these control strategies impacts the energy storage size, inverter capacity, and any other operational tradeoffs. In the next section, we investigate these sensitivities.

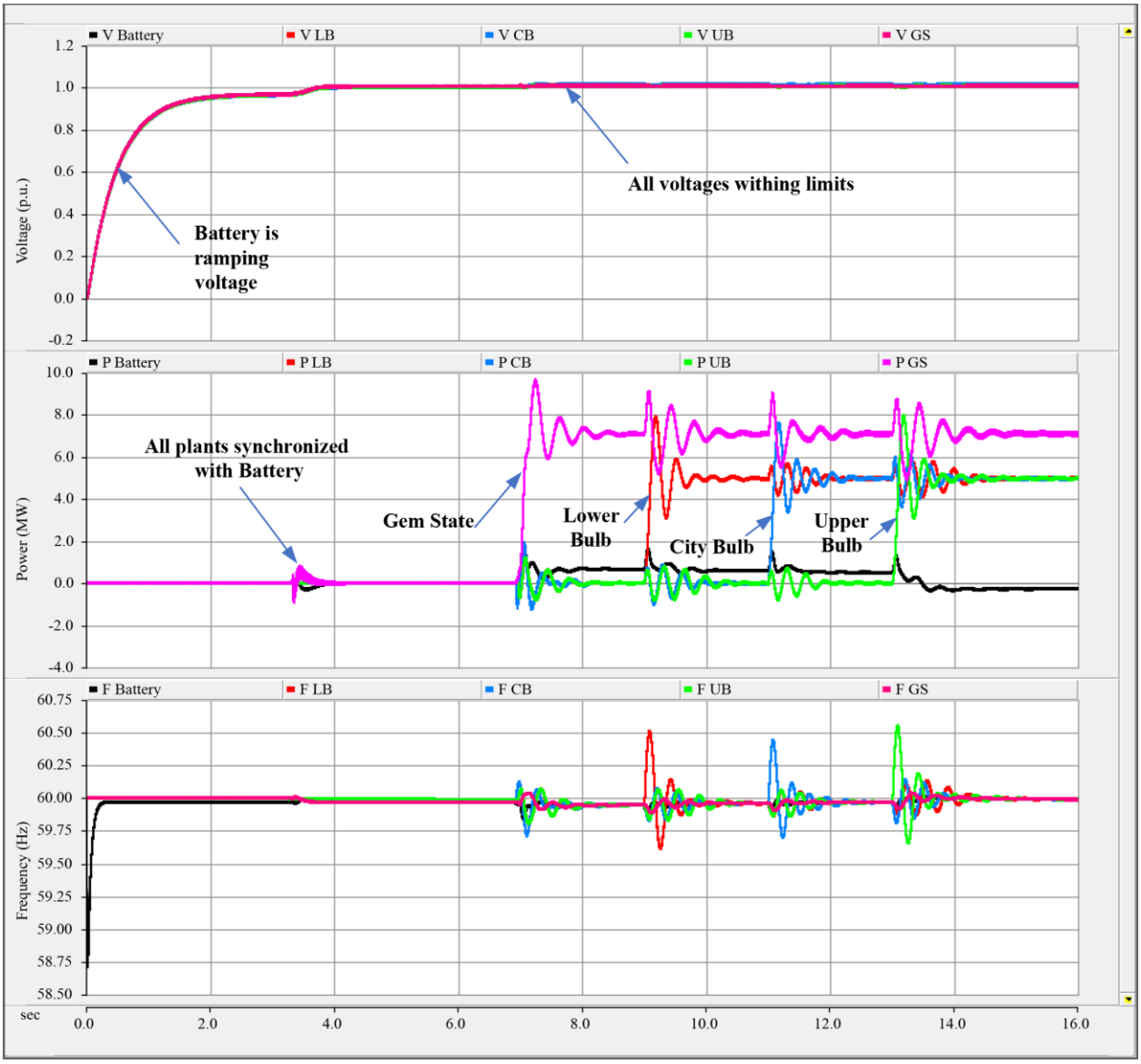

Figure 28. Multi-plant black start using coordination between hydropower plant control and load step changes.

4. IMPACTS OF ENERGY STORAGE SYSTEM SIZING AND CONTROL ON FREQUENCY STABILITY

Key Takeaways:

- Electric loading of an islanded run-of-river hydropower plant and associated transients are simulated on a computer-based transient simulation platform. The simulation included dynamic model of Idaho Falls Power's Lower Bulb hydropower plant. Model of grid-following inverter with ultracapacitor is also included to simulate frequency droop based active power support.
- The simulation is run across the variation of different parameters: (1) ultracapacitor size (in capacitance, F), (2) inverter capacity (in kVA), (3) deadband in inverter's frequency-Watt settings, and (4) slope of inverter's frequency-Watt settings.
- From the transient simulations, frequency stabilities are assessed in terms of frequency nadir and multiple frequency dips. Impact on ultracapacitor is assessed through state of charge.
- Selection of energy storage size, inverter capacity, and control strategy needs to address the tradeoff among frequency stability requirement, storage status, and cost.

We have observed the tradeoff between frequency stability improvement and the state of charge (SoC) of the energy storage (Sections 2 and 3). For example, narrower deadband in the f-Watt setting or GFM operation can accelerate decline in the SoC causing double dips (Section 2) and risking the synchronization of multiple hydropower plants (Section 3).

This section reports the alternative simulation-based studies to determine the impact of storage (ultracapacitor) sizing, grid-following inverter capacity, and frequency (f)-Watt droop settings used to make fast frequency response during black start of a ROR hydropower plant. Multiple scenarios, as discussed in Appendix B, are simulated to help draw conclusions on the impact of various parameters, including ultracapacitor sizing and f-Watt settings on the overall frequency response. The ultracapacitor used in the field demonstration has a capacitance of 6.5 F with a grid-following inverter capacity of 375 kVA. The DC operating voltage of the inverter used is 950 ~ 650 Vdc. However, for the simulation, no restriction has been applied to DC cutoff voltage. Furthermore, the following attributes are considered for each of the design and control parameters that might have an impact on frequency response during black start performance:

- Ultracapacitor size: 6.5 F, 13 F
- Inverter capacity: 375 kVA, 2 x 375 kVA
- f-Watt settings
    - dP/df: steep, gentle
    - Deadband: wide, narrow.

These additional features in f-Watt settings are illustrated in Figure 29 through settings #3–5. Settings #1, 2 from Figure 10 are also shown in Figure 29 and used in the frequency response impact analysis.

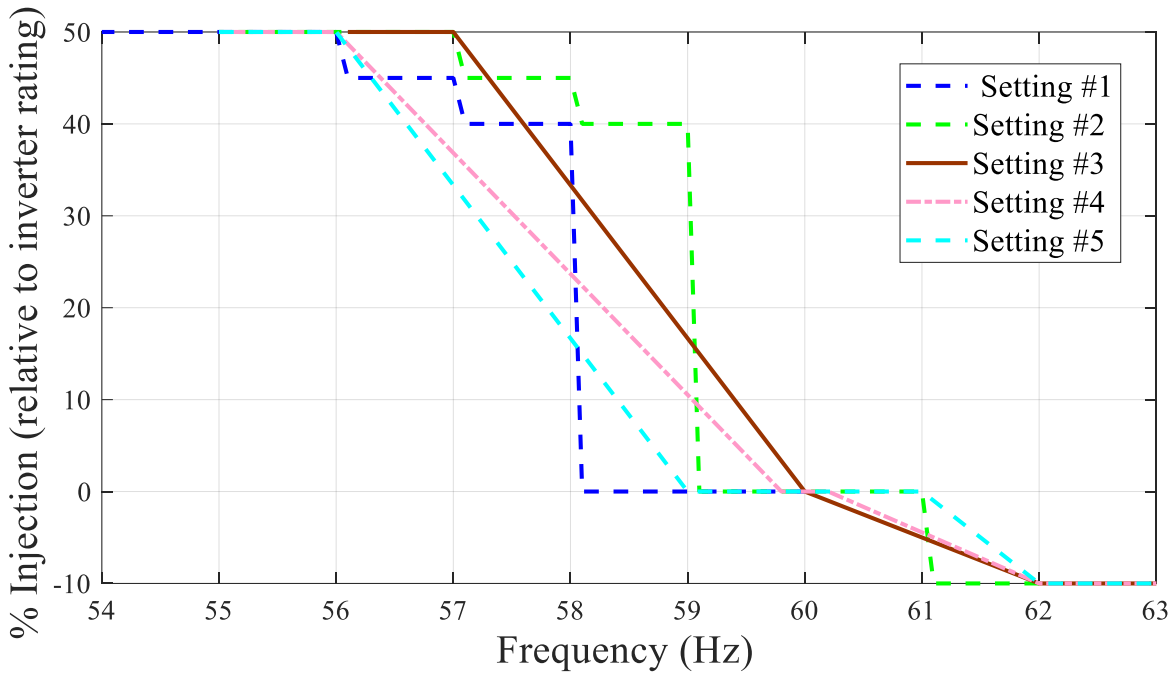

Figure 29. f-Watt settings used for testing the efficacy of ultracapacitor in frequency recovery.

The following variables of interest and their corresponding metrics are monitored and analyzed to determine how the parameters discussed above impacts black start performance:

- Ultracapacitor SoC profiles
- Frequency nadir improvement
- Presence of multiple frequency dips.

Based on the simulation studies performed (details provided in Appendix B), sensitivity of frequency stability to storage sizing, and f-Watt settings can be summarized (see Figure 30). It can be observed that an increase in storage size, for a given f-Watt setting, has an overall positive impact on reducing the second frequency dips during black start. However, with increased storage size, the cost of the system goes up. This means a right balance between the storage size and the f-Watt settings is required to optimize both the frequency response performance and the cost of the system.

It can also be observed, that for a given storage size and f-Watt settings, increment in inverter rating can have a negative impact on both the second frequency dip in the system and the overall cost but can also have a positive impact on the frequency nadir improvement. The frequency nadir improvement can be attributed to the early supply of a large burst of power as soon as drop in frequency is observed.

From the simulation studies, it can also be seen that the wider deadband used in the f-Watt settings lowers the possibility of second frequency dips and preserves the SoC of the storage. However, the larger deadband used in the f-Watt settings would lead to poorer frequency response since the frequency nadir following the addition of loads in the system is not improved as much when compared to a setting with narrower deadband. Some key simulation results based on the different scenarios considered are summarized next.

Inverter		
Cause	**Attribute**	**Effect**
Increase capacity	Frequency nadir	↑
	Multiple frequency dips	✓
	State of charge	↓
	Cost	↑
Widen deadband	Frequency nadir	↓
	Multiple frequency dips	X
	State of charge	↑
	Cost	None
Gentler dP/df	Frequency nadir	↓
	Multiple frequency dips	None
	State of charge	↑
	Cost	None

Energy Storage		
Cause	**Attribute**	**Effect**
Increase size	Frequency nadir	None
	Multiple frequency dips	X
	State of charge	↑
	Cost	↑

↑	Improves, sustains
↓	Degrades
↑	Undesired increase
✓	Undesired presence
X	Absent as desired

Figure 30. Storage size, inverter capacity, and control settings each impact frequency stability performance, SoC, and cost.

Frequency stability with support from storage devices like UCAP is dependent on both the f-Watt setting and the storage sizing (see Figure 32). Figure 31 shows that with the increase in inverter rating along with the ultracapacitor size, the frequency response of the system (frequency nadir) improves as soon as a disturbance occurs; however, if the energy storage device does not have enough stored energy, there can be a possibility of second dip in system frequency, depending on the system inertia and hydrogovernor's frequency response. A gentler slope in dP/df of f-Watt setting #2 removes the second frequency dips across different inverter capacities and ultracapacitor sizes at the cost of lower frequency nadir (see Figure 32).

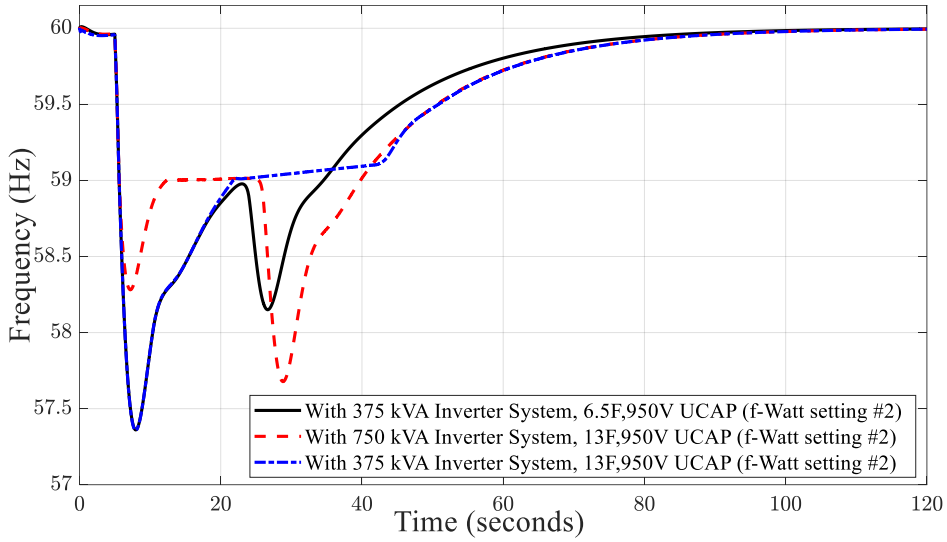

Figure 31. Comparison of system frequency response for different inverter and ultracapacitor ("UCAP") configurations using same f-Watt setting (setting #2).

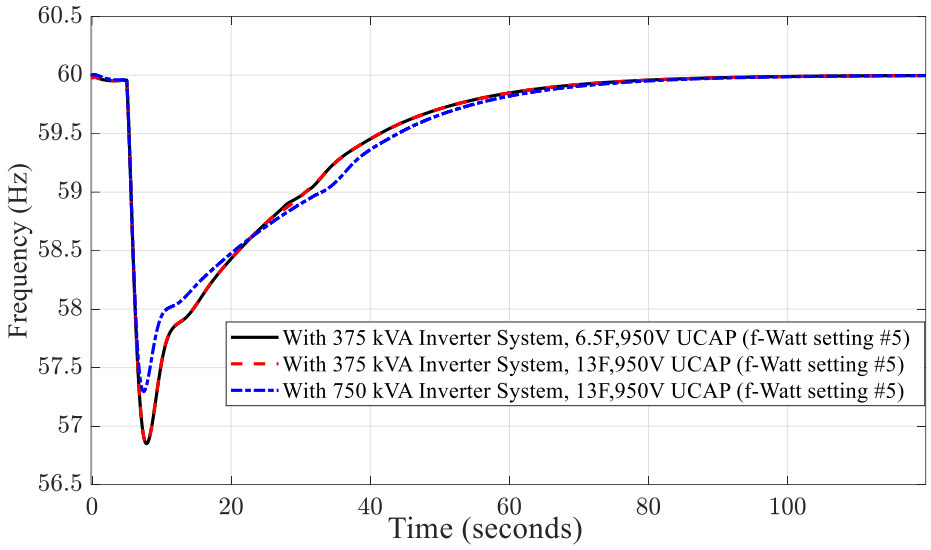

Figure 32. Comparison of system frequency response for different inverter and ultracapacitor ("UCAP") configuration using same f-Watt settings (setting #5).

These results also show that the optimum storage configuration and setting are those that provide enough bursts of energy without completely depleting their SoC before the hydrogovernor response kicks in to bring the frequency close to the nominal frequency.

The sensitivities of frequency nadir, multiple frequency dips, and SoC across the variation of f-Watt settings suggest an asymmetric strategy in designing the f-Watt droops that is adaptive to rate-of-change-frequency (ROCOF) and aware of the SoC profile. This can be achieved by providing the inverter the ability to make transition among different control settings (e.g., steeper dP/df for faster excursion of frequency while gentler dP/df for slower recovery of frequency).

5. REFINEMENT OF HYDROPOWER UNIT TRANSIENT MODELS TO MATCH FIELD DEMONSTRATION MEASUREMENTS

Key Takeaways:

- This section compares the field demonstration measurements (Section 2) and simulation results (Section 4).
- Simulations were helpful to identify potential solutions, but field demonstration led to unique insights not possible through simulation.
- Field demonstration measurements suggest potential approaches to introduce more realism into transient simulation models, such as stochastic perturbation factors to account for bubbles during rapid changes in gate or blade position.
- For Idaho Falls Power, the comparison of field demonstration measurements with simulation results suggests adjustment in the hydropower transient model's (a) inertia constant according to water flow rate and (b) operating head according to steady-state electric loading and hydrogovernor settings.

Offline simulation enables a comprehensive assessment of a phenomena and its overall impact over a broad range of scenarios without risking physical assets. The associated simulation model is expected to match the reality as close as possible since it de-risks the field test and hence accelerates deployment. For example, offline transient simulation enabled a comprehensive study of the hydropower-based black start of IFP's entire distribution system (Section 3) and overall assessment of energy storage control strategy for stable black start (Section 4).

As mentioned earlier, electric loading in steps is performed as part of the load restoration during black start, and the associated dynamics reflect the frequency stability performance and load-carrying capability. To conduct such a procedure in transient simulation environment, a high-fidelity dynamic model of the hydropower unit is utilized (see Figure 33). The dynamic model of the hydropower unit consists of (a) turbine, (b) hydrogovernor, and (c) synchronous generator. Furthermore, a dynamic load model is interconnected with the hydropower unit to simulate load step changes. The transient simulation is executed through complex interaction among the sub-models, and its accuracy depends upon how the various parameters are set throughout the model.

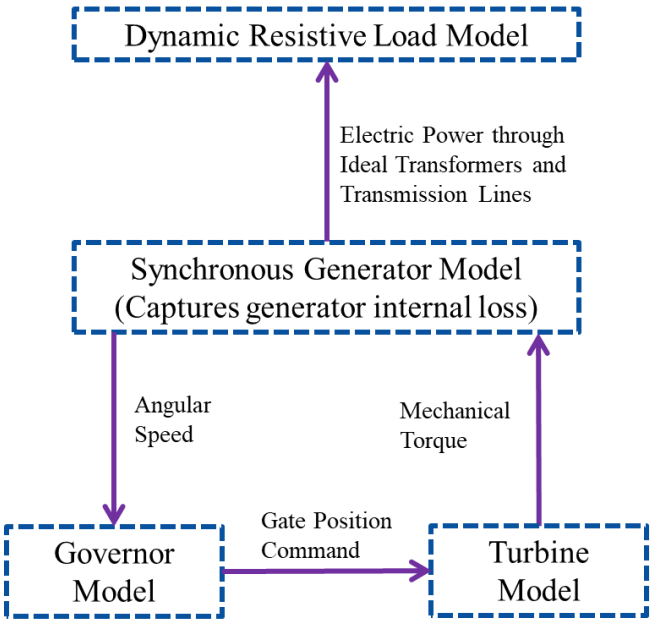

Figure 33. Elements of dynamic model for transient simulation of black start.

Field demonstration, on the other hand, brings a technology closer to deployment through testing on a limited set of physical assets. In Section 2, the improvement in frequency stability during black start has been demonstrated through the field testing of ultracapacitor with IFP's islanded hydropower. Such demonstration raises awareness among the industry stakeholder about the viability of a proof-of-concept technological solutions. For example, the Northwest Public Power Association (NWPPA) featured an article about INL and IFP's black start field demonstration [46]. Furthermore, measurements collected during the field test enable identifying gaps in simulation models and guide additional refinement (see Figure 34). This interdependence plays an important role in technical innovation, simulating, testing, and deployment of similar solutions to small hydropower's grid islanding capabilities in other systems.

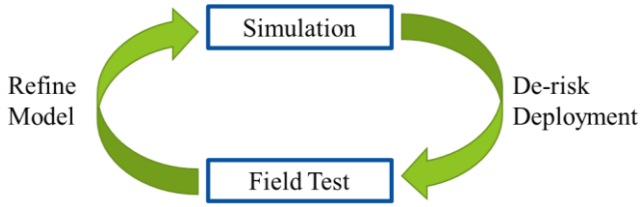

Figure 34. Conceptual interdependence between simulation and field test.

Based on the field demonstration with IFP, we present two such instances where the necessity of the simulation model refinement is captured. First, we investigate the Lower Bulb (LB) unit's inertia constant and capture any variation or dependence to steady-state conditions. We repeat the same for the operating head parameter called *hdam*. It should be noted that the synchronous generator model utilizes inertia constant of the rotary mass to reflect rate-of-change-of-frequency (ROCOF) during transients. Whereas the turbine model utilizes *hdam*, which is typically kept at 1 p.u. (per unit).

5.1 Flow-Rate Dependent Inertia Constant in Synchronous Generator Model

During the preparation of the field demonstration, high-fidelity dynamic model of IFP's LB hydropower plant has been developed. The inertia constant used for this is 1.33 MW-s/MVA—estimated from the micro-phasor measurement unit (micro-PMU) data of December 2017 black start test, using the method described in [47]. Notice the lower inertia constant compared to what is typical for hydropower (2~4) [48].

Similar approach has been taken with the micro-PMU data from April 2021 black start field demonstration to investigate any variation in the inertia constant. It appears that the inertia constant of the LB hydropower unit varies across electric loading. Furthermore, the average inertia constants on April 19 and 22, 2021 are 1.4 MW-s/MVA and 1.42 MW-s/MVA, respectively (see Figure 35).

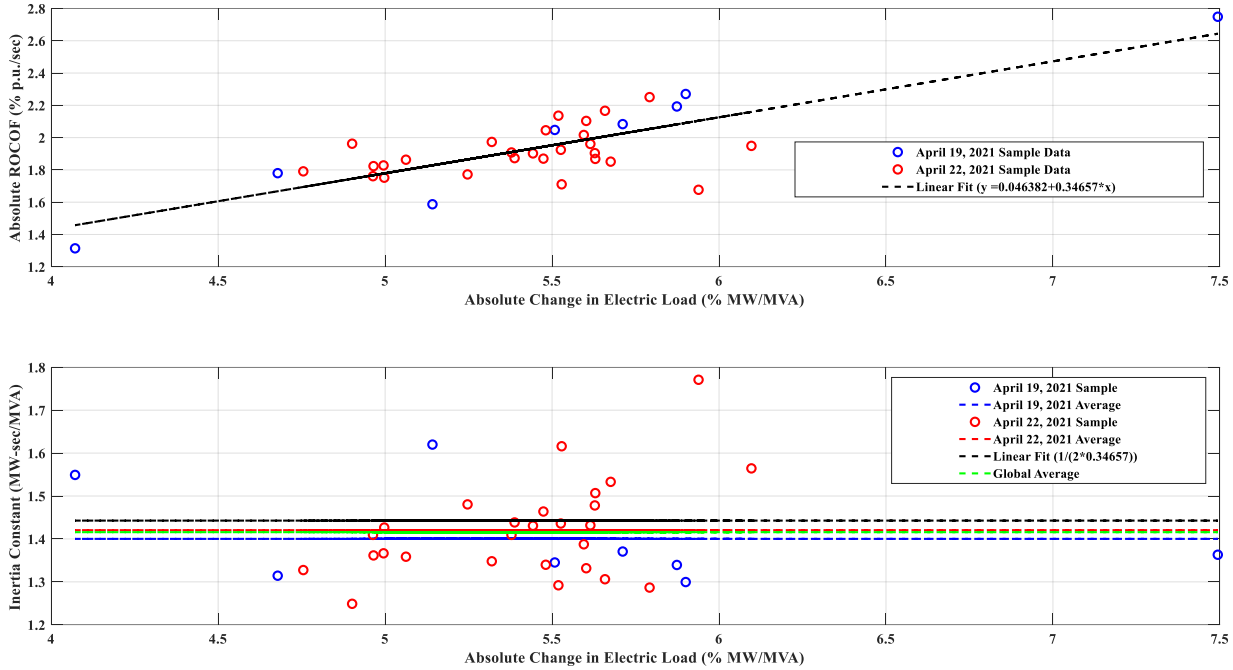

Figure 35. Effective inertia constant of LB unit's rotary mass. Variation across electric loading and days are observed.

While investigating the flow-rate data from the nearby USGS stream gauge # 13060000, the average flow rates on April 19 and 22, 2021 are 3600 CFS and 4300 CFS, respectively. Seemingly, the inertia constant of the LB unit's rotary mass increases with flow rate—reflecting the contribution of additional volume of water body in the inertia increment. Such relation needs to be accurately captured in the dynamic model of synchronous generator by keeping a provision of flow-rate dependent inertia constant adjustment.

5.2 Load and Hydrogovernor Dependent Operating Head Parameter in Turbine Model

In this case, the goal is to compare the hydrogovernor response recorded during the field demonstration with that from the transient simulation of the Simulink Kaplan Bulb-turbine model [41]. During the field demonstration, the hydrogovernor programmable logic controller (PLC) recorded the gate servo stroke (%) and speed (%) in response to an electric loading. A fair comparison of this field measurement with simulated response can be obtained by ensuring the same hydrogovernor settings are

applied, and steady-state electric loadings are matched (see Figure 33). The hydrogovernor settings from the field are matched in the Simulink model by setting the same proportional-integral-derivative (PID) gains. To match the steady-state electrical loading, a loss-less transmission line and ideal transformer has been considered, while the stator resistance of the synchronous generator are kept very small (2.8544 mΩ).

The following sequence of three steps are then applied to match the simulation load with measured electric load as close as possible:

- Step 1: In the Simulink, set the load value (P_L^{old}) as the steady-state electric load measured (P_L^m), run load flow, and capture the power being delivered by the synchronous generator (P_{SG}). This includes the generator's internal loss (P_{SG}^{loss}).
- Step 2: Calculate $P_{SG}^{loss} = P_{SG} - P_L^{old}$.
- Step 3: Adjust the load value in the Simulink model, $P_L^{new} = P_L^m - P_{SG}^{loss}$. This ensures P_L^m is now set as the P_{SG}.

The steady-state electric load matching is done for all the electric loading to the LB unit only (see Table 5-1). It can be observed the actual load power decreases after the 1 MW load command. Two instances of the matched steady-state electric load are shown in Figure 36.

Table 5-1. Simulink model adjustment to match electric loading from field test.

Load bank setting (MW)	Steady-state electric power measured, P_L^m (MW); $P_L^{old} = P_L^m$	Loss captured in the Simulink model, $P_{SG}^{loss} = P_{SG} - P_L^{old}$ (MW)	Load value set in the Simulink model, $P_L^{new} = P_L^m - P_{SG}^{loss}$ (MW)
0.5	0.5533	0.000098	0.553202
	0.5422333	0.00009466667	0.5421386
1.0	1.037	0.00034	1.03666
	1.04	0.00035	1.03965
	1.021333	0.00033666667	1.0209966
	1.0045	0.00032	1.00418
1.5	1.427	0.00065	1.42635
	1.423	0.00065	1.42235
	1.4776666667	0.000703333	1.476963333
	1.466333	0.000687	1.465646
2.0	1.908	0.00117	1.90683
	1.929	0.00119	1.92781
	1.918666	0.001184	1.917482
2.5	2.37	0.0018	2.3682
	2.324333	0.00173666	2.3225963
	2.309	0.00171	2.30729
3.0	2.844	0.00259	2.84141
	2.846	0.0026	2.8434
	2.75726666	0.0024334	2.75483326

Load bank setting (MW)	Steady-state electric power measured, P_L^m (MW); $P_L^{old} = P_L^m$	Loss captured in the Simulink model, $P_{SG}^{loss} = P_{SG} - P_L^{old}$ (MW)	Load value set in the Simulink model, $P_L^{new} = P_L^m - P_{SG}^{loss}$ (MW)
	2.77	0.00246	2.76754
3.5	3.327	0.00355	3.32345
	3.185333	0.003256666	3.18207633

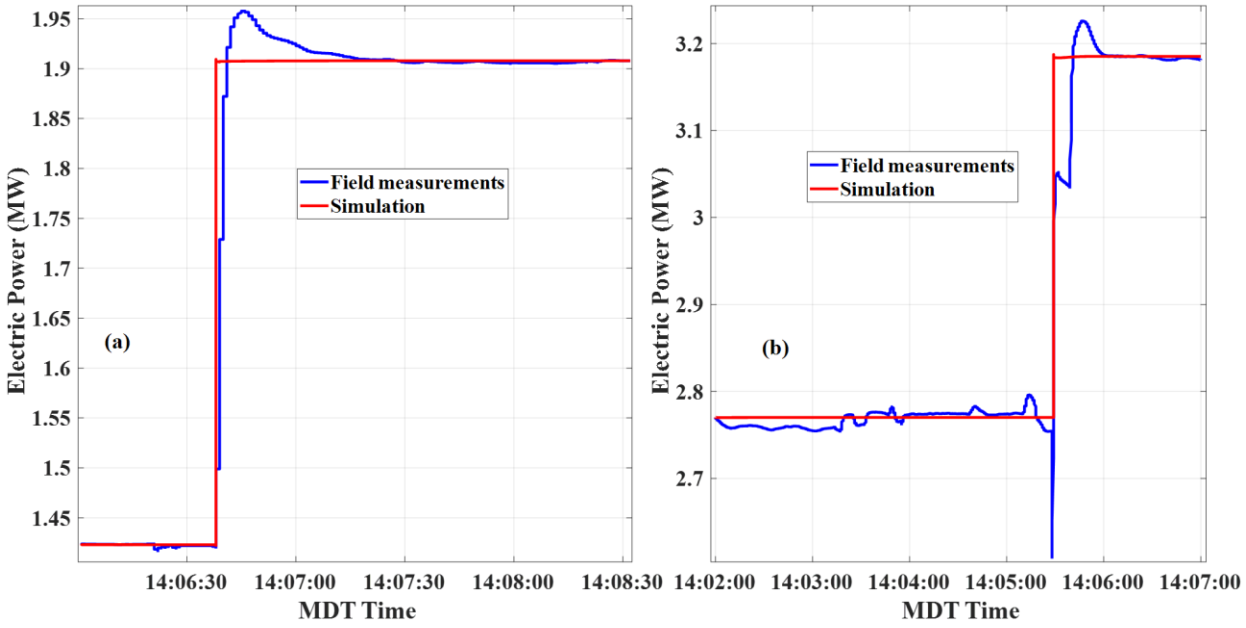

Figure 36. Simulink model electric loading matched to field measurements. (Left) 1.5 MW → 2.0 MW on April 19, 2021 (Right) 3.0 MW → 3.5 MW on April 22, 2021.

Once the steady-state electric loads are matched, the gate servo stroke from the field test is compared with that from the simulation. It has been observed that for the same electric loading and same hydrogovernor setting, the simulated gate servo stroke is either overestimating or underestimating the servo stroke from the actual hydrogovernor unit. In this regard, a greedy trial-and-error approach has been taken to adjust the operating head parameter (*hdam*) in the turbine model to visually match the simulated gate servo stroke with that from actual hydrogovernor unit. The turbine model's operating head adjustment is thus obtained for all steady-state electric loading of the LB unit with two different hydrogovernor settings (see Figure 37).

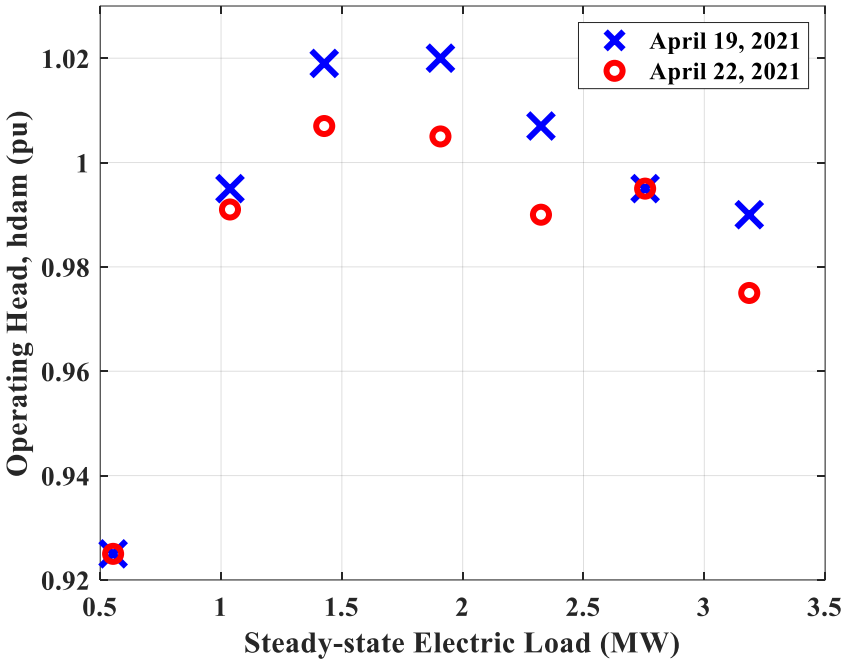

Figure Notes: hdam look up table used to match the simulation and field measurement of gate servo stroke given the same electric loading. Different P,I,D settings used for the 2 days (1.5, 0.08, 0.75 on April 19, 2021 and 0.9, 0.09, 0.75 on April 22, 2021) in the hydrogovernor. Blade bias not considered here.

Figure 37. Hydroturbine simulation model adjustment, which varies based on loading and day.

Adjustment of operating head (*hdam*) is motivated by the fact that it directly impacts the flow rate (*q*) and hence the mechanical torque (i.e., turbine output power [*Pturb*] [see Figure 38]). Given the steady-state loading condition, the hydrogovernor will sense corresponding rotational speed and will adjust the gate servo stroke accordingly (see Figure 33). For example, overestimation of the gate servo stroke is resolved by increasing *hdam*, which would increase *Pturb*, and hence, the simulated gate servo stroke will be reduced through feedback (see Figure 39).

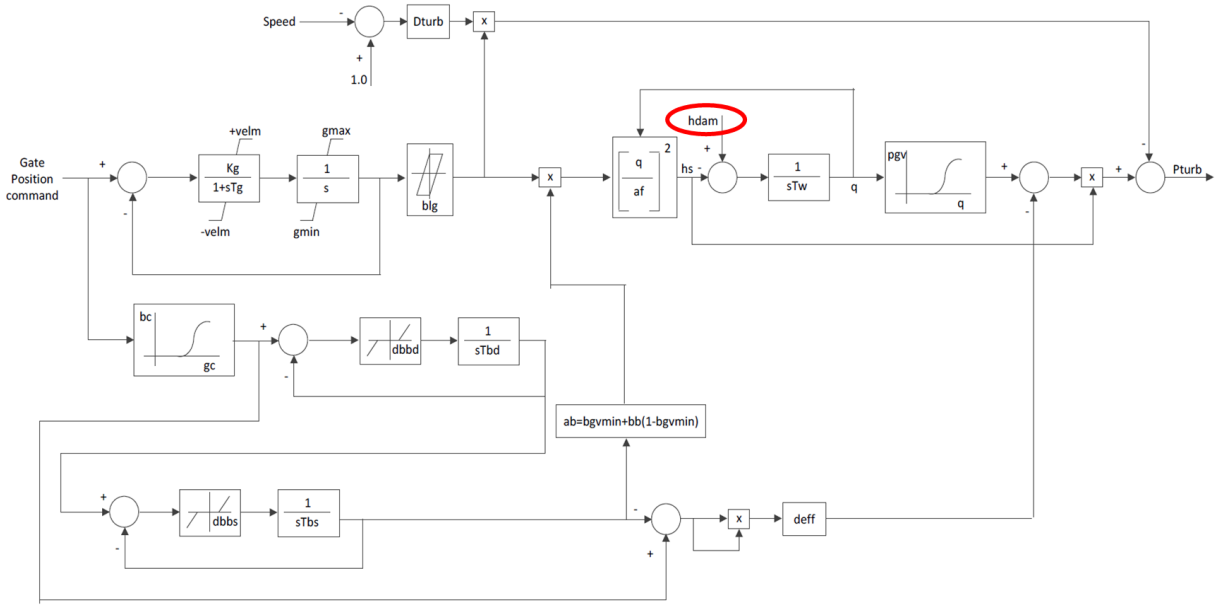

Figure 38. Block diagram for Kaplan turbine model. Red eclipse shows the *hdam parameter* [49].

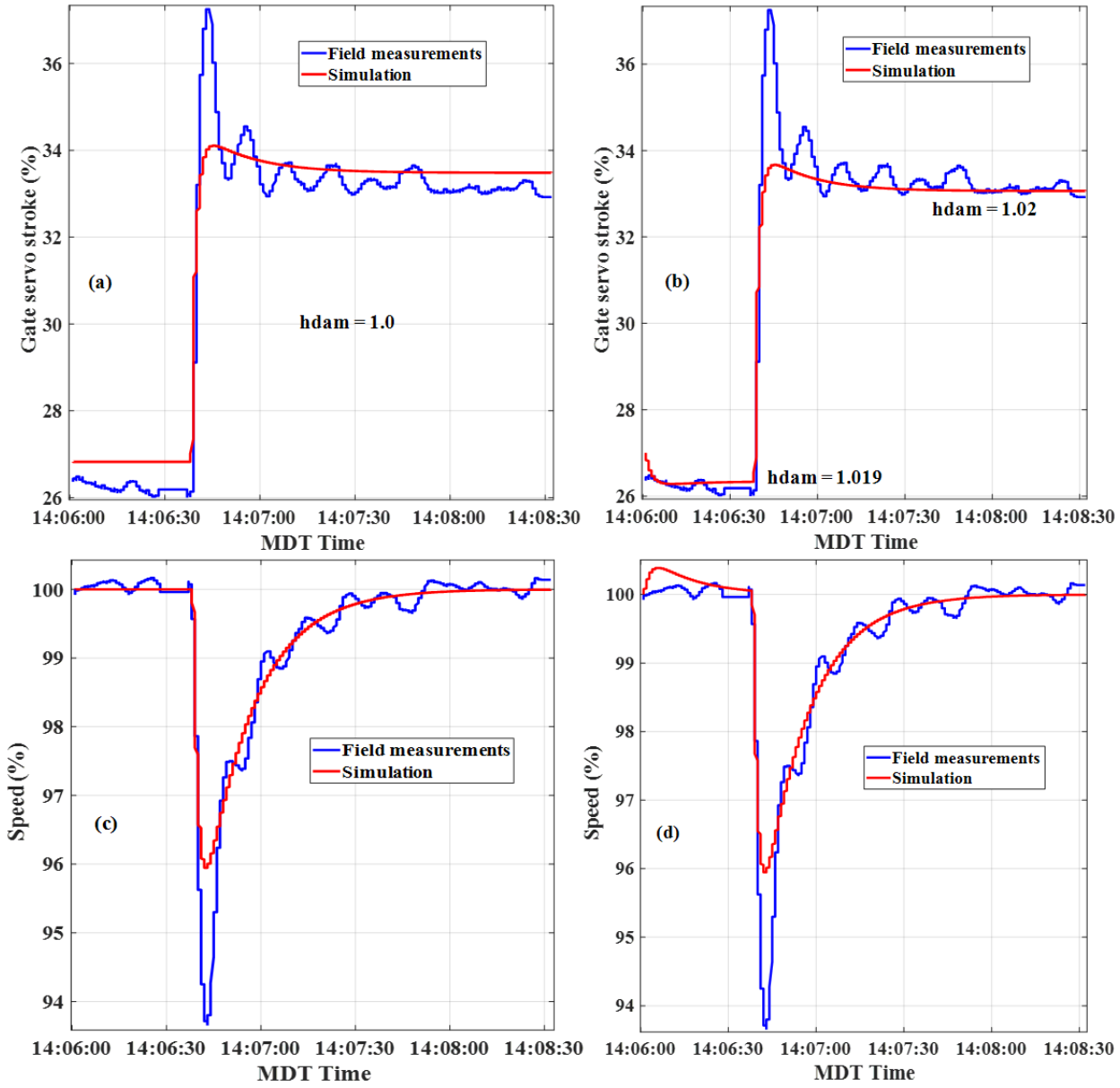

Figure Notes: Tests conducted on April 19, 2021 with P = 1.5, I = 0.08, D = 0.75. For (a) and (c) hdam = 1.0; for (b) and (d) hdam = {1.019, 1.02}.

Figure 39. Impact of hydroturbine simulation model adjustment on gate servo stroke (a and b) and speed (c and d) when stepping load from 1.5 MW to 2.0 MW without ultracapacitor.

On the other hand, underestimation of gate servo stroke is resolved by decreasing *hdam*, which would decrease *Pturb*, and hence, simulated gate servo stroke will be increased through feedback (see Figure 40).

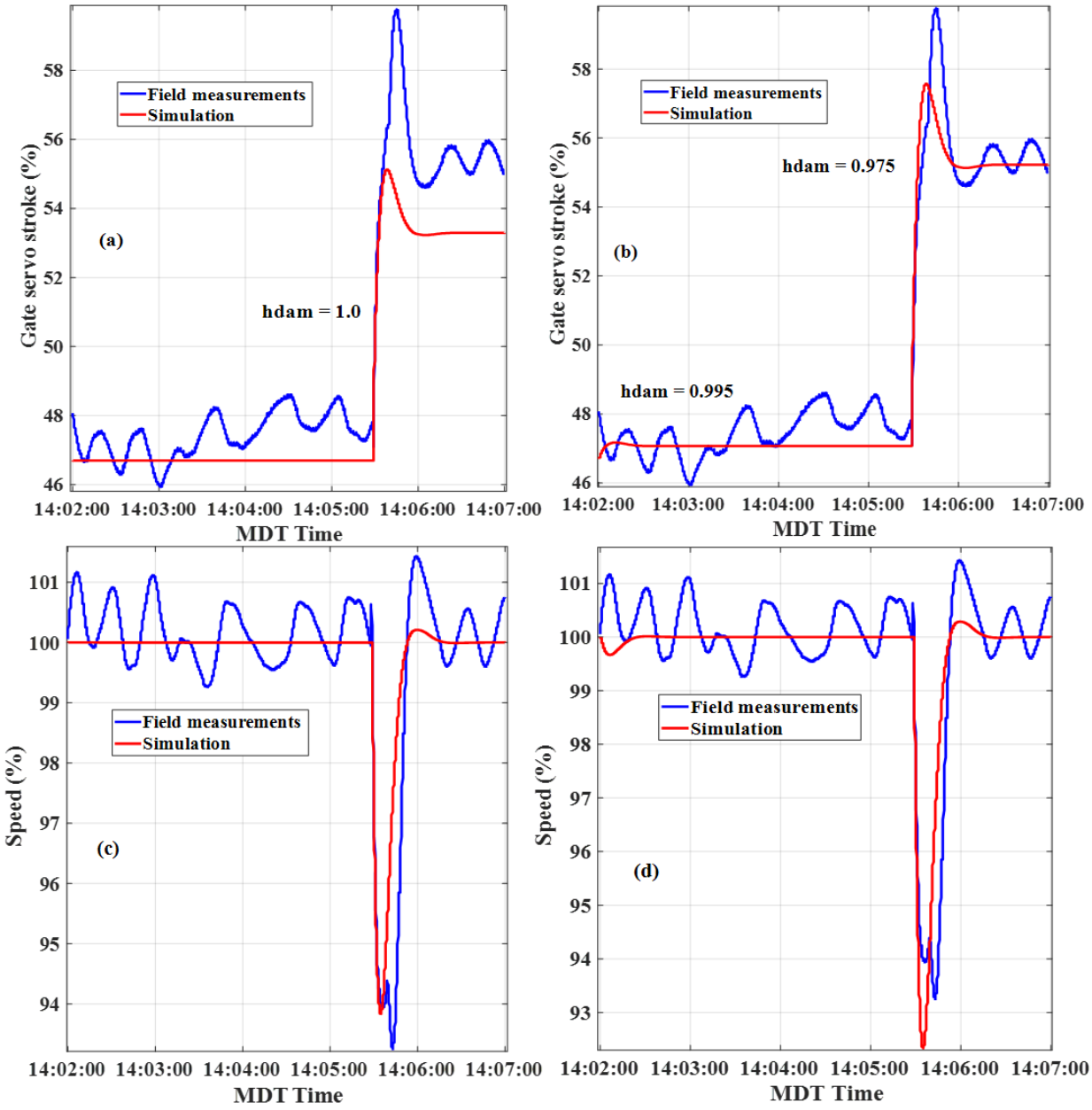

Figure Notes: Tests conducted on on April 22, 2021 with P = 0.9, I = 0.09, D = 0.75. For (a) and (c) hdam = 1.0; for (b) and (d) hdam = {0.995, 0.975}.

Figure 40. Impact of hydroturbine simulation model adjustment on gate servo stroke (a and b) and speed (c and d) when stepping load from 3.0 MW to 3.5 MW. The field measurements included the ultracapacitor while the simulations did not. Thus, the *hdam* adjustment not only resolves gate position mismath (b) but also corrects speed nadir (d).

Thus, steady-state electric loading and hydrogovernor setting based operating head adjustment is needed inside the turbine model to resolve the mismatch in steady-state gate servo strokes. However, the existing model does not capture the oscillaory behavior in the measuremed gate servo stroke (probably caused by insuffcient water flow rate and may vary with electric loading). This presents the necessity to investigate into other degrees of freedom in the model as well as identify modeling gaps [50].

6. CONCLUSION: SCALING-UP SMALL HYDROPOWER DISTRIBUTION BLACK START CAPABILITIES

Key Takeaways:

- Small hydropower with appropriate integration of energy storage can offer the capability of a distribution grid black start. This is demonstrated through a field demonstration with Idaho Falls Power (see Section 2).
- The sizing, placement, and control modes of energy storage that facilitates small hydro-based black start are driven by the desired performance in stability and storage health.
- Additional field demonstration, associated model refinement, and simulation works will enable the generalization of small hydro's islanded mode response and energy storage integration requirement for black start. This will thereby reduce the hesitancy in accepting hydro + storage as a local grid resilience solution across the risk averse utilities.
- Besides local grid resilience, energy storage integration with hydropower has the potential of capturing additional revenue streams. This can promote new hydropower development at non-powered dams and through irrigation modernization.

This report presents the small hydropower's ability to power distribution grid black starts and islanded operation. The core of the report focuses on simulations and field demonstrations conducted with IFP to show how adding energy storage such as ultracapacitors could enhance the capabilities of their existing five ROR hydropower plants. The field demonstration consisted of multiple tests to compare the impact of synchronizing multiple hydropower plants, integrating ultracapacitors, and modifying the hydrogovernor controls to improve performance. Each of these interventions improved key performance indicators, such as magnitude of frequency excursion and maximum load-carrying capacity. The simulations expanded on the field demonstration to analyze black start for the entire distribution system and optimal energy storage placement. Both the field demonstration and simulations provide critical insights and are necessary to continue proving this capability. Simulations are helpful for exploring a large set of options, but field demonstration is key to understand factors impossible to represent in simulation, such as impact of bubbles in the turbine or operator response to dynamic conditions.

The field demonstration confirmed that in all scenarios the ultracapacitors had a measurable positive impact on performance. The increase in performance was most notable for scenarios that included either only the LB plant or the LB and OL plants, where adding ultracapacitors reduced the frequency excursions by approximately 30% and reduced the time below 58 Hz by 25% to 50% for experiments at the upper end of the load-carrying capacity. This represents a significant improvement in islanded stability. Notably, this performance could likely be enhanced even further if a larger energy storage system was used. For the multi-plant black start, the ultracapacitor still increased performance, but the greater impact was from synchronization of the multiple plants to carry the load. In this scenario, the limiting factor on load-carrying capacity was the size of the load banks rented for the field demonstration. Modifying the hydrogovernor controls to include blade biasing had a small impact on performance but holds promise if refinements are made, particularly if modified controls include coordination between hydropower units and energy storage.

The field demonstration, simulations, and associated analysis presented herein collectively shows the significant potential role that small hydropower can play in increasing local grid resilience. The impact will likely be greatest where small hydropower is co-located with critical loads that are within small utilities or remote regions of the grid. The utilities and other organizations with these facilities are typically risk averse when it comes to using their assets in new ways. Additionally, simulations and field demonstrations to prove the potential capability are expensive. Expansion of this work through additional field demonstration and generalizing the energy storage sizing and controls for a wider range of

hydropower unit types would help to reduce such hesitancy in deploying new technology. Furthermore, there is no doubt that utilities have well-trained and experienced personnel to operate their grid and generation asset in a normal and emergency situation. However, utilizing the existing assets to execute a non-traditional operation (such as the DGBS) would require a feasibility study of the assets as well as new training and operational guidebook.

The resilience benefit of small hydropower can also help motivate development of new hydropower, especially at sites near critical loads. For example, energy storage integration with non-powered dams to hydropower plant conversions [51], [52] and in-conduit or open channel turbines [53], [54] as part of irrigation modernization [55] can provide additional value for these projects. During normal grid operations, the energy storage can increase firm capacity of the hydropower plant and enable energy arbitrage (i.e., shift power from low-value hours to high-value hours).

Utilization of small hydropower to increase local grid resilience would be accelerated through:

- Developing restoration plans that include this capability and account for its attributes. One example is adjusting the amount of load being restored according to water conditions and frequency dynamics [56].
- Developing controls to provide synthetic inertia via the energy storage component. Section 2 showed that additional inertial support improves the frequency nadir and other stability metrics during black start. Consequently, power injection according to ROCOF (i.e., synthetic inertia contribution) from energy storage can play an important role in enabling stable black start in a distribution grid. Flexibility in real-time switching and system specific priority of control modes (between ROCOF and droop-based power injection) for the commercial off-the-shelf inverters needs to be investigated through hardware-in-the-loop testing and field demonstration before deployment.
- Exploring grid-forming inverters. The grid-forming inverter with battery was simulated to significantly improve frequency oscillation damping and keep the frequency nadir at an acceptable level in a multi-plant black start simulation (Section 3). However, the resulting impact on battery's (or energy storage in general) SoC (Section 4 shows the case of grid-following inverter) and life-cycle performance seeks additional assessment. This would better inform the decision-makers about the cost-benefit tradeoffs of choosing one type of inverter over other.
- Learning from deployment. The activities involved in the deployment of proven technology (e.g., modeling, simulation, testing, and demonstration) can show gaps in modeling and operation—raising new research questions. Research and innovations that can address the newly identified challenges can further accelerate the next deployment. Similar to the interdependence among simulation and field testing (Section 5), lessons learned from deployment promotes innovation through research, while the later de-risks and accelerates further deployment.

Overall, a systematic approach of evaluating the energy storage provision for grid islandability, identifying and demonstrating the technological solution, and developing a readily available decision and operational guidebook are among the significant outstanding needs for widespread hydro + storage deployment. This hybrid solution can enhance the socioeconomic value small hydro can offer to its serving communities through local grid resilience against extreme weather and manmade events. Hydropower operators and owners can also be benefited by adopting this hybrid solution as it will unfold new service revenue streams. Initiatives from Water Power Technologies Office, such as HydroWIRES, can bolster hydro + storage research and demonstration to make this hybrid a resilient, affordable, and reliable technoeconomic solution.

7. REFERENCES

[1] P. Brickley, "PG&E Loses Challenge to Law Holding It Liable for Fire Damage," The Wall Street Journal, 27 November 2019. [Online]. Available: https://www.wsj.com/articles/pg-e-loses-challenge-to-law-holding-it-liable-for-fire-damage-11574910091#:~:text=Under%20the%20doctrine%20of%20inverse,pay%20them%20about%20%2413.5%20billion. [Accessed 9 March 2022].

[2] *Glossary of Terms Used in NERC Reliability Standards,* North American Electric Reliability Corporation, 2021.

[3] J. Gracia, L. Markel, D. Rizy, P. O'Connor, R. Shan and A. Tarditi, "Hydropower Plants as Black Start Resources," Oak Ridge National Laboratory , Oak Ridge, 2019 .

[4] M. A. Gonzalez-Salazar, T. Kirsten and L. Prchlik, "Review of the operational flexibility and emissions of gas- and coal-fired power plants in a future with growing renewables," *Renewable and Sustainable Energy Reviews,* p. 1497–1513, 2018.

[5] F. Qiu, J. Wang, C. Chen and J. Tong, "Optimal Black Start Resource Allocation," *IEEE Transactions on Power Systems,* p. 2493–2494, 2016.

[6] W. Sun, C. Liu and L. Zhang, "Optimal generator start-up strategy for bulk power system restoration," in *IEEE Power and Energy Society General Meeting*, San Diego, 2012.

[7] C. Liu, K. Liou, R. Chu and A. T. Holen, "Generation capability dispatch for bulk power system restoration: a knowledge-based approach," *IEEE Transactions on Power Systems*, p. 316–325, 1993.

[8] D. Wang, X. Gu, G. Zhou, S. Li and H. Liang, "Decision-making optimization of power system extended black-start coordinating unit restoration with load restoration," *International Transactions on Electrical Energy Systems,* 2017.

[9] B. Chen, C. Chen, J. Wang and K. L. Butler-Purry, "Multi-Time Step Service Restoration for Advanced Distribution Systems and Microgrids," *IEEE Transactions on Smart Grid,* p. 6793–6805, 2018.

[10] North American Electric Reliability Corporation, "M-1 Reserve Margin," [Online]. Available: https://www.nerc.com/pa/RAPA/ri/Pages/PlanningReserveMargin.aspx. [Accessed 9 March 2022].

[11] C. Grande-Moran and J. W. Feltes, "An Overview of Restoration Issues and Blackstart Analysis," in *50th Annual Minnesota Power Systems Conference*, Minnesota, 2014.

[12] Y. Guo, E. Torabi-Makhsos, G. Rossa-Weber, W. Gawlik, R. Schmaranz, P. Hinkel, M. Ostermann, W. Wellbow and E. Traxler, "Review on Network Restoration Strategies as a Part of the RestoreGrid4RES Project," in *Symposium Energieinnovation*, Graz, 2018.

[13] N. Kang, J. Wang, R. Singh and X. Lu, "Interconnection, Integration, and Interactive Impact Analysis of Microgrids and Distribution Systems," Argonne National Laboratory, Lemont, 2017.

[14] J. Reichl, M. Schmidthaler and F. Schneider, "The value of supply security: The costs of power outages to Austrian households, firms and the public sector," *Energy Economics,* pp. 256-261, 2013.

[15] T. Schroder and W. Kuckshinrichs, "Value of Lost Load: An Efficient Economic Indicator for Power Supply Security? A Literature Review," *Front. Energy Res.,* 2015.

[16] M. Schmidthaler and J. Reichl, "Assessing the socio-economic effects of power outages ad hoc," *Computer Science - Research and Development,* pp. 157-161, 2016.

[17] P. Centolella, M. Farber-DeAnda, L. Greening and T. Kim, "Estimates of the Value of

Uninterrupted Service for The Mid-West Independent System Operator," SAIC, 2010.

[18] D. Lineweber and S. McNulty, "The Cost of Power Disturbances to Industrial & Digital Economy Companies," PRMEN, Madison, 2001.

[19] R. Campbell, "Weather-Related Power Outages and Electric System Resiliency," Congressional Research Service , Washington, 2012.

[20] A. C. Melhorn, N. Heine and B. Deaver, "Distribution System State Estimation: A Primer for Application Based Research," in *IEEE PES Transmission & Distribution Conference and Exhibition*, Montevideo, 2020.

[21] "Power Island Strength and Stability in support of Black Start," Black Start from Non-Traditional Generation Technologies, National Grid ESO, London, 2019.

[22] C. Strunck and C. Rehtanz, "Definition of Key Indicators to Identify Optimal Distribution Grid Restoration Strategies," in *ENERGY-21 – Sustainable Development & Smart Management*, Irkutsk, 2020.

[23] S. Lee, *Power Systems Dynamics Tutorial*, Palo Alto: Electric Power Research Institute, 2009.

[24] *Smart, Clean Neighborhood Grids: Redesigning Our Electric System To Help Communities Power Through Blackouts,* San Francisco: Sunrun, 2021.

[25] High Share of Inverter-Based Generation Task Force, *Grid-Forming Technology in Energy Systems Integration,* Energy Systems Integration Group, 2022.

[26] L. Darío, A. Klingmann, D. Fetzer, G. Lammert, C. Hachmann, T. Paschedag and M. Braun, *Black start and island operation of distribution grids with significant penetration of renewable resources,* Integration Workshops, 2017.

[27] NERC, *Fast Frequency Response Concepts and Bulk Power System Reliability Needs,* Atlanta: North American Electric Reliability Corporation, 2020.

[28] Z. Xu, P. Yang, Z. Zeng, Y. Zhang, J. Peng and Q. Zheng, "Study on black start strategy for multi-microgrids," in *IEEE Innovative Smart Grid Technologies - Asia (ISGT-Asia)*, Melbourne, 2016.

[29] *Black Start Strategy: Produced in accordance with Standard Condition C16 of the NGET Transmission License,* National Grid , 2017.

[30] U.S. Energy Information Administration, "About 25% of U.S. power plants can start up within an hour," 19 November 2020. [Online]. Available: https://www.eia.gov/todayinenergy/detail.php?id=45956. [Accessed 15 April 2022].

[31] CISA, *A Guide to Critical Infrastructure Security and Resilience,* Washington D.C.: Cybersecurity and Infrastructure Security Agency, U.S. Department of Homeland Security, 2019.

[32] *Idaho Falls Power Annual Report,* Idaho Falls: Idaho Falls Power, 2017.

[33] NHA, "Small Hydro," National Hydropower Association, [Online]. Available: https://www.hydro.org/policy/technology/small-hydro/. [Accessed 9 March 2022].

[34] B. Jenkins, M. Panwar and R. Hovsapian, "Experiences from Field Testing for Black Start of a Run-of-the-river Hydropower Plant in Idaho Falls Power Distribution Grid," in *Hydrovision International Conference*, Portland, 2019.

[35] "Idaho Falls Power Annual Report," Idaho Falls Power, Idaho Falls, 2020.

[36] J. S. Paine and L. E. Felton, "Bulb Turbine/Generators for the Idaho Falls Hydroelectric Project," *IEEE Transactions on Power Apparatus and Systems,* Vols. PAS-103, no. 9, pp. 2405 - 2409, 1984.

[37] "Southeastern Idaho Transmission Projects," PacifiCorp, [Online]. Available: https://www.pacificorp.com/transmission/transmission-projects/southeastern-idaho.html. [Accessed 10 March 2022].

[38] "Eastern Idaho power outage affects 53K," Morgan Murphy Media, 4 December 2013. [Online]. Available: https://www.kxly.com/eastern-idaho-power-outage-affects-53k/. [Accessed 10 March

2022].

[39] N. Sunderland, "Rocky Mountain Power investigates blackout, substation fire," East Idaho News, 20 July 2016. [Online]. Available: https://www.eastidahonews.com/2016/07/rocky-mountain-power-investigating-blackout-substation-fire/. [Accessed 10 March 2022].

[40] S. M. S. Alam, A. Banerjee, C. Loughmiller, B. Bennett, N. Smith, T. M. Mosier, V. Gevorgian, B. Jenkins and M. Roberts, "Idaho Falls Power Black Start Field Demonstration - Preliminary Outcomes Report," Idaho National Laboratory, Idaho Falls, 2021.

[41] A. Banerjee, S. M. S. Alam, T. M. Moier and J. Undrill, "Modeling a Bulb-Style Kaplan Unit Hydrogovernor and Turbine in Mathworks-Simulink and RTDS-RSCAD," in *IEEE PES T&D Conference and Exposition*, New Orleans, 2022.

[42] S. M. S. Alam, A. Banerjee and T. M. Mosier, "Power Hardware-In-the-Loop Hydropower and Ultracapacitor Hybrid Testbed," in *IEEE PES General Meeting*, 2022, 2022.

[43] "USGS 13060000 SNAKE RIVER NR SHELLEY ID," United States Geological Survey, [Online]. Available: https://waterdata.usgs.gov/nwis/inventory?agency_code=USGS&site_no=13060000. [Accessed 10 March 2022].

[44] "PSCAD," Manitoba Hydro International Ltd., [Online]. Available: https://www.pscad.com/. [Accessed 10 March 2022].

[45] "Milsoft," Milsoft Utility Solutions, [Online]. Available: https://www.milsoft.com/. [Accessed 10 March 2022].

[46] N. Rydalch, "Idaho Falls Power Discovers Big Value in Small Hydropower," *NWPPA Bulletin*, pp. 30-33, February 2022.

[47] U. Tamrakar, N. Guruwacharya, N. Bhujel, F. Wilches-Bernal, T. M. Hansen and R. Tonkoski, "Inertia Estimation in Power Systems using Energy Storage and System Identification Techniques," in *International Symposium on Power Electronics, Electrical Drives, Automation and Motion (SPEEDAM)*, Sorrento, 2020.

[48] M. Shafiullah, H. Rahman, M. I. Hossain and M. M. Ahsan, "The study of dependency of power system stability on system inertia constant for various contingencies," in *International Conference on Electrical Engineering and Information & Communication Technology*, Dhaka, 2014.

[49] P. Zadkhast, *Powertech h6e benchmarking results*, Western Electric Coordinating Council, 2019.

[50] R. Bhattarai, *Gaps in Modeling Hydro Power Plant in Steady-state and Dynamic Analysis*, WECC Model Validation Subcommittee Workshop, 2021.

[51] C. Hansen, M. Musa, C. Sasthav and S. DeNeale, "Hydropower development potential at non-powered dams: Data needs and research gaps," *Renewable and Sustainable Energy Reviews*, vol. 145, no. 111058, 2021.

[52] USACE, "HYDROPOWER RESOURCE ASSESSMENT AT NON-POWERED USACE SITES," US Army Corps of Engineers, 2013.

[53] M. Sari, M. Badruzzaman, C. Cherchi, M. Swindle, N. Ajami and J. Jacangelo, "Recent innovations and trends in in-conduit hydropower technologies and their applications in water distribution systems," *Journal of Environmental Management*, vol. 228, pp. 416-428, 2018.

[54] S. Chesney, "Hydropower in canal called energy ‘game-changer’," Denver Water, 26 June 2017. [Online]. Available: https://www.denverwater.org/tap/hydropower-in-canal-called-energy-game-changer. [Accessed 10 March 2022].

[55] "NEW IRRIGATIONVIZ TOOL PROMOTES WATER, ENERGY, ENVIRONMENT FOR COMMUNITIES," Idaho National Laboratory, 17 June 2021. [Online]. Available: https://inl.gov/article/new-irrigationviz-tool-promotes-water-energy-environment-for-communities/. [Accessed 10 March 2022].

[56] Q. Zhang, Z. Ma, Y. Zhu and Z. Wang, "A Two-Level Simulation-Assisted Sequential Distribution System Restoration Model With Frequency Dynamics Constraints," *IEEE Transactions on Smart Grid*, vol. 12, no. 5, pp. 3835-3846, 2021.

[57] W. Sun, C. Liu and Z. L., "Optimal Generator Start-Up Strategy for Bulk Power System Restoration," *IEEE Transactions on Power Systems*, p. 1357–1366, 2011.

[58] D. Wang, X. Gu, G. Zhou, S. Li and H. Liang, "Decision-making optimization of power system extended black-start coordinating unit restoration with load restoration," *International Transactions on Electrical Energy Systems*, 2017.

[59] L. H. Sheldon, "Optimizing Kaplan Turbine Efficiency with Minimal Cost, Effort, and Time," POWER magazine, 1 April 2019. [Online]. Available: https://www.powermag.com/optimizing-kaplan-turbine-efficiency-with-minimal-cost-effort-and-time/. [Accessed 10 March 2022].

[60] C. Koplin, "Cordova Electric Cooperative-Black Start for Microgrids," Electricity Advisory Committee (EAC), Virtual, 2021.

Appendix A
Postprocessing the Micro-PMU Data

In order to perform a strategic way to create a code that simultaneously opens, reads, rearranges, and plots graphs, we needed to analyze the process of the data. The following flowchart is a representation taken to achieve the desire process (see Figure 41).

A.1 Mountain Daylight Time (MDT) Time / Reading Bad Rows

The first task was able to understand the file format and what it has recorded. There were couple of complicated errors that needed to be address within the large number of rows that the micro-PMU recorded. This process needed to be achieved in order to organize every row based on their correct time. For these, we need to skip all the bad rows and then transform the Epoch time to MDT time which eventually would allow for organizing based on time (see Figure 41).

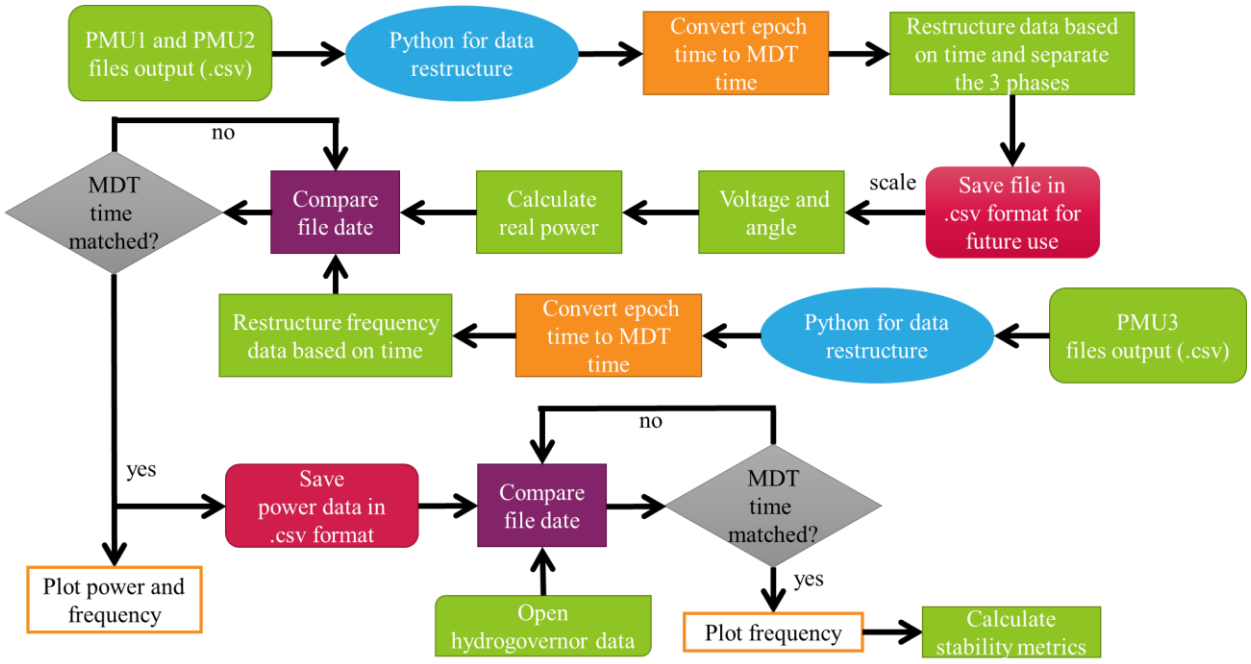

Figure 41. Flowchart showing the overall process of postprocessing of micro-PMU data.

PPA:262	BPA_PMU	PMU2-PM	22:35.0	1.62E+09	0.235103	Good	Pmu2 L1MagAng + Voltage Magnitude
PPA:263	BPA_PMU	PMU2-PA1	22:35.0	1.62E+09	50.76862	Good	Pmu2 L1MagAng + Voltage Phase Angle
PPA:264	BPA_PMU	PMU2-PM	22:35.0	1.62E+09	0.087987	Good	Pmu2 L2MagAng + Voltage Magnitude
PPA:265	BPA_PMU	PMU2-PA2	22:35.0	1.62E+09	-94.2715	Good	Pmu2 L2MagAng + Voltage Phase Angle
PPA:266	BPA_PMU	PMU2-PM	22:35.0	1.62E+09	0.166771	Good	Pmu2 L3MagAng + Voltage Magnitude
PPA:267	BPA_PMU	PMU2-PA3	22:35.0	1.62E+09	-132.797	Good	Pmu2 L3MagAng + Voltage Phase Angle
PPA:268	BPA_PMU	PMU2-PM	22:35.0	1.62E+09	0.000175	Good	Pmu2 C1MagAng + Current Magnitude
PPA:269	BPA_PMU	PMU2-PA4	22:35.0	1.62E+09	-171.195	Good	Pmu2 C1MagAng + Current Phase Angle
PPA:270	BPA_PMU	PMU2-PM	22:35.0	1.62E+09	3.00E-06	Good	Pmu2 C2MagAng + Current Magnitude
PPA:271	BPA_PMU	PMU2-PA5	22:35.0	1.62E+09	-42.4277	Good	Pmu2 C2MagAng + Current Phase Angle
PPA:272	BPA_PMU	PMU2-PM	22:35.0	1.62E+09	8.11E-05	Good	Pmu2 C3MagAng + Current Magnitude
PPA:273	BPA_PMU	PMU2-PA6	22:35.0	1.62E+09	130.6753	Good	Pmu2 C3MagAng + Current Phase Angle
PPA:262	BPA_PMU	PMU2-PM	22:35.0	1.62E+09	0.236627	Good	Pmu2 L1MagAng + Voltage Magnitude
PPA:263	BPA_PMU	PMU2-PA1	22:35.0	1.62E+09	50.15436	Good	Pmu2 L1MagAng + Voltage Phase Angle
PPA:264	BPA_PMU	PMU2-PM	22:35.0	1.62E+09	0.084049	Good	Pmu2 L2MagAng + Voltage Magnitude
PPA:265	BPA_PMU	PMU2-PA2	22:35.0	1.62E+09	-95.0525	Good	Pmu2 L2MagAng + Voltage Phase Angle
PPA:266	BPA_PMU	PMU2-PM	22:35.0	1.62E+09	0.175699	Good	Pmu2 L3MagAng + Voltage Magnitude
PPA:267	BPA_PMU	PMU2-PA3	22:35.0	1.62E+09	-134.049	Good	Pmu2 L3MagAng + Voltage Phase Angle
PPA:268	BPA_PMU	PMU2-PM	22:35.0	1.62E+09	0.000162	Good	Pmu2 C1MagAng + Current Magnitude
PPA:269	BPA_PMU	PMU2-PA4	22:35.0	1.62E+09	-164.095	Good	Pmu2 C1MagAng + Current Phase Angle

Figure 42. Raw data screenshot.

A.2 Restructure Data Based On Line Current, Voltage, and Angle

Using the Pandas library was needed for data restructure. Pandas is a data frame software library that allows the user to have data manipulation. After scanning and filtering out all the lines, they were filtered by column and at the same time were separated based on their time stamps. This process is repeated for PMU 1 and PMU 2 to restructure voltage and line current time series, and for PMU 3 to restructure frequency time series (see Figure 43 for a snapshot of restructured voltage and line current time series).

0	MDT_Time	Current Magnitude1	Line_1 _x	Current Phase1	Line_1 _y	Volate Magnitude1	Line_1_x	Volate Phase1	Line_1_y
1	2021-04-22 13:20:00.000000000	0.09236792	Pmu1 C1MagAng + Current Magnitude	35.88927	Pmu1 C1MagAng + Current Phase Angle	122.1516	Pmu1 L1MagAng + Voltage Magnitude	-142.918	Pmu1 L1MagAng + Voltage Phase Angle
2	2021-04-22 13:20:00.000000000	0.09236792	Pmu1 C1MagAng + Current Magnitude	35.88927	Pmu1 C1MagAng + Current Phase Angle	122.1516	Pmu1 L1MagAng + Voltage Magnitude	97.18809	Pmu1 L2MagAng + Voltage Phase Angle
3	2021-04-22 13:20:00.000000000	0.09236792	Pmu1 C1MagAng + Current Magnitude	35.88927	Pmu1 C1MagAng + Current Phase Angle	122.1516	Pmu1 L1MagAng + Voltage Magnitude	-22.81747	Pmu1 L3MagAng + Voltage Phase Angle
4	2021-04-22 13:20:00.000000000	0.09236792	Pmu1 C1MagAng + Current Magnitude	35.88927	Pmu1 C1MagAng + Current Phase Angle	121.9033	Pmu1 L2MagAng + Voltage Magnitude	-142.918	Pmu1 L1MagAng + Voltage Phase Angle
...	...	...	...	...	...	...	...	...	...
13381301	2021-04-22 13:43:00.000000000	0.000276	Pmu1 C3MagAng + Current Magnitude	-150.8135	Pmu1 C3MagAng + Current Phase Angle	0.058141	Pmu1 L2MagAng + Voltage Magnitude	-143.8329	Pmu1 L2MagAng + Voltage Phase Angle
13381302	2021-04-22 13:43:00.000000000	0.000276	Pmu1 C3MagAng + Current Magnitude	-150.8135	Pmu1 C3MagAng + Current Phase Angle	0.058141	Pmu1 L2MagAng + Voltage Magnitude	-138.3784	Pmu1 L3MagAng + Voltage Phase Angle
13381303	2021-04-22 13:43:00.000000000	0.000276	Pmu1 C3MagAng + Current Magnitude	-150.8135	Pmu1 C3MagAng + Current Phase Angle	0.053261	Pmu1 L3MagAng + Voltage Magnitude	-128.3909	Pmu1 L1MagAng + Voltage Phase Angle
13381304	2021-04-22 13:43:00.000000000	0.000276	Pmu1 C3MagAng + Current Magnitude	-150.8135	Pmu1 C3MagAng + Current Phase Angle	0.053261	Pmu1 L3MagAng + Voltage Magnitude	-143.8329	Pmu1 L2MagAng + Voltage Phase Angle
13381305	2021-04-22 13:43:00.000000000	0.000276	Pmu1 C3MagAng + Current Magnitude	-150.8135	Pmu1 C3MagAng + Current Phase Angle	0.053261	Pmu1 L3MagAng + Voltage Magnitude	-138.3784	Pmu1 L3MagAng + Voltage Phase Angle

Figure 43. Output data restructure.

A.3 Power Calculation and Frequency Matching

After having new data structure, a code has been developed that could rescale the voltage and current magnitude based on the potential transformer (PT) and current transformer (CT) ratios for real power calculation. The PT and CT ratios for the three micro-PMUs used during the field demonstration are given below.

Table A-1. PT and CT ratios for micro-PMU connection.

PMU #	Location of installation (see Figure 9)	PT ratio	CT ratio
1	4B1-1 (Rack substation)	12.47 kV (L-L) : 120 V (L-L)	1200:5
2	EPC Converter	480 V (L-L) : 480 V (L-L)	1000:5
3	3B1-10 (LB unit)	4.16 kV (L-L) : 69.3 V(L-N)	1500:5

The real power calculation is executed in the following steps:

- Step 1: Check the voltage magnitude recordings from L1, L2, L3 and scale them using the PT ratios to present line-to-neutral voltages in kV (PMU 1) and V (PMU 2).
- Step 2: Check the voltage phase angles for PMU 1 and PMU 2. For each time instance, the three voltages should be 120 degree out-of-phase from each other.
- Step 3: Check the current magnitude recordings from L1, L2, L3 and scale them using the CT ratios to present line currents in kA for both PMU 1 and PMU 2.

- Step 4: Check the current phase angles. For each time instance, the three currents should be 120 degrees out-of-phase from each other. If any phase appears only 60 degrees out-of-phase from the rest due to CT's orientation, affix corresponding phase angle with a negative sign for correction.
- Step 5: Utilize scaled voltage and current values from PMU 1 to calculate the real power being consumed by the load bank.

$$P_{PMU1}[MW] = \sum_{i=1}^{3} \left|V_i^{PMU1}(L-N)\right|[kV] \times \left|I_i^{PMU1}\right|[kA] \times \cos(\angle V_i^{PMU1}(L-N) \sim \angle I_i^{PMU1}).$$

- Step 6: Utilize scaled voltage and current values from PMU 2 to calculate real power being injected by the UCAP ESS

$$P_{PMU2}[kW] = \sum_{i=1}^{3} \left|V_i^{PMU2}(L-N)\right|[V] \times \left|I_i^{PMU2}\right|[kA] \times \cos(\angle V_i^{PMU2}(L-N) \sim \angle I_i^{PMU1}).$$

- Step 7: Repeat steps 1–6 for each time instance and create real power time series (see Figure 44).

	MDT_Time	FinalPower
0	2021-04-22 13:20:00.000000000	4.885646e-01
1	2021-04-22 13:20:00.007999897	4.866681e-01
2	2021-04-22 13:20:00.016000032	4.882875e-01
3	2021-04-22 13:20:00.023999929	4.864306e-01
4	2021-04-22 13:20:00.032999992	4.882854e-01
...	...	...
164614	2021-04-22 13:42:59.966000080	2.079651e-07
164615	2021-04-22 13:42:59.973999977	1.695036e-07
164616	2021-04-22 13:42:59.983000040	2.144630e-07
164617	2021-04-22 13:42:59.990999937	1.279320e-07
164618	2021-04-22 13:43:00.000000000	2.876404e-07

Figure 44. Output Real Power Calculation from Lines in PMU1.

A.4 Power and Frequency Instance Matching

The power with frequency match was accomplished based on the time stamp they both shared, at which we would ignore any point where the time stamp did not match. Few occurrences of such mismatch out of 120 samples every second can be ignored without significant deterioration in the quality of stability metric calculations. This provided a better alignment for power and frequency. It should be noted that both the power and frequency data need to have the same data and time to ensure proper alignment of frequency excursion and change of power events (see Figure 45).

	MDT_Time	FinalPower	F	H
0	2021-04-22 13:20:00.000000000	4.885646e-01	NaN	NaN
1	2021-04-22 13:20:00.007999897	4.866681e-01	60.02368	Pmu3 Frequency
2	2021-04-22 13:20:00.016000032	4.882875e-01	60.07468	Pmu3 Frequency
3	2021-04-22 13:20:00.023999929	4.864306e-01	60.02399	Pmu3 Frequency
4	2021-04-22 13:20:00.032999992	4.882854e-01	60.07655	Pmu3 Frequency
...	...	...	...	...
167055	2021-04-22 13:42:59.973999977	1.695036e-07	72.89332	Pmu3 Frequency
167056	2021-04-22 13:42:59.983000040	2.144630e-07	72.96069	Pmu3 Frequency
167057	2021-04-22 13:42:59.990999937	1.279320e-07	73.02621	Pmu3 Frequency
167058	2021-04-22 13:43:00	NaN	73.08771	Pmu3 Frequency
167059	2021-04-22 13:43:00.000000000	2.876404e-07	NaN	NaN

Figure 45. Output from matching time with frequency.

Appendix B
UCAP Sizing Simulation

To determine UCAP sizing along with the proper f-Watt settings for a particular UCAP size and system response requirements, various simulation scenarios considering different capacitor configurations and f-Watt settings were considered. The following configurations of UCAP and inverter were selected:

- 6.5 F, 950 V UCAP with 375 kVA inverter
- 13 F, 950 V UCAP with 750 kVA inverter
- 13 F, 950 V UCAP with 375 kVA inverter
- 6.5 F, 950 V UCAP with 750 kVA inverter.

For the f-Watt settings, variations with respect to dP/df slope and deadband sizes are considered as shown in Figure 29.

Below is a brief description of various f-Watt settings used:

- For setting #1, a larger deadband was used around 60 Hz. A deadband of 1.9 Hz was used for a frequency below 60 Hz, and a steep power injection rate (400% per Hz) was used between frequency 58.1 and 58 Hz. This ensures a sudden burst of power injection as soon as frequency drops below 58.1 Hz. The rationale for using such a steep dP/df slope between 58 and 58.1 Hz was to quickly capture any fast drop in frequency of the system below 58.1 Hz. After the first injection of power at 40% of the inverter rated capacity, a stepped approach is used to arrest the further decline in frequency. A constant power injection was used between frequency of 57.1 Hz and 58 Hz and was increased to 45% for frequency between 57 Hz and 56.1 Hz. For frequency below 56 Hz, the power injection is increased to 50% of inverter rated capacity. Such a stepped approach with wider deadband was used to study the impact of the failure to capture the drop of frequency early on after the disturbance but injecting a large burst of power after a certain lower frequency threshold is reached.
- For setting #2, a similar stepped approach as setting #1 is used but with a narrower deadband around 60 Hz. A deadband of 0.9 Hz below 60 Hz was used for setting #2. Once a frequency below 59 Hz is reached a large injection of power at 40% of inverter rating is supplied to the system. This ensures early capture of frequency deviation compared to setting #1. However, depending on the system inertia, level of disturbance, system's primary frequency response, etc., setting #2 could result in power injection for longer period, resulting in faster depletion of stored energy within the ultracapacitor. This faster depletion of stored energy before the system frequency settles in and the primary frequency response from the governor starts to kick in can result in second dip in system frequency. Such phenomena for certain ultracapacitor and inverter configurations are discussed below.
- For setting #3, no deadband was selected; a steady increment of power injection at 16.67% of inverter rated capacity/Hz was used for frequency below 60 Hz. Such setting would allow the ultracapacitor to respond to small deviations around 60 Hz, but due to the slower injection rate, it may not be as suitable as a stepped approach. For example, at 59 Hz, setting #3 injects about 16.67% of rated inverter capacity; whereas for setting #1 at 59 Hz, power injection is at 40% of rated inverter capacity. However, the slow response from the ultracapacitor with setting #3 means improved primary response from the governor and faster achievement of steady-state frequency as can be seen from results later.

- For setting #4, a small deadband of 0.2 Hz below 60 Hz was used. This was used to conserve the energy in the UCAP and prevent continuous injection of power even for small frequency deviations around 60Hz. Also a less steep slope of 10.52 %/Hz was used for frequency between 59.8 Hz and 56 Hz. For frequency below 56 Hz a constant power injection rate of 50% of inverter rated capacity was used. This setting ensures a steady injection of power if frequency falls below 56 Hz but adjusts the rate of injection linearly when frequency is between 56 Hz to 59.8 Hz.
- For setting #5, a slightly larger deadband of 1Hz was used below 60 Hz; an injection rate determined by slope of 16.67%/Hz was used for frequency between 59 Hz and 56 Hz. The rational for this setting was to facilitate early kick in of primary governor response by delaying the response from the ultracapacitor.

B.1. Simulations with 6.5 F Capacitor and 375 kVA Inverter System

The frequency response studies were started with a UCAP rating of 6.5 F, 950 V, and an inverter rating of 375 kVA. Each of the five different f-Watt settings were tested for this UCAP and inverter configuration. Figure 46 below shows the system frequency response with different f-Watt settings with 375 kVA inverter and 6.5 F, 950 V ultracapacitor. It can be seen from the figure that with addition of ultracapacitor the overall frequency nadir has been improved irrespective of the f-Watt setting used. However, on closer look, it can be observed that aggressive f-Watt settings with steep slope like setting #2 results in better frequency nadir than the rest. However, the issue with setting #2 is evident once we move past the arresting period; due to the aggressive nature of setting #2, it can be observed that the ultracapacitor runs out of available energy shortly after 20 s resulting in sudden increase in demand from the synchronous generator, which led to the second dip in frequency. For setting #1, which has a wider deadband than setting #2, it can be observed that the frequency nadir is lower (due to the late injection of power). However, setting #2 takes less time to reach to the steady-state frequency as opposed to the setting #1, and no second dip in frequency occurs with setting #1 as the SoC of ultracapacitor is not fully depleted. For setting #1, the frequency rises slowly once it reaches 58 Hz until it rises to 58.1 Hz, and this is associated to the steep setting around 58 and 58.1 Hz for setting #1. The phenomena that lead to the slow increase of frequency around the region with steep slope for settings #1 and #2 (for other configurations of ultracapacitor and inverter) is described in Section B.5.

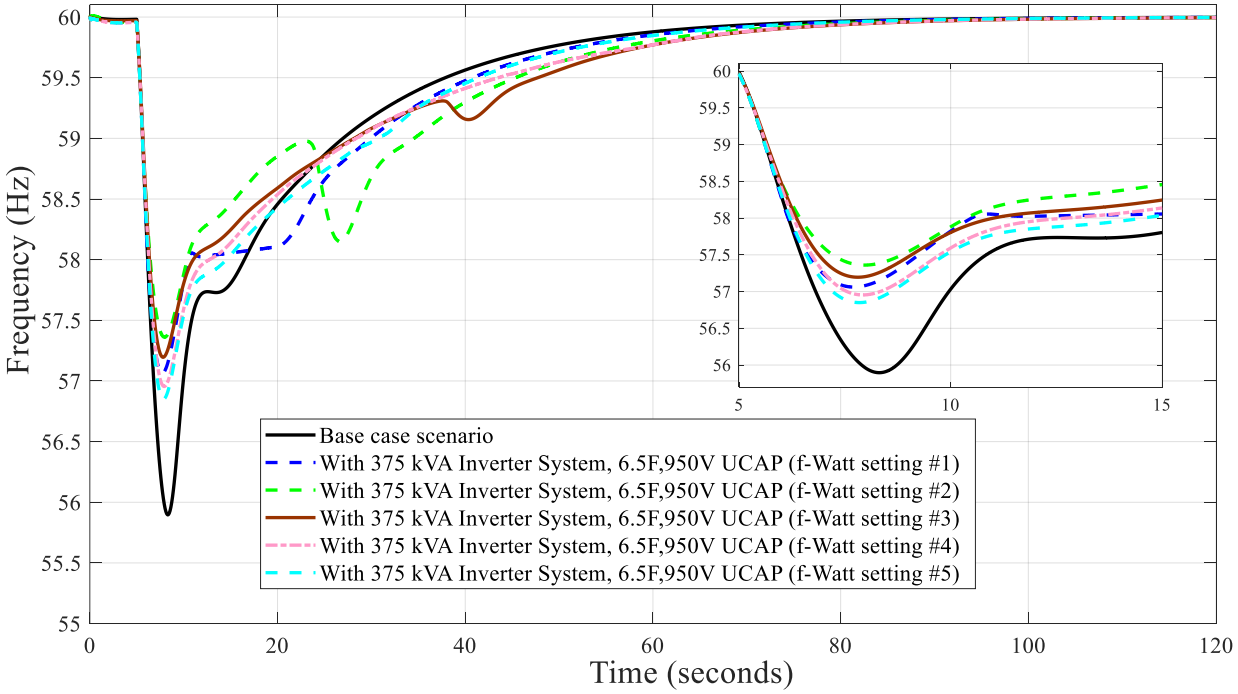

Figure 46. System frequency response with different f-Watt settings with 375 kVA inverter and 6.5 F, 950 V UCAP.

For settings #3 to #5, setting #3 has the better frequency nadir, but due to lack of deadband in setting #3, which results in continuous injection of power from ultracapacitor, UCAP SoC falls down to zero at around 40 s, resulting in second dip in the frequency (albeit small). Setting #4 has marginally better frequency nadir than setting #5, due to its smaller frequency deadband below 60 Hz, but setting #5 has a better time to reach to steady-state frequency. This can be attributed to earlier withdrawal of power injection from ultracapacitor for setting #5 owing to its larger deadband below 60 Hz.

Also, from Figure 47, and Figure 48, it can be observed that setting #1 and setting #5 end up at the same SoC and final terminal voltage, indicating both these settings have equal amount of energy injection; however, setting #1 has a better frequency nadir than setting #5, indicating the larger injection of power for frequency below 58 Hz with setting #1 resulted in better frequency nadir.

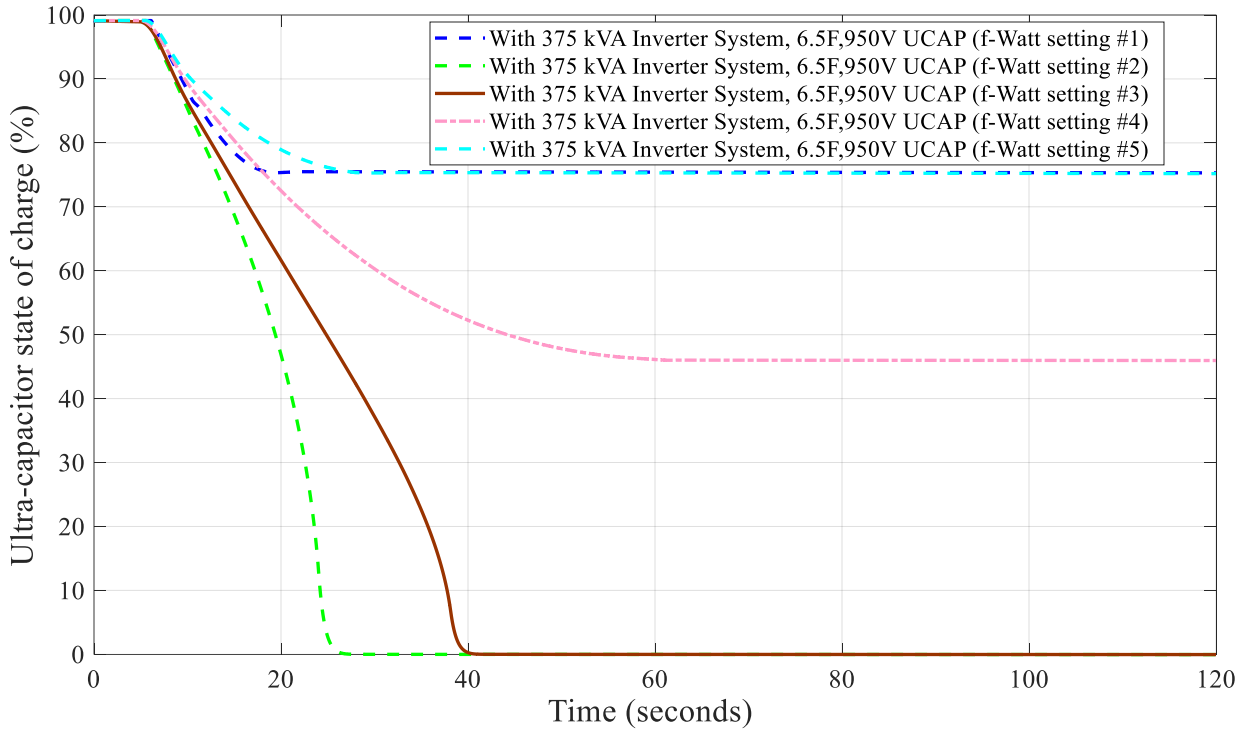

Figure 47. State of charge for 6.5 F, 950 V ultracapacitor with 375 kVA inverter when providing frequency support with different f-Watt settings.

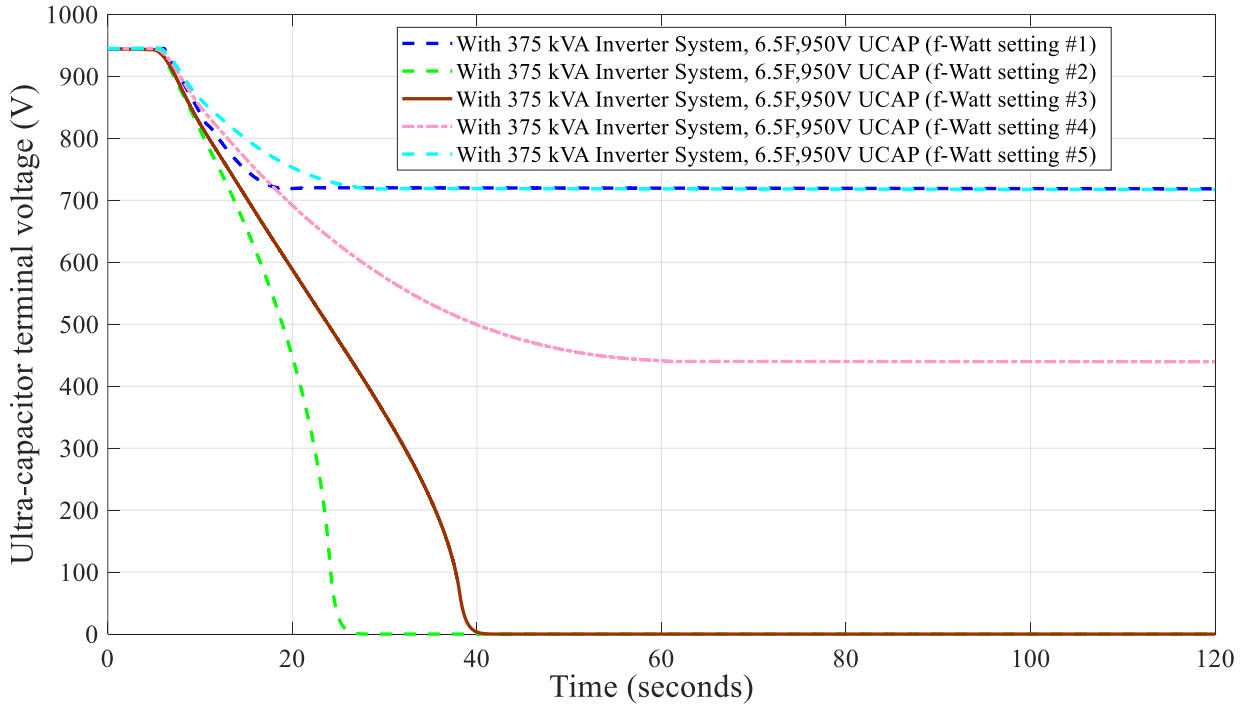

Figure 48. Terminal voltage for 6.5 F, 950 V ultracapacitor with 375 kVA inverter when providing frequency support with different f-Watt settings.

B.2. Simulations with 13 F Capacitor and 750 kVA Inverter System

The rationale for this second simulation study is to determine how the ratings of the inverter along with the capacity of ultracapacitor affect the system frequency response when the f-Watt settings remain unchanged. Note the f-Watt curves are designed based on the percentage of inverter ratings; so when a larger size inverter is in use, a larger amount of power is injected in the grid. The initial thesis is that the overall system frequency response improves when both larger size inverter and capacitors are used, and a larger amount of power is injected in the grid.

The results in Figure 49 below show that with the larger rating of the inverter used, the frequency nadir is improved as much as 1 Hz with f-Watt setting #2; however, due to faster depletion of the energy stored in ultracapacitor, a second dip in frequency is observed, with the second dip in frequency being larger the initial frequency nadir. A second dip in frequency is also observed with setting #3; however, the second dip in frequency is not as much as the initial drop in frequency. This is due to a less steep dP/df slope in setting #3 resulting in lower withdrawal of power from the system when ultracapacitor charge depletes. These results show that the higher injection rate from ultracapacitor improves the initial drop in frequency, but a less steep dP/df curve or a higher deadband is required to prevent the possibility of second dip in system frequency.

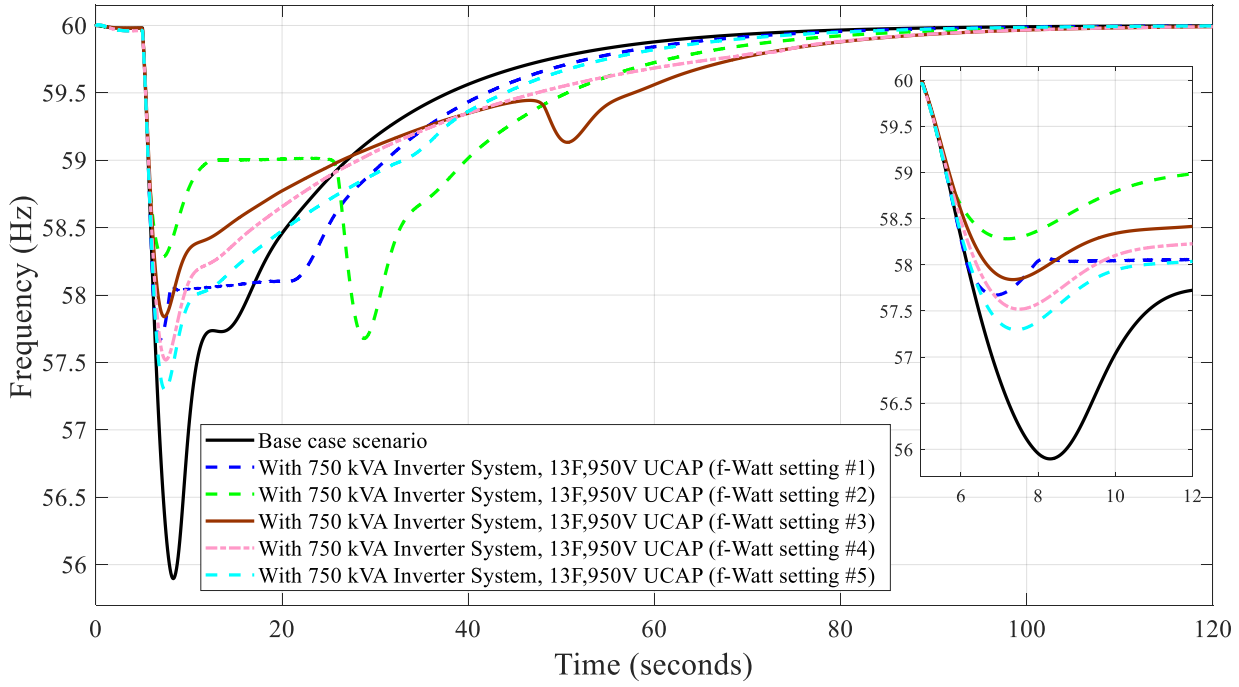

Figure 49. System frequency response with different f-Watt settings with 750 kVA inverter and 13 F, 950 V UCAP.

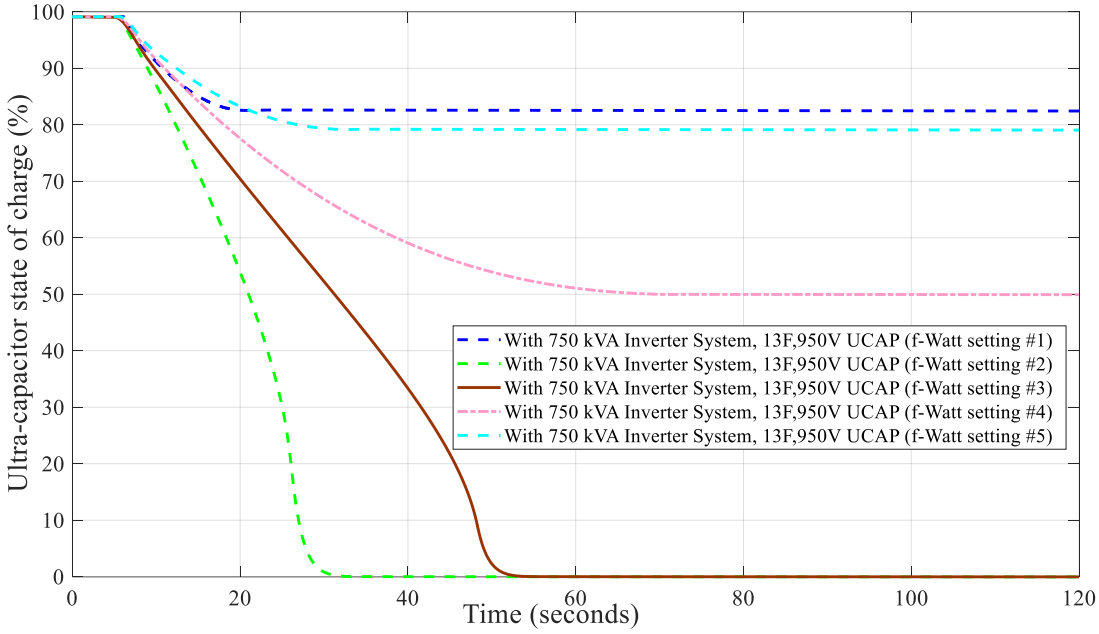

Figure 50. State of charge for 13 F, 950 V ultracapacitor with 750 kVA inverter when providing frequency support with different f-Watt settings.

B.3. Simulations with 13 F Capacitor and 375 kVA Inverter System

The rational for these set of simulations is based on the response observed for 375 kVA, 6.5 F capacitor with f-Watt setting #2. It was observed in the frequency response for that particular case (see Figure 46) that the frequency nadir was lower and was recovering faster than any other scenario for that capacitor and inverter configuration before the frequency double dip, which was the result of depletion of state of charge of the ultracapacitor (see Figure 47). So, the rational for these set of simulations was to keep the same amount of power injection as the previous case but increase the amount of stored energy in the ultracapacitor; hence, the inverter rating was kept fixed at 375 kVA, and the ultracapacitor size was increased to 13 F. The results below in Figure 51 show that the frequency nadir is improved, and a frequency double dip is avoided; however, in between the frequency range 59 to 59.1 Hz, the rate of frequency recovery slows down. As between the range of 59 to 59.1 Hz, the ultracapacitor power output fluctuates between 40% of inverter rating to 0%. Similarly, slowing down of frequency recovery is seen for results with curve #1 settings around 58 Hz.

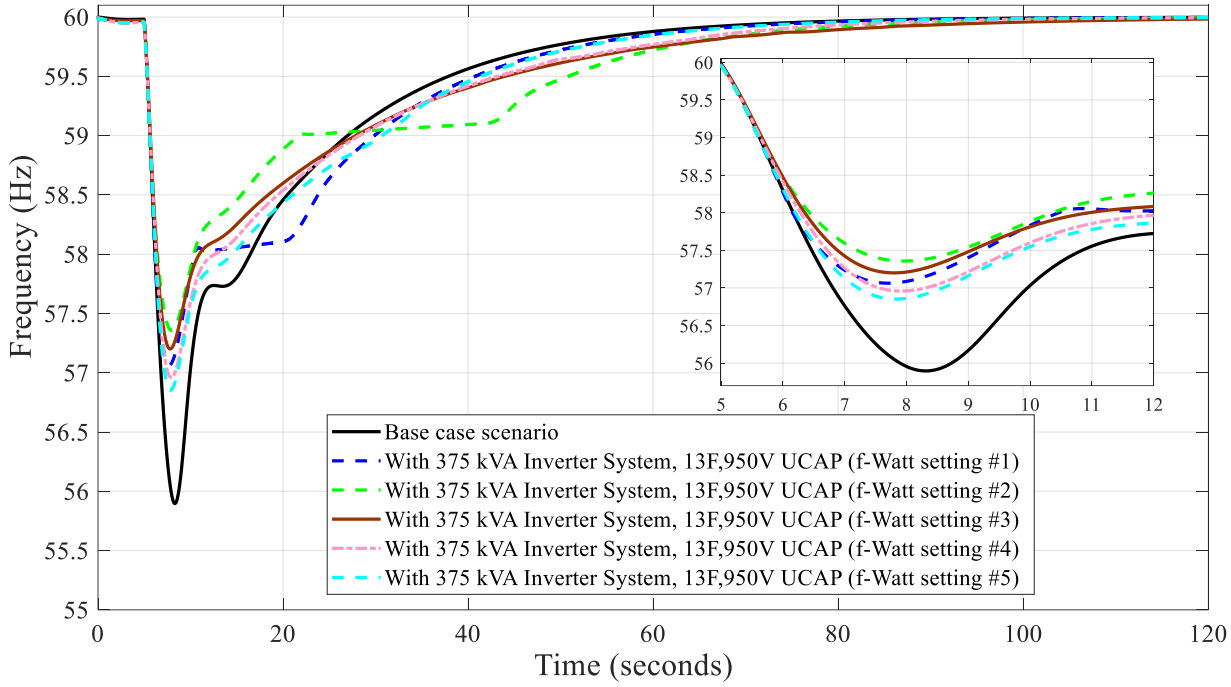

Figure 51. Frequency response comparison with various f-Watt settings with 375 kVA inverter system and 13 F, 950 V UCAP.

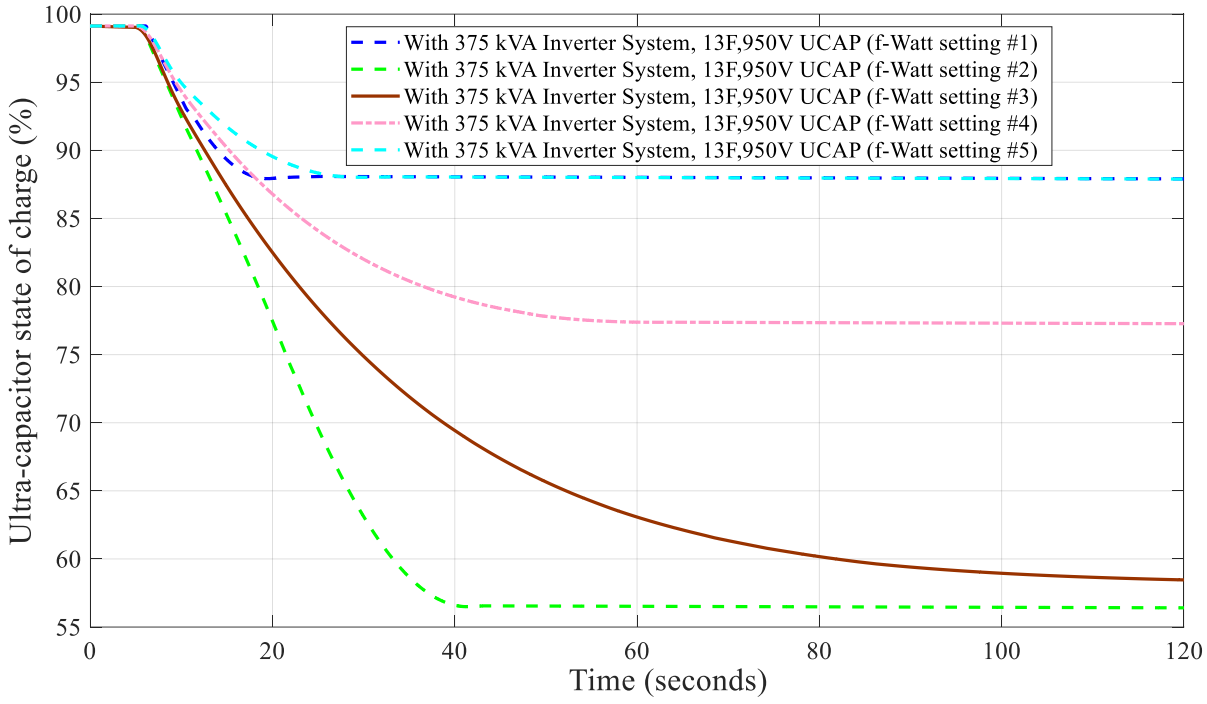

Figure 52. State of charge for 13 F, 950V UCAP with 375 kVA inverter when providing frequency support with different f-Watt settings.

B.4. Simulations with 6.5F Capacitor and 750kVA Inverter System

The rational for these set of simulations is based on the response observed for 750 kVA, 13 F UCAP with f-Watt setting #1 and #5. It was observed in the frequency response for that case, the frequency recovery was faster with setting #1 and #5, the frequency nadir was better compared to the base case, and the SoC of the ultracapacitor was still high (i.e., greater than 80%). Because of the observations made with capacitor and inverter configuration of 13 F, 750 kVA with available SoC at the end of disturbance, the capacitor and inverter configuration with lower capacitor rating of 6.5 F and same inverter rating of 750 kVA were tested. The results showed that the frequency nadir was comparable to the 13 F, 750 kVA configuration for setting #1 and #5, and a double dip in frequency was observed for setting #4 due to insufficient SoC in ultracapacitors. Also, with setting #2, a second dip in frequency larger than the original dip was observed, even though the initial nadir was improved when compared to the 6.5 F, 375 kVA inverter case. Thus, it can be observed that a combination of the inverter and capacitor ratings along with the proper choice of f-Watt setting is essential to obtain the desired frequency response from the system with support from ultracapacitor-based energy storage.

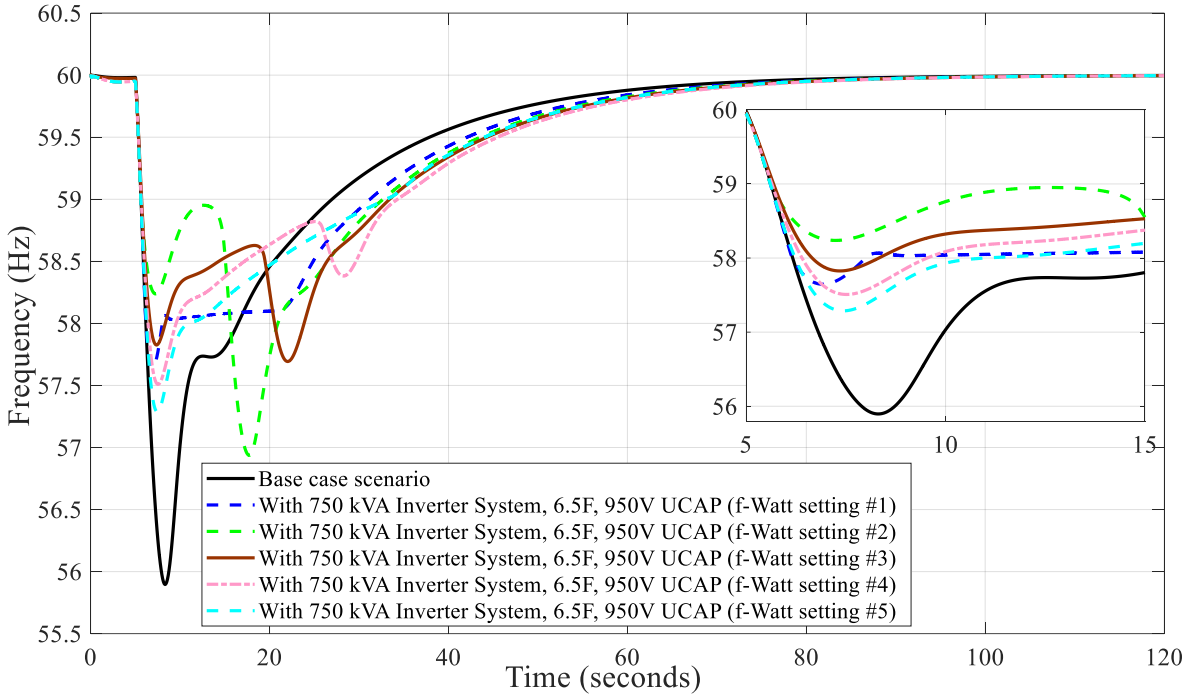

Figure 53. Frequency response comparison with various f-Watt settings with 750 kVA inverter system and 6.5 F, 950 V UCAP.

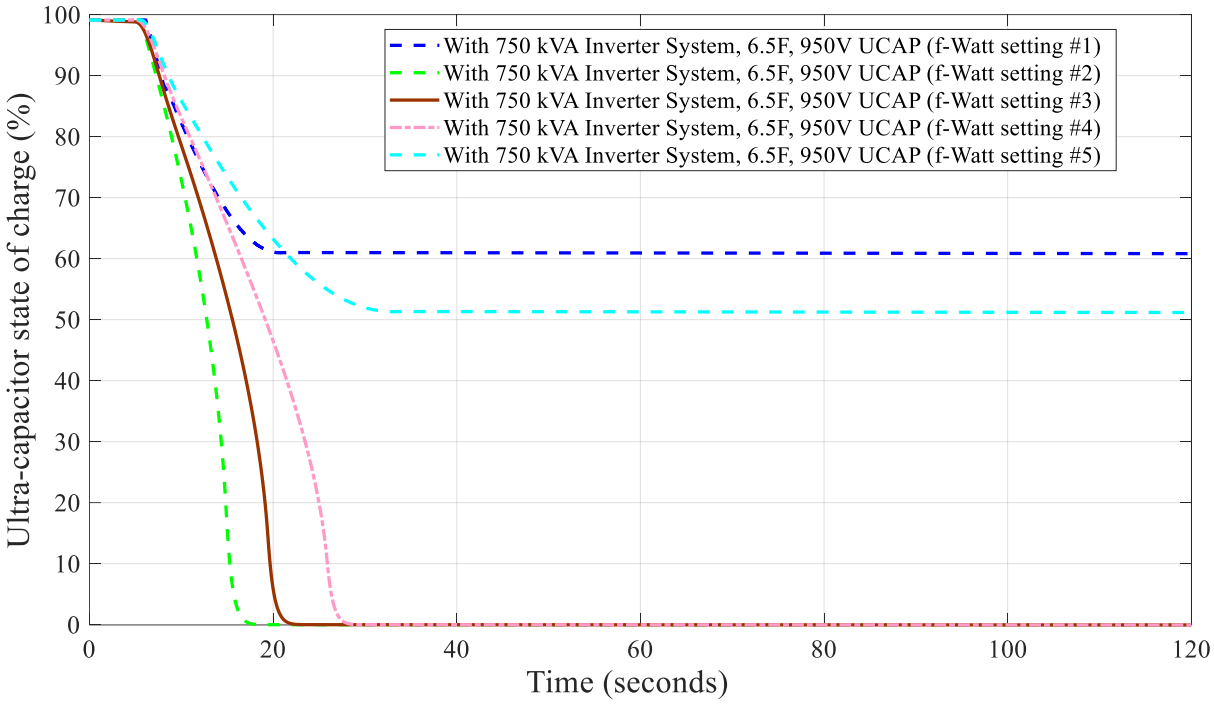

Figure 54. State of charge for 6.5 F, 950 V UCAP with 750 kVA inverter when providing frequency support with different f-Watt settings.

B.5. Study to Determine How dP/df Slope in F-Watt Settings Impacts Overall Frequency Response with Sufficient Energy Storage Availability

To determine the impact of the dP/df slope on the overall system frequency response when the maximum injection, as well as when the capacitor configuration is kept fixed, is discussed in this section. Setting #2 is used as an example, and two new settings #5 and #6 are created with the difference being reduction of deadband, as well as the slope between frequency of 59 Hz and 60 Hz (as shown in Figure 55).

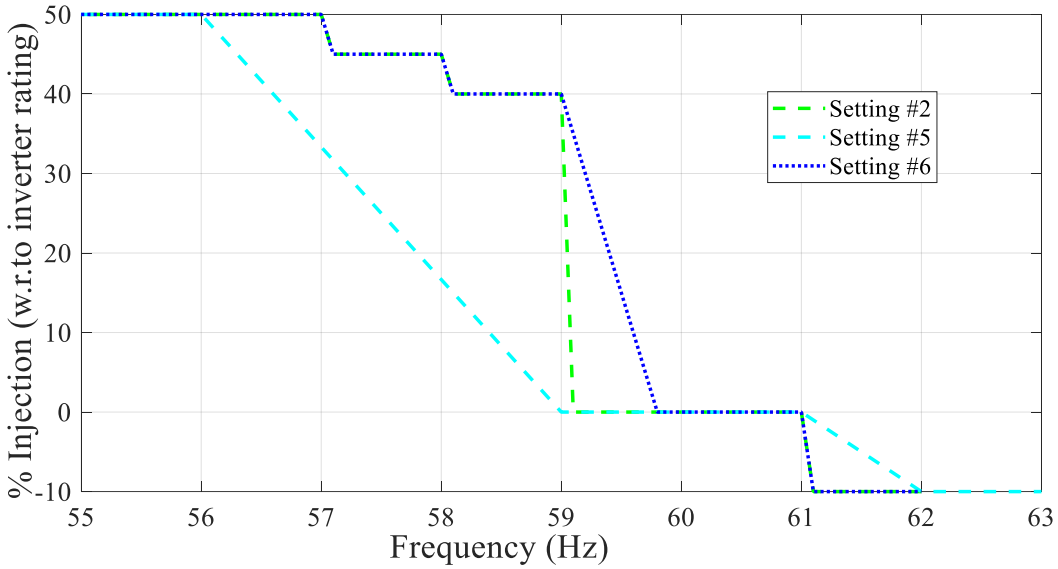

Figure 55. New f-Watt setting used for with modification in setting #2 and original setting #2.

Figure 56 compares the frequency response of the system with settings #2, #5, and #6 with the 375 kVA inverter and the, 6.5 F, 950 V capacitor system. It can be observed that for settings #2 and #6, an almost similar response is obtained with setting #6 being marginally better in minimizing the amount of frequency nadir. However, for both cases due to the insufficient amount of energy in the ultracapacitor, a second dip in frequency is observed. However, with setting #5 of deadband as in #2 but with less steep slope, the frequency nadir has not improved as much; however, the primary frequency response is better as the capacitor does not get fully discharged as in settings #2 and #6.

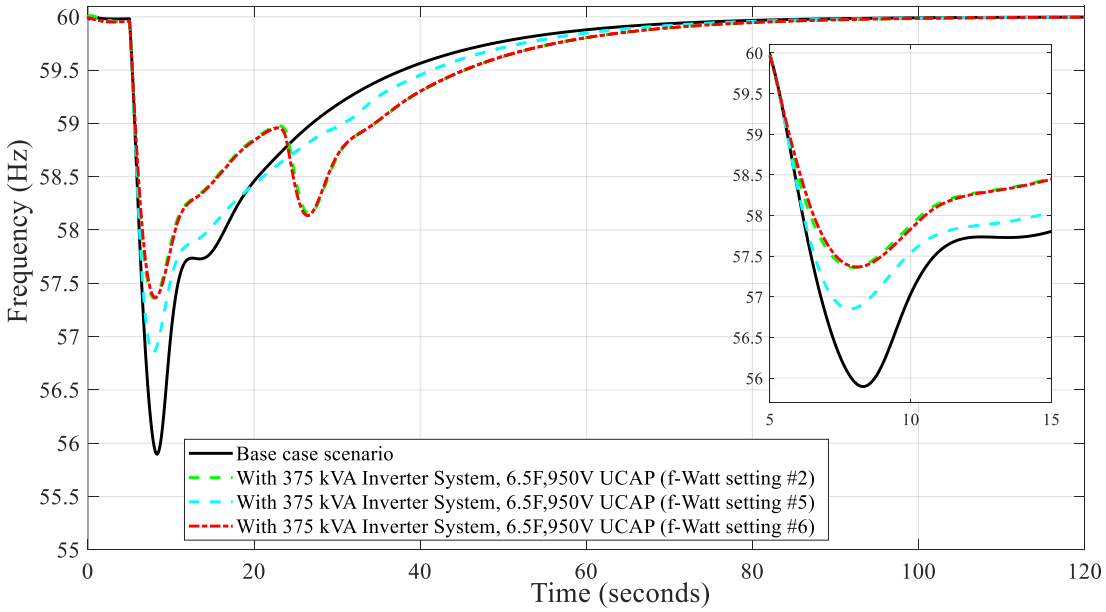

Figure 56. Frequency vs. time when setting #6 modified from #2 is used, with 375 kVA inverter, 6.5F, 950 V UCAP system.

To study what would happen if ultracapacitor had more energy available, a second set of simulation with a 375 kVA inverter and 13 F capacitor is performed. Figure 57 shows that in such a case, the less steep slope in setting #6 allows frequency to rise faster after it reaches 59 Hz letting the governor response to kick in; however, a narrower deadband causes more discharge of energy from the ultracapacitor, resulting in depletion of SoC of UCAP (see Figure 58), and a minor second dip in frequency with #6. For setting #5, we however see a larger frequency nadir but higher SoC available at the end of frequency response and shorter time to get to steady-state frequency.

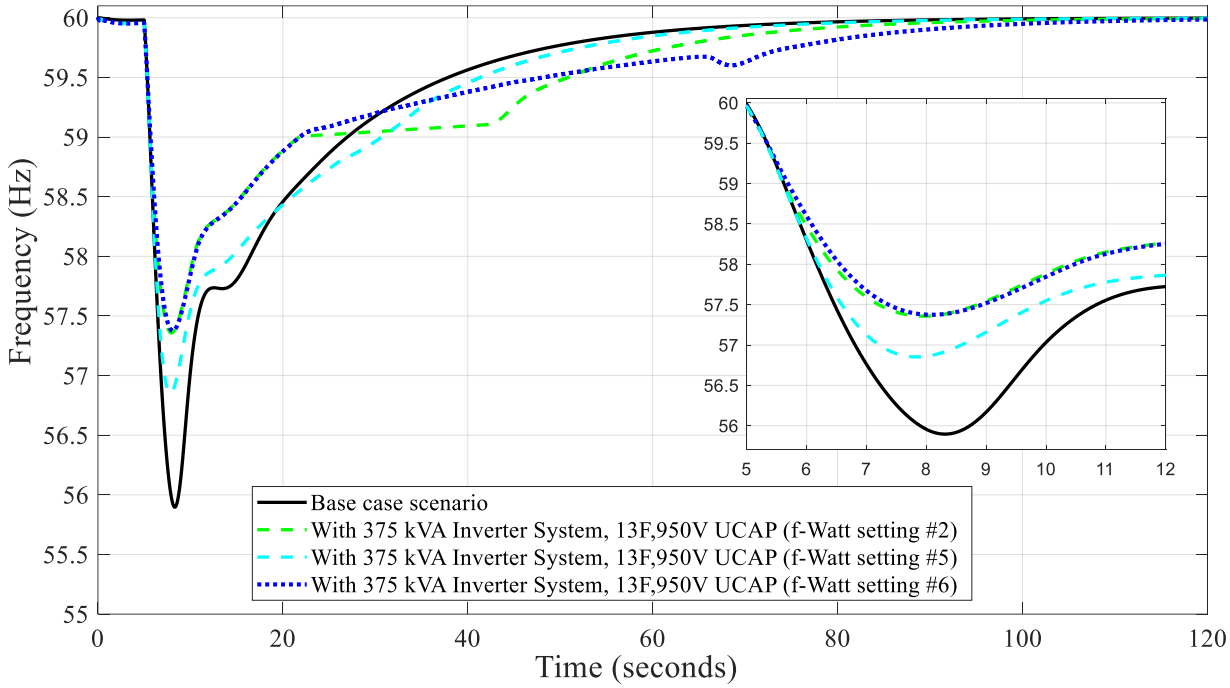

Figure 57. Frequency vs. time when setting #6 modified from #2 is used, with 375 kVA inverter, 13 F, 950 V UCAP system.

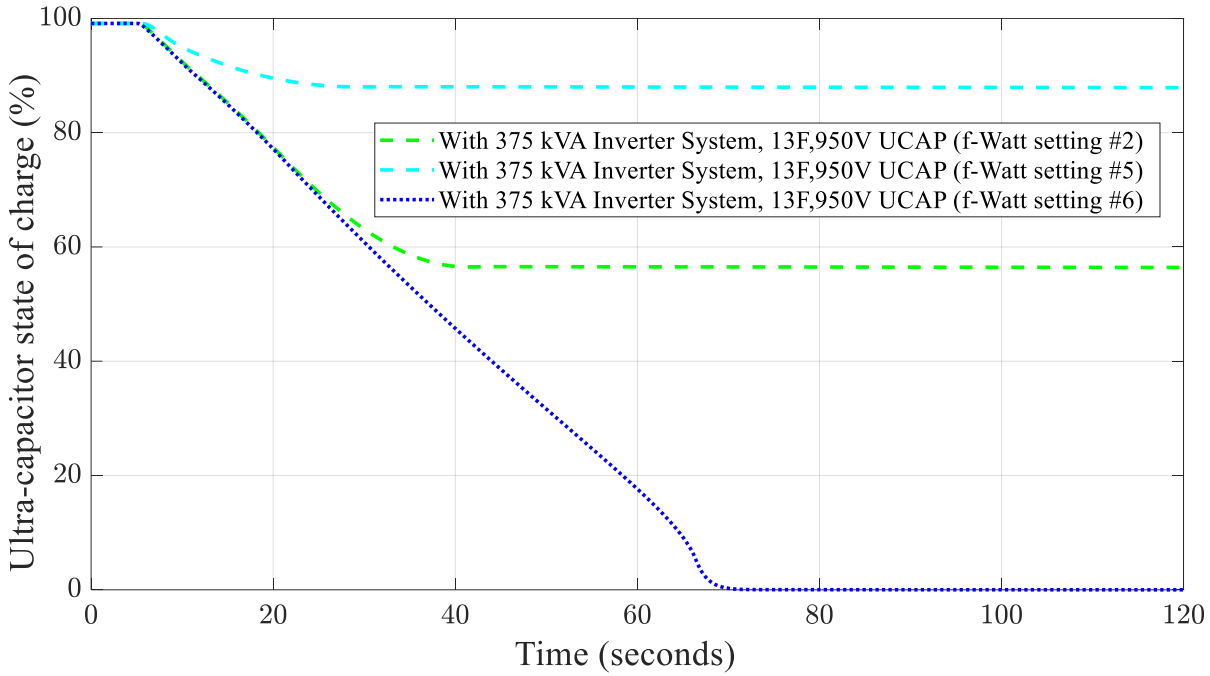

Figure 58. State of charge comparison with 375 kVA inverter, 13 F, 950 V UCAP system when using setting #2 and setting #6.

This report is being prepared for the U.S. Department of Energy (DOE). As such, this document was prepared in compliance with Section 515 of the Treasury and General Government Appropriations Act for fiscal year 2001 (public law 106-554) and information quality guidelines issued by DOE. Though this report does not constitute "influential" information, as that term is defined in DOE's information quality guidelines or the Office of Management and Budget's Information Quality Bulletin for Peer Review, the study was reviewed both internally and externally prior to publication.

NOTICE

Available electronically at OSTI.gov http:/www.osti.gov

Available for a processing fee to U.S. Department of Energy
and its contractors, in paper, from:

U.S. Department of Energy Office of Scientific and Technical Information
P.O. Box 62
Oak Ridge, TN 37831-0062
OSTI http://www.osti.gov
Phone: 865.576.8401
Fax: 865.576.5728
Email: reports@osti.gov

Available for sale to the public, in paper, from:

U.S. Department of Commerce
National Technical Information Service
5301 Shawnee Road
Alexandria, VA 22312
NTIS http://www.ntis.gov
Phone: 800.553.6847 or 703.605.6000
Fax: 703.605.6900
Email: orders@ntis.gov

How to cite this report: Alam, S M S.; Bhattarai, R.; Hussain, T.; Gevorgian, V.; Shah, S.; Velaga, N., Y.; Roberts, M.; Mosier, M., T.; Alzamora, A., J.; Jenkins, B.; Koralewicz, P. September 2022. Enhancing Local Grid Resilience with Small Hydropower Hybrids – Proving the concept through demonstration, simulation, and analysis with Idaho Falls Power. Idaho National Laboratory. INL/RPT-22-69038.

HydroWIRES
U.S. DEPARTMENT OF ENERGY

https://energy.gov/hydrowires